Journal of Ophthalmology

Effects of Ageing on the Eye Structure and Function 2019

Special Issue Editor in Chief: Alejandro Cerviño

Guest Editors: Jose F. Alfonso, Hema Radhakrishnan, Jose M. González-Meijome, and Rune Brautaset

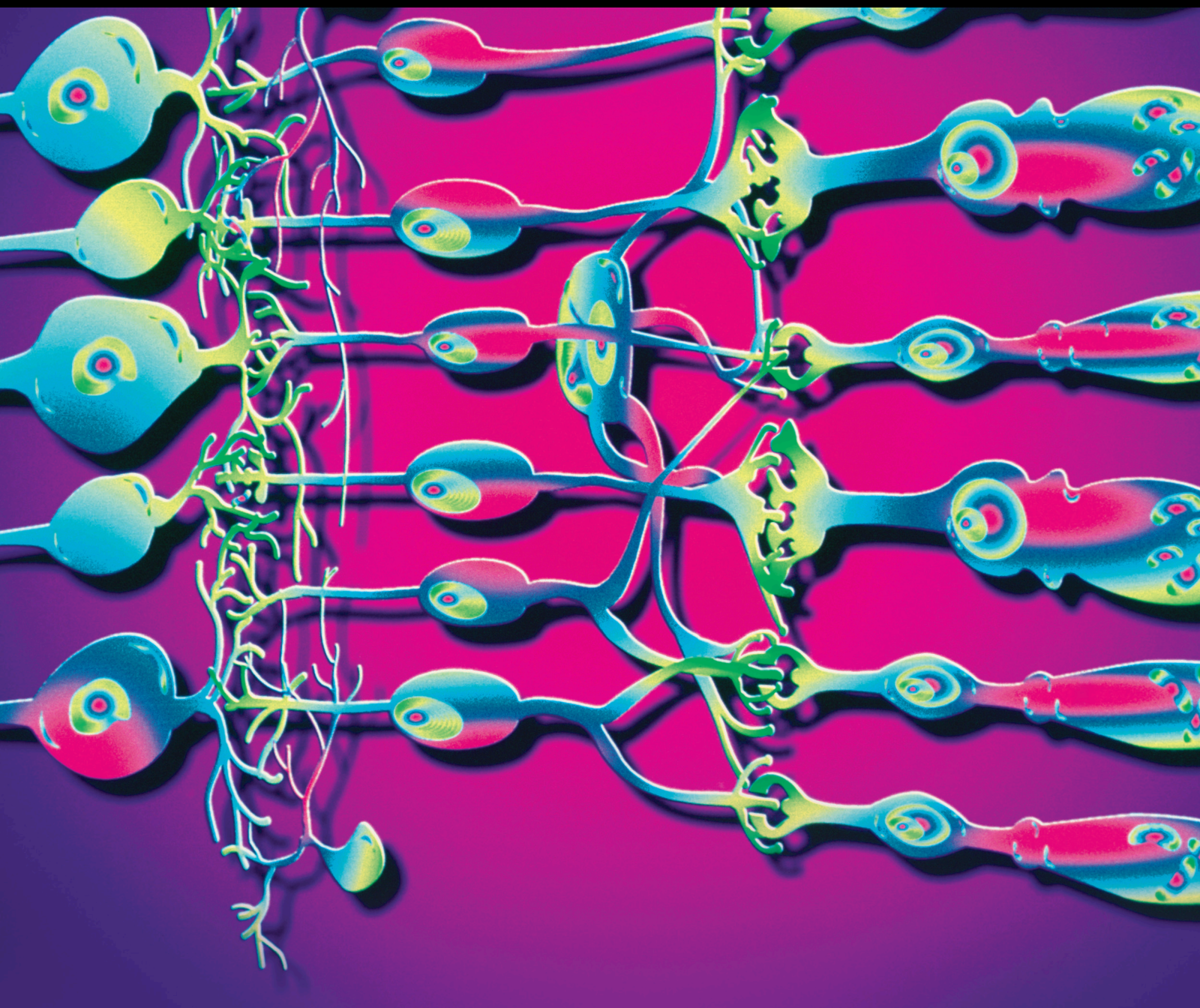

Effects of Ageing on the Eye Structure and Function 2019

Journal of Ophthalmology

Effects of Ageing on the Eye Structure and Function 2019

Special Issue Editor in Chief: Alejandro Cerviño
Guest Editors: Jose F. Alfonso, Hema Radhakrishnan, Jose M. González-Meijome, and Rune Brautaset

Contents

Hindawi
Journal of Ophthalmology
Volume 2020, Article ID 5192491, 2 pages
https://doi.org/10.1155/2020/5192491

Editorial

Effects of Ageing on the Eye Structure and Function 2019

Alejandro Cerviño,[1] **Jose F. Alfonso**,[2] **Hema Radhakrishnan**,[3] **Jose M. González-Meijome**,[4] **and Rune Brautaset**[5]

[1]*Department of Optics and Optometry and Vision Sciences, University of Valencia, Valencia, Spain*
[2]*Fernández-Vega Ophthalmological Institute, Oviedo, Spain*
[3]*University of Manchester, Manchester, UK*
[4]*Department of Physics (Optometry), University of Minho, Braga, Portugal*
[5]*Karolinska Institutet, Stockholm, Sweden*

Correspondence should be addressed to Alejandro Cerviño; alejandro.cervino@uv.es

Received 21 February 2020; Accepted 22 February 2020; Published 23 March 2020

The world's population is growing older, with persons over the age of 65 being the fastest-growing age group. According to data from World Population Prospects 2019 [1], one in 11 people in the world was over the age of 65 in 2019 (9%), and this number is expected to increase to one in six (16%) by 2050 since life expectancy is also expected to increase from current 72.6 years to 77.1. In 2018, for the first time in history, persons aged 65 or above outnumbered children under five years of age.

Aging is a natural process that affects the function of many organs, including the eyes, having both structural and functional consequences for the visual system, affecting all ocular structures and causing a variety of effects. Improving quality of life as well as reducing age-related disability is of increasing importance for health systems. Determining the mechanisms behind age-related conditions and healthy ageing may help creating tools to improve early detection of involutive changes and prognosis, delay the onset of disease, and allow the optimization of resources through the treatment at earlier stages of the condition.

The eye is usually considered a window for findings of systemic disease, due to its high metabolic demands to keep transparency on its media, its sensitivity to vascular compromise, and the possibility of observing the different structures in a noninvasive manner. When age-related changes turn into age-related conditions, they manifest into eye disease, such as age-related macular degeneration (AMD), cataract, or pseudoexfoliation (PEX) syndrome. Several signalling pathways have been implicated in the aging process. In the paper titled "Repressed Wnt Signaling Accelerates the Aging Process in Mouse Eyes," Y. Zhang et al. suggest that disruption of Wnt signalling homeostasis in the eye is associated with accelerated aging.

One of the important aspects to understand is the anatomical change in the different ocular structures occurring with healthy aging and how they differ from age-related disease. In the paper titled "Panoramic Observation of Crystalline Lenses with 25 MHz Ultrasonography," W. Xue and H. Zou use 25 MHz B-scan ultrasound to assess change in the entire lens contour and the radii of curvatures of the central anterior and posterior lens surfaces. They confirm that the lens grows equatorially and axially with age while its central anterior lens surface steepens and its posterior central surface curvature does not change.

Age-related overproduction or overaggregation of elastic microfibrillar components on the lens results in PEX. The role of its inheritance has been explored in the past in different populations, and several genes were found likely to play a role in PEX, such as clusterin. In the paper titled "CLU Polymorphisms in Patients with Pseudoexfoliation Syndrome in Polish Population," H. Lesiewska et al. investigate this possible association in the Polish population concluding that clusterin variants may contribute to the risk of PEX.

Various retinal degenerative processes, such as AMD, concur with selective outer retinal degeneration. In the paper titled "Outer Retinal Layers' Thickness Changes in Relation

to Age and Choroidal Thickness in Normal Eyes," M. K. Abdellatif et al. identify and correlate age-related changes in outer retinal layers' thickness and choroidal thickness in normal eyes using spectral-domain optical coherence tomography and investigate factors affecting these changes. They report significant thinning of retinal pigment epithelium/outer-segment layer thickness with increasing age.

Similarly, in the paper titled "Distribution of Choroidal Thinning in High Myopia, Diabetes Mellitus, and Aging: A Swept-Source OCT Study," F. A. Bartol-Puyal et al. analyse the distribution of choroidal thinning in high myopia, diabetes mellitus, and aging, showing different thinning pattern that may help identifying conditions. They report the choroidal thickness pattern in young healthy individuals as resembling a mountain range; with age, a mountain peak; in high myopia, an inverted gorge; and in aged type 2 diabetic patients, gathered hills. The thicker the zone is in healthy subjects, the thinner it becomes with any pathology.

Age-related anatomical changes as described have functional consequences. Age-related changes in the eye may arise from several sources and affect visual function in different ways. Difficulty in adaptation to light level changes is a common complaint associated with ageing, particularly regarding night driving, and with significant impact in quality of life. Photostress is one of the methods that test adaption of the visual system and might be, therefore, useful to determine functional differences due to impairment of photopigment regeneration. In the paper titled "An Alternative Psychophysical Diagnostic Indicator of the Aging Eye," J. D. Rodriguez et al. explore the use of photostress with the addition of flickering stimuli, less dependent on refractive error or straylight, for assessing the health of the aging retina. They report that photostress recovery of flicker sensitivity under mesopic conditions agrees with subject-reported complaints in reduced luminance conditions after exposure to bright lights, such as night driving, highlighting the potential usefulness of the method for the clinical assessment in diseased eyes.

Finally, older persons generally have greater susceptibility to infections than younger adults. Aging is associated with immune dysfunction, especially in cell-mediated immunity, and elderly persons also suffer from a variety of chronic disorders, some of which affect the integrity of host resistance to infections.

Elderly individuals have an increased susceptibility to skin infections due to age-related anatomical, physiological, and environmental factors. The skin of the elderly is structurally and functionally different from that of other age groups. Mites are found on almost all normal adult skin. Demodex is a host-specific obligate parasite, and clinical observations based on large samples are important for exploring the relationship between its presence and clinical signs. In the paper titled "The Prevalence of *Demodex folliculorum* and *Demodex brevis* in Cylindrical Dandruff Patients," J. Zhong et al. carry out a large sample study in China designed to determine the prevalence of Demodex and the effect of host-related factors such as gender, age, and eyelid inflammation on this prevalence. They report higher prevalence in Demodex spp. in older subjects and greater prevalence on subjects with cylindrical dandruff than healthy subjects. Furthermore, in subjects with cylindrical dandruff, the number of *Demodex spp*. was reported as positively correlated with age and exacerbated the severity of eyelid congestion, providing, therefore, a good clinical reference.

We know that significant challenges remain in understanding the full extent of structural and functional changes in the eye which results from ageing. Some of these changes are outlined in this special issue. We hope that these stimulate ideas which will further advance our understanding of the ageing eye.

Conflicts of Interest

The editors declare that they have no conflicts of interest regarding the publication of the special issue.

Alejandro Cerviño
Jose F. Alfonso
Hema Radhakrishnan
Jose M. González-Meijome
Rune Brautaset

References

[1] United Nations, Department of Economic and Social Affairs, Population Division, *World Population Prospects 2019: Highlights*, United Nations, Department of Economic and Social Affairs, Population Division, New York, NY, USA, 2019.

Hindawi
Journal of Ophthalmology
Volume 2019, Article ID 8319027, 6 pages
https://doi.org/10.1155/2019/8319027

Research Article

Panoramic Observation of Crystalline Lenses with 25 MHz Ultrasonography

Wenwen Xue[1] **and Haidong Zou**[1,2]

[1]*Department of Ophthalmology, Shanghai Eye Disease Prevention and Treatment Center, Shanghai Eye Hospital, Shanghai 200040, China*
[2]*Department of Ophthalmology, Shanghai General Hospital, Shanghai Jiao Tong University School of Medicine, Shanghai 200080, China*

Correspondence should be addressed to Haidong Zou; zouhaidong@sjtu.edu.cn

Received 8 April 2019; Revised 24 September 2019; Accepted 19 October 2019; Published 11 November 2019

Academic Editor: Alejandro Cerviño

Purpose. To visualize and assess in vivo the age-related changes in crystalline lens size and contour. *Methods*. Seventy-nine healthy volunteers, 39 females and 40 males, with a mean age of 41.53 + 11.32 years (range: 21 to 60 years) were enrolled in this study. The axial lens thickness (ALT), equatorial lens diameter (ELD), and anterior (R_a) and posterior (R_p) lens surface radii of curvatures of the subjects' left eyes were measured with a 25 MHz ultrasound probe. *Results*. The mean ALT and ELD were 4.178 mm + 0.288 mm and 9.209 mm + 0.214 mm, respectively. There was a statistically significant increase in both ALT (slope = 11 μm/year, $r = 0.88$, $p < 0.01$) and ELD (slope = 6 μm/year, $r = 0.60$, $p < 0.01$) with age. R_a negatively correlated, and R_p did not change with age. *Conclusion*. There were no statistically significant relationships between any studied values and gender. Independent of gender, the lens grows equatorially and axially with age while its central anterior lens surface steepens and its posterior central surface curvature does not change.

1. Introduction

Understanding the normal functioning of the human lens and its role in the development of refraction, accommodation and presbyopia requires a thorough knowledge of how lens size and contour change with age. The central 1 mm-to-6 mm zone of the lens within the pupillary area is easily visualized. Axial lens thickness (ALT), central lens radius of curvature, can be measured using anterior segment optical coherence tomography or Scheimpflug photography. Although these devices have proven to provide high resolution and valid in vivo images of the lens of the eye, none of these devices can visualize the contour of the lens equator because the iris blocks the penetration of light. Although 50 MHz ultrasound biomicroscopy can visualize a small portion of the lens equator, only magnetic resonance imaging (MRI) has been able to visualize the entire contour of the lens including its equator [1–3]. However, MRI has low resolution and is infrequently used in the field of ophthalmic clinical observation because it is time-consuming and expensive.

In this study a 25 MHz B-scan ultrasound device was used to visualize and assess the age-related changes in the entire lens contour including ALT and ELD and the radii of curvatures of the central anterior and posterior lens surfaces.

2. Materials and Methods

2.1. Subjects. This healthy volunteer prospective study was completed within 1 year (January 1, 2014, to December 1, 2015). The inclusion criteria were the following: Chinese Han race; 21–60 years of age; no history of systematic diseases, such as hypertension, diabetes, or other diseases; best-corrected visual acuity 6/6 or higher in both

eyes; and a refractive error between −3.00 D and +3.00 D and otherwise normal ophthalmic examination. Children or teenagers were not enrolled because of their intolerance to corneal-contact examinations. Volunteers with eye diseases, such as cataracts, glaucoma, retinal diseases, or strabismus, and in whom the equator of the lens was not clearly identifiable with the 25 MHz B-scan ultrasound probe were excluded. All volunteers received a routine eye examination without mydriasis that included best-corrected visual acuity, auto-refraction (RM-8900, Topcon, Tokyo, Japan), biomicroscopy, and ophthalmoscopy. This investigation complied with the Declaration of Helsinki and was approved by the Institutional Ethical Board at the Shanghai General Hospital, Shanghai Jiao Tong University. All examination procedures were clearly explained to the subjects, and informed consent was obtained.

2.2. Ultrasonography. A 25 MHz B-scan ultrasonography device (AVISO Diagnostic Ultrasonography, Quantel Medical, France) was used to visualize the entire contour of the lens. In previous studies, this device has been shown to make highly reliable repeatable measurements [4]. The axial and lateral resolutions of the 25 MHz B-scan ultrasonographic probe are estimated to be 60 μm and 120 μm, respectively. Two experienced ophthalmologists (HZ and WX) conducted the following procedures. Each subject was placed in the supine position on an examination table in natural light. After a topical anesthetic drop was administered to the left eye, the 25 MHz B-scan probe ultrasound probe with an attached water bladder was gently placed vertically onto the center of the left cornea. Starting from the 12 o'clock position, the probe was rotated once 360°. The gain, dynamic range, time-gain compensation, contrast, and intensity of the ultrasound were adjusted to ensure maximum visualization of the entire left lens including its equator while the subject stared with the right eye at a 3 m high ceiling. An ultrasound image was frozen when the whole equator of the lens was clearly observed, as shown in Figure 1. The caliber of the ultrasound device was used to measure 3 times the ELD, anterior (ALT_a), and posterior (ALT_p) lens thicknesses as shown in Figure 2. In addition, a 10 MHz A-scan ultrasonographic probe (AVISO Diagnostic Ultrasonography, Quantel Medical, France) was used to measure ALT. The 10 MHz probe was gently placed in contact with the center of the left cornea while the subject fixated at the light within the center of the probe.

2.3. Analysis. The central 1 to 3 mm of the lens anterior and posterior surfaces were assumed to be spherical, and the radius of the central anterior lens surface was calculated using the following formula:

$$R_a = \left[\frac{ELD^2}{8 * ALT_a}\right] + 0.5 * ALT_a. \quad (1)$$

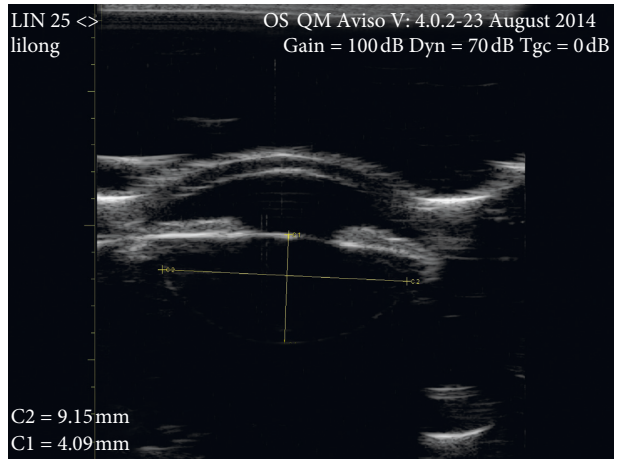

Figure 1: A 25 MHz ultrasonographic image of the left eye of a 40-year-old female. The gain was set to 100 dB, the dynamic range to 70 dB, and the time gain compensation to 0 dB. The entire contour of the lens, including the equator anterior and posterior surfaces, was clearly visible. Using the calipers, yellow lines, shown in the image, the axial lens thickness and equatorial lens diameter were calculated as 4.09 mm (C1) and 9.15 mm (C2), respectively.

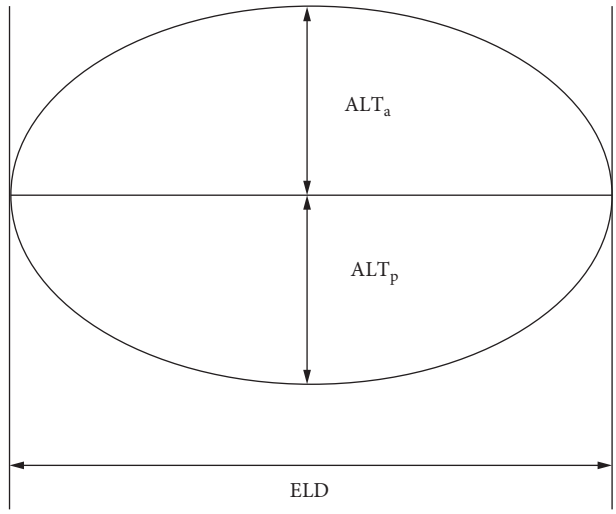

Figure 2: A schematic drawing of a lens. ELD represents the equatorial lens diameter, ALT_a represents the anterior part of axial lens thickness, and ALT_p represents the posterior part of the axial lens thickness.

The curvature of the central anterior surface (K_a) was calculated as the reciprocal of R_a. The radius (R_p) and curvature (K_p) of the central posterior lens surface were calculated with the same method.

2.4. Statistics. Consistency between the ALT results measured by 25 MHz B-scan and 10 MHz A-scan ultrasonography were analyzed using an intragroup coefficient (ICC). Correlations between ALT and ELD were evaluated using Pearson's correlation analysis. The relation between studied

Table 1: Dimensions by gender of 79 crystalline lenses measured with a 25 MHz B-scan ultrasonic probe.

	Males	Females	Student's t-test	p value
Axial lens thickness (mm)	4.190 ± 0.285	4.167 ± 0.295	0.35	0.727
Equatorial lens diameter (mm)	9.216 ± 0.193	9.202 ± 0.236	0.293	0.77
Radius of anterior lens surface (mm)	10.513 ± 0.977	10.485 ± 0.985	0.125	0.901
Radius of posterior lens surface (mm)	4.980 ± 0.128	4.982 ± 0.143	0.083	0.934
Curvature of anterior lens surface (mm)	0.096 ± 0.009	0.096 ± 0.009	0.123	0.902
Curvature of posterior lens surface (mm)	0.201 ± 0.005	0.201 ± 0.006	0.059	0.953

Note. Data are presented as mean ± standard deviation.

values and gender were assessed with the Student's t-test. A statistical package (SPSS V10.0, Chicago, IL, USA) was used for database setup and analysis. The level of statistical significance was set at $p < 0.05$.

3. Results

3.1. Subjects. One hundred and fifty-seven healthy volunteers were screened; however, 78 subjects were excluded because their lens equators were too fuzzy to identify; i.e., only 79 subjects (50.3%) met the inclusion criteria. Of the 79 enrolled subjects, 40 (50.63%) were male and 39 (49.37%) were female. The average age was 41.53 ± 11.32 years old. There were 17 (21.5%) subjects in the 21-to-30-year-old age group, 20 (25.3%) in the 31-to-40-year-old age group, 21 (26.6%) in the 41-to-50-year-old age group, and 21 (26.6%) in the 51-to-60-year-old age group. The refractive error of the left eye of these 79 subjects was between −2.00 D and +2.50 D.

3.2. Measurements. The mean (standard deviation) of the 25 MHz B-scan ultrasonographic ALT, ELD, R_a, K_a, R_p, and K_p was 4.178 mm (+0.288 mm), 9.209 mm (+0.214 mm), 10.499 mm (+0.975 mm), 0.096/mm (+0.009/mm), 4.981 mm (+0.135 mm), and 0.201/mm (+0.005/mm), respectively. There were no statistically significant gender differences in these measurements as shown in Table 1.

The 10 MHz A-scan ultrasonography measured ALT was 4.168 mm (+0.291 mm). An intragroup correlation analysis of the ALT measured by the 25 MHz B-scan and 10 MHz A-scan probes showed that the two techniques were highly statistically significantly consistent (ICC = 0.962, $p < 0.01$).

The ALT, ELD, R_a, K_a, R_p, and K_p using 25 MHz B-scan ultrasonography of the 79 eyes are shown in Table 2.

3.3. Correlations. A positive correlation was found between age and ALT and ELD (slope = 11 μm/year and 6 μm/year, Pearson's correlation coefficient, $r = 0.880$, $p < 0.01$ and $r = 0.600$, $p < 0.01$, respectively). There was a negative correlation between age and R_a. There was no statistically significant correlation between age and R_p or K_p ($p > 0.05$) as shown in Figure 3.

4. Discussion

In the present study, a panoramic observation of the entire crystalline lens contour was obtained with a 25 MHz B-scan ultrasonography. This technique has relatively high axial and lateral resolutions estimated to be 60 μm and 120 μm, respectively. The accuracy of the measurements in the present study was confirmed by the highly statistically significant correlation between the 25 MHz B-scan and 10 MHz A-scan probe ALT measurements. However, even though the technique has good resolution, 50% of subjects screen failed because the lens equator contour was ambiguous. Possible reasons for the difficulty in imaging the equatorial region in these screened failed subjects were poor fixation with their right eyes or that their pupils were naturally more dilated resulting in a thicker peripheral iris causing a decrease in penetration of the ultrasound.

In the 79 enrolled subjects, there was a statistically significant non-gender-related and age-related increase in both ALT and ELD and a decrease in R_a; however, R_p did not change with age. Other studies have also confirmed an age-related increase in ALT [2, 5, 6, 7]. For example, and similar to the present study, Atchison et al. found with A-scan ultrasonography an age-related ALT increase of 0.0235 mm/year in 106 emmetropes aged 18 to 69 years [2]. And with optical coherence tomography (Lenstar LS900, Haag-Streit Diagnostics, Köniz, Switzerland), Adnan et al. also reported a similar age-related increase in ALT of 0.020 mm/year [6].

The observed age-related increase in ELD is consistent with *in vitro* ELD [8, 9] and *in vivo* MRI measurements [2, 3]. Using Scheimpflug photography, Dubbelman and Heijde found that the radius of curvature of the central 3 mm zone of the anterior lens surface decreases with age according to the following equation: $R_a = 12.9–0.057 * \text{age}$ [10]. Similar to the present study Atchison et al. found that there was not a statistically significant decrease in R_p. Consistent with the present study, previous studies found that the age-related decrease in R_a was not gender dependent [2, 10].

Some inherent limitations of the present study should be noted. First, the observed subjects were in a single race over a limited age range. Second, since all subjects were asked to stare at the 3 m high ceiling, it was assumed that during all measurements the subjects were not or only minimally accommodating. Consistent with this assumption, the mean $R_a = 10.5$ mm (range: 8.97 to 11.82 mm). Third, in the present study, it was assumed that the lens is axisymmetric; however, Atchinson et al. found with MRI that the horizontal and vertical lens equatorial diameters slightly differ [2].

Table 2: Mean axial lens thickness, equatorial lens diameter, radius, and curvature of the anterior and posterior lens surfaces of each of the 79 eyes measured by 25 MHz B-scan ultrasonography.

Age (years)	Number	Axial lens thickness (mm)	Equatorial lens diameter (mm)	Anterior lens surface		Posterior lens surface	
				Radius (mm)	Curvature (mm)	Radius (mm)	Curvature (mm)
21	1	3.54	8.9	11.112	0.09	5.099	0.196
23	2	3.765	8.78	10.379	0.097	4.87	0.206
24	2	3.775	8.8	10.825	0.093	4.832	0.207
25	2	3.865	9.015	11.344	0.088	4.948	0.203
26	3	3.873	9.14	10.977	0.091	5.073	0.197
27	2	3.78	8.865	10.107	0.1	4.952	0.202
28	3	3.787	9.083	10.849	0.092	5.093	0.197
29	2	3.805	9.2	10.788	0.093	5.202	0.193
31	2	4.07	9.23	10.321	0.097	5.067	0.198
32	2	3.955	9.3	10.596	0.094	5.211	0.192
33	2	3.98	9.23	10.534	0.095	5.115	0.196
34	1	3.98	8.97	10.463	0.096	4.871	0.205
35	2	3.955	9.165	11.022	0.091	5.032	0.199
36	2	4.175	9.17	10.274	0.098	4.944	0.203
37	2	4.085	9.165	10.263	0.098	4.997	0.201
38	4	4.103	9.108	10.659	0.094	4.913	0.204
39	2	4.085	8.945	10.181	0.098	4.805	0.208
40	1	4.14	9.11	10.062	0.099	4.926	0.203
41	1	4.45	9.48	11.734	0.085	4.981	0.201
42	3	4.34	9.313	10.926	0.092	4.939	0.203
43	3	4.36	9.263	10.985	0.093	4.894	0.205
44	1	4.23	9.47	13.179	0.076	5.021	0.199
46	3	4.207	9.203	10.021	0.1	4.974	0.201
47	2	4.235	9.395	11.534	0.087	5.032	0.199
48	4	4.258	9.253	10.011	0.101	4.992	0.201
49	1	4.29	9.52	10.849	0.092	5.146	0.194
50	3	4.37	9.237	10.319	0.098	4.901	0.204
52	4	4.358	9.315	10.446	0.097	4.977	0.201
53	2	4.395	9.45	10.3	0.098	5.063	0.198
54	2	4.455	9.33	9.396	0.107	4.993	0.2
55	2	4.565	9.505	10.668	0.096	5.012	0.2
56	2	4.475	9.545	10.904	0.092	5.062	0.198
57	3	4.687	9.293	9.054	0.11	4.877	0.205
58	3	4.433	9.147	8.971	0.111	4.879	0.205
59	2	4.46	9.3	10.3	0.099	4.912	0.204
60	1	4.65	9.56	11.816	0.085	4.959	0.202

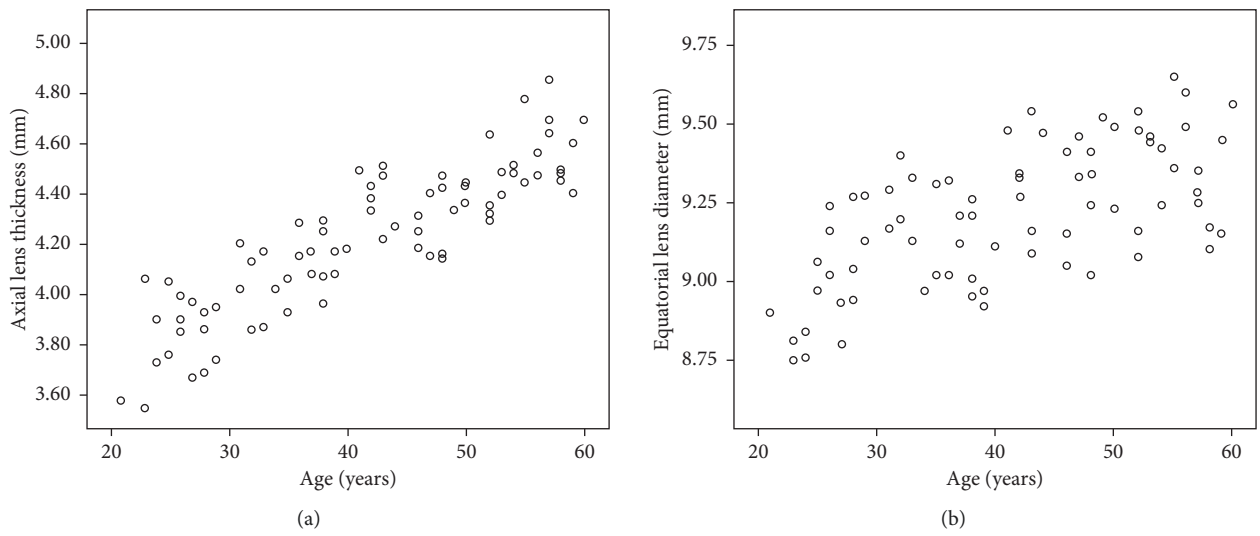

Figure 3: Continued.

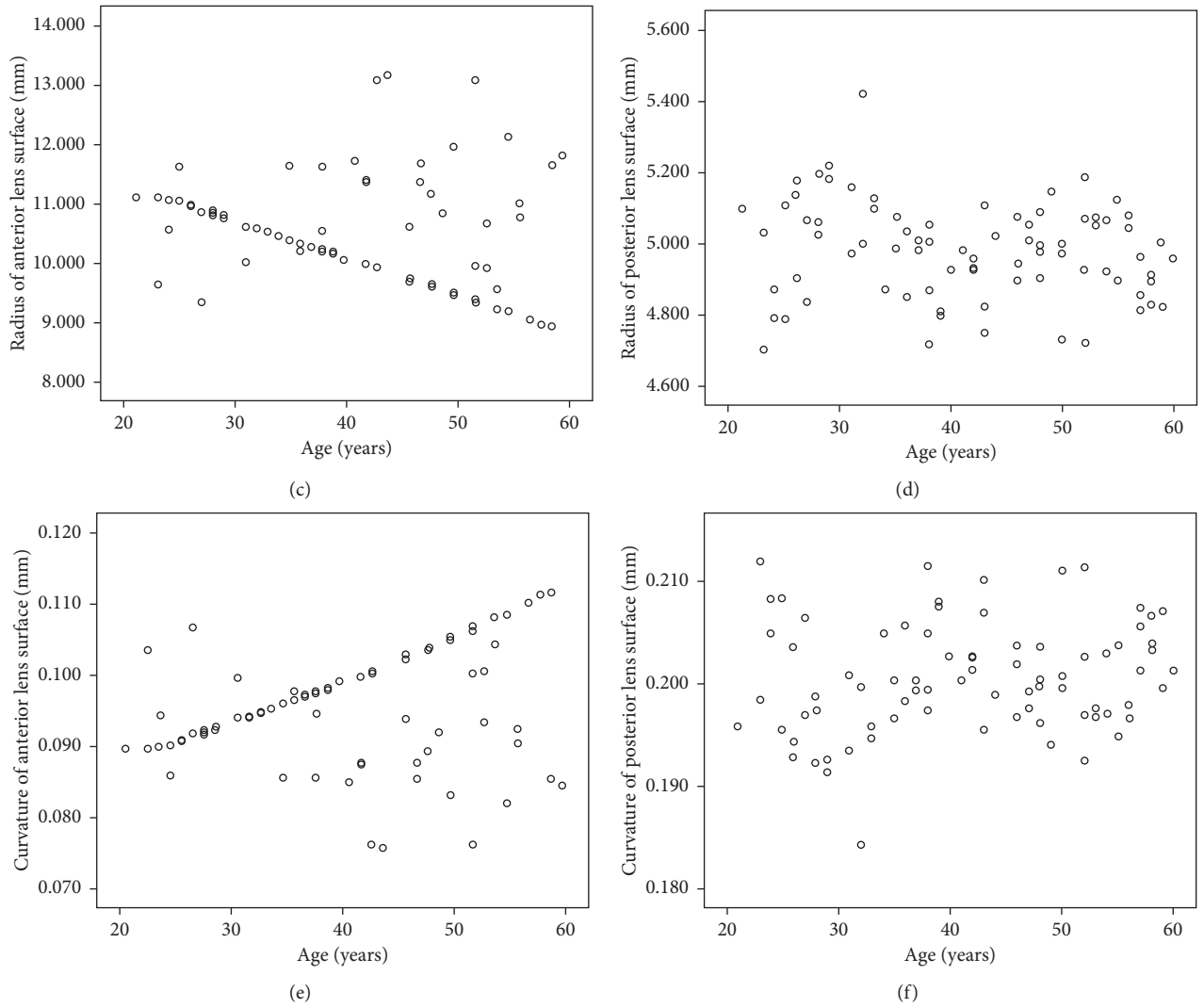

Figure 3: Scatter plots of ALT, ELD, radius, and curvature of the central anterior and posterior lens surface versus age for the entire 79 healthy left eyes using 25 MHz B-scan ultrasonography.

5. Conclusions

ALT and ELD increase with age while the R_a decreases and the R_p does not change. Gender does not appear to affect the size or contour of the lens. The age-related increase in ELD is consistent with Schachar's theory of presbyopia [11] and probably plays a role in altering the stress on the lens resulting in cortical cataracts [12].

Abbreviations

ALT: Axial lens thickness
ALT_a: Anterior portion of the axial lens thickness
ALT_p: Posterior portion of the axial lens thickness
ELD: Equatorial lens diameter
K_a: Anterior lens surface curvature
K_p: Posterior lens surface curvature
R_a: Anterior lens surface radius of curvature
R_p: Posterior lens surface radius of curvature.

Data Availability

The data used to support the findings of this study are available from the corresponding author upon request.

Ethical Approval

The study was approved by the Institutional Ethical Board of the Shanghai General Hospital, Shanghai Jiao Tong University, and adhered to the tenets of the Declaration of Helsinki.

Consent

All participating subjects signed an informed consent form.

Conflicts of Interest

The authors declare that they have no conflicts of interest.

Authors' Contributions

WX and HZ were responsible for the concept, design of the study, conducting the study, subject recruitment, data entry, data analysis, and manuscript writing. Both authors contributed to appraising and finalizing the manuscript.

References

[1] S. A. Strenk, J. L. Semmlow, L. M. Strenk, P. Munoz, J. Gronlund-Jacob, and J. K. DeMarco, "Age-related changes in human ciliary muscle and lens: a magnetic resonance imaging study," *Investigative Ophthalmology and Visual Science*, vol. 40, no. 6, pp. 1162–1169, 1999.

[2] D. A. Atchison, E. L. Markwell, S. Kasthurirangan, M. P. James, S. George, and G. S. Peter, "Age-related changes in optical and biometric characteristics of emmetropic eyes," *Journal of Vision*, vol. 8, no. 4, p. 29, 2008.

[3] S. Kasthurirangan, E. L. Markwell, D. A. Atchison, and J. M. Pope, "MRI study of the changes in crystalline lens shape with accommodation and aging in humans," *Journal of Vision*, vol. 11, no. 3, p. 19, 2011.

[4] M. Caixinha, D. A. Jesus, E. Velte, M. J. Santos, and J. B. Santos, "Using ultrasound backscattering signals and Nakagami statistical distribution to assess regional cataract hardness," *IEEE Transactions on Biomedical Engineering*, vol. 61, no. 12, pp. 2921–2929, 2014.

[5] S. Kasthurirangan, E. L. Markwell, D. A. Atchison, and J. M. Pope, "In vivo study of changes in refractive index distribution in the human crystalline lens with age and accommodation," *Investigative Opthalmology & Visual Science*, vol. 49, no. 6, pp. 2531–2540, 2008.

[6] X. Adnan, M. Suheimat, N. Efron et al., "Biometry of eyes in type 1 diabetes," *Biomedical Optics Express*, vol. 6, no. 3, pp. 702–715, 2015.

[7] A. Glasser and M. C.W. Campbell, "Biometric, optical and physical changes in the isolated human crystalline lens with age in relation to presbyopia," *Vision Research*, vol. 39, no. 11, pp. 1991–2015, 1999.

[8] R. A. Schachar, "Growth patterns of fresh human crystalline lenses measured by in vitro photographic biometry," *Journal of Anatomy*, vol. 206, no. 6, pp. 575–580, 2005.

[9] P. Smith, "Diseases of lens and capsule. 1. On the growth of the crystalline lens," *Transactions of the Ophthalmology Society of the United Kingdom*, vol. 3, pp. 79–99, 1883.

[10] M. Dubbelman and G. L. Van der Heijde, "The shape of the aging human lens: curvature, equivalent refractive index and the lens paradox," *Vision Research*, vol. 41, no. 14, pp. 1867–1877, 2001.

[11] R. A. Schachar, *The Mechanism of Accommodation and Presbyopia*, Kugler Publications, Amsterdam, The Netherlands, 2012.

[12] R. Michael, L. Pareja-Aricò, F. G. Rauscher, and R. I. Barraquer, "Cortical cataract and refractive error," *Ophthalmic Research*, vol. 62, no. 3, pp. 157–165, 2019.

Hindawi
Journal of Ophthalmology
Volume 2019, Article ID 2036192, 5 pages
https://doi.org/10.1155/2019/2036192

Research Article

An Alternative Psychophysical Diagnostic Indicator of the Aging Eye

John D. Rodriguez[1], **Garrick Wallstrom**[2], **Divya Narayanan**[1], **Donna Welch**[1] and **Mark B. Abelson**[1,3]

[1]*Ora, Inc., Andover, MA, USA*
[2]*Statistics & Data Corporation, Tempe, AZ, USA*
[3]*Harvard Medical School, Department of Ophthalmology, Boston, MA, USA*

Correspondence should be addressed to John D. Rodriguez; jrodriguez@oraclinical.com

Received 15 February 2019; Accepted 9 October 2019; Published 3 November 2019

Academic Editor: Alejandro Cerviño

Purpose. Impaired adaptation to changes in lighting levels as well as mesopic visual function is a common complaint in those over the age of 65. The use of photostress is a well-established method to test the adaption rate and the response of the visual cycle. In this study, we test visual function recovery to mesopic luminance stimuli following a long duration photostress in young and elderly subjects. If successful in strongly differentiating aging macular function, these methods may also be useful in the study of pathologies such as age-related macular degeneration. *Methods*. A group of 12 older normal subjects (mean age 75.1 ± 4.79) and a control group of 5 younger normal subjects (mean age 26.2 ± 4.19) were subjected to macular photostress using the OraLux photostress system. The OraLux system provides a diffuse light source bleaching 84% of cone photopigment while maintaining an exposure safety factor of 200 times less than the maximum safe exposure. After each photostressing session, macular recovery was tracked using a foveal, variable contrast, flickering stimulus of mean luminance in the high mesopic range. Recovery was tracked for 300 seconds. The endpoint was time to recovery to each individual's baseline sensitivity as determined by two static sensitivity trials prior to photostress. *Results*. Proportional hazards analysis of recovery time yielded a statistically significant difference between the older group and the young group (HR = 0.181; $p = 0.0289$). The estimated hazard ratio of 0.181 indicates that older subjects return to baseline at less than one-fifth the rate of younger subjects. The hazards ratio remained statistically significant after adjusting for visual acuity (HR = 0.093; $p = 0.0424$). *Conclusion*. Photostress recovery of flicker sensitivity under mesopic conditions is a strong differentiator of aging macular function. This agrees with subject-reported complaints in reduced luminance conditions after exposure to bright lights such as night driving. The qualitative similarity between the aging retina and changes in early AMD suggests that flicker recovery following photostress may be useful as a surrogate endpoint in AMD clinical trials.

1. Introduction

The use of photostress is a well-established method to test the adaption rate of the visual system and the response of the visual cycle [1, 2]. The regeneration of photopigment can be impaired either due to retinal disease [3–6] or as a normal consequence of aging [7]. In the elderly, difficulties in adaptation to changes in lighting levels as well as mesopic luminance visual function are a common quality of life complaint, particularly regarding night driving [8].

Age-related changes in the eye may arise from several sources and affect visual function. In particular, changes in the cornea and lens have strong effects on visual acuity. Age-related changes in the retina are less well studied. The use of flickering stimuli is less dependent on refractive error or straylight and is useful for this purpose [9]. The addition of photostress with a flicker endpoint is thus a possibly useful stress test for assessing the health of the aging retina.

Retinal diseases may also result in diminished robustness of the visual cycle and adaptation to changing light levels.

Both age-related macular degeneration (AMD) and diabetic retinopathy have been shown to be important examples [5, 6, 10–14]. The use of photostress in this context is as a stress test of the visual cycle analogous to the widely used cardiovascular stress test in order to more easily detect pathology in the early disease state.

Both aging and AMD have been shown to result in rod photoreceptor loss and diminished sensitivity in short wavelength (blue) photoreceptors [15, 16]. Thus, in addition to improved understanding of adaptive visual processes in the elderly, the study of the normal aging retina may yield insight into retinal disease as well.

A considerable number of studies using photostress have been reported since the initiation of this method. Studies have included both normal aging subjects [17–26] and subjects with retinal disease [5, 6, 10–14, 22]. A common difficulty of many of these studies has been inconsistency of the hardware apparatus used for the bleaching process [21]. Following the bleach process, recovery has been determined using various outcomes, most commonly recovery of visual acuity.

In recent studies, the introduction of computer-based stimuli using central foveal disks or blobs with sinusoidal time-varying flickering stimuli has permitted much greater flexibility in testing methodology [9, 27, 28]. As a stand-alone endpoint, foveal flicker sensitivity has shown declines with age in both photopic and mesopic luminance levels [9, 29]. In addition, recent studies of AMD subjects have found that computer-based methods using variable contrast flickering stimuli are a particularly useful and effective endpoint [27, 28].

The purpose of the present study is to improve the understanding of photostress recovery using a time-varying flickering stimulus in an aged population. Results are compared to a group of young subjects. Within the context of clinical trials, these results may be useful to provide control data for the clinical application of variable contrast flickering stimuli to pathological conditions such as AMD.

2. Methods

2.1. Subjects. Two groups of subjects were enrolled: young subjects (early thirties and younger) and older subjects (60 years of age and older). All subjects were recruited from a single general ophthalmology practice. All subjects provided written informed consent, and study protocols were approved by a properly constituted Institutional Review Board (Alpha IRB, San Clemente, CA). The study was conducted in accordance with the ethical principles of the Declaration of Helsinki.

All subjects provided medical and ocular history and were tested for ETDRS visual acuity at baseline and following photostress. Retinal imaging, including OCT and dilated fundus photography, was used to confirm absence of retinal disease. All subjects, young and old, were required to have no evidence or history of ocular disease or any medical condition that the investigator felt put the subject at significant risk, confounded the study results, or interfered significantly with study participation. All subjects were required to present with visual acuity of 20/25 or better in at least one eye (the study eye). If different, the eye with better visual acuity was chosen as the study eye. If both eyes were tested at equal visual acuity, the right eye was chosen as the study eye. Data were collected on all qualified eyes.

2.2. Baseline Cone Function and Recovery. Baseline retinal cone photoreceptor sensitivity was measured using a Python-based software program developed in-house for this study. A foveal, flickering sinusoidal time-varying stimulus of approximately 2° visual angle was presented on a background of luminance intensity in the upper mesopic range. The luminance range chosen was based on the earlier work of Collins and Brown in a study of an AMD population [13, 14]. The contrast between maximum stimulus brightness and background was the outcome variable. The flicker frequency of the target stimulus was based on a range chosen to bracket the sensitivity of the human visual system to this stimulus [30]. Based on previous studies of AMD subjects [27, 28], we investigated stimuli at several frequencies. The stimulus was viewed monocularly from a distance of one meter. The visual task was the subject identifying the presence of the stimulus. All subjects were first required to complete a demonstration run to ensure that each subject could properly identify the presence or absence of the stimulus based on ten trials. Subjects were required to correctly identify the presence or absence of the stimulus at least 80% of the time. The sensitivity of the subject to the stimulus was first determined before photostress as a baseline based on two trials. After assessing baseline flicker threshold, photostress was applied as described below. Recovery was measured by the subjects identifying the presence of the stimulus through the resulting afterimage. The test was terminated five minutes after exposure to the bleaching lamp. The study outcome was the time to return to baseline sensitivity. A simple staircase procedure was used to track recovery following photobleach.

During the photostress recovery process, fixation lines were presented to assist the subject in maintaining gaze on the area of the screen in which the stimulus was presented. In addition, a fixation circle of diameter corresponding to the bleaching area was presented. The subject was instructed to center the resulting afterimage within the circle.

A second measurement of ETDRS visual acuity was made following photostress testing as a safety check. In addition, subjects who had not returned to baseline after five minutes were retested one hour following photostress to confirm recovery of visual function before visit termination.

2.3. Photobleach Procedure. The photostress procedure was performed using a custom-designed full-spectrum diffused fluorescent light source (Ora LUX) [31]. The level of retinal irradiance of the Ora LUX source yields at least 84% cone photoreceptor bleach. The center of the bleaching light was aligned with the center of each subject's gaze in the vertical and horizontal directions as required. Subjects were instructed to maintain their gaze on the center of the bleaching light and to avoid squinting, but were allowed to

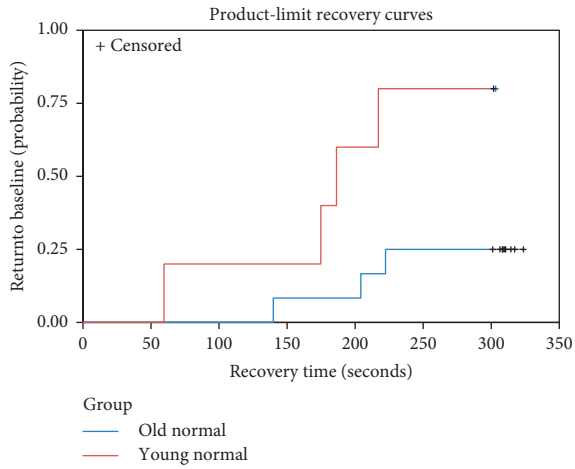

Figure 1: Kaplan–Meier recovery curves for the older group (blue) and the younger group (red).

blink normally during the procedure. Compliance by the subject was monitored by the technician. A safety analysis found that the maximum exposure level of the Ora LUX light source was 200 times less than maximum permissible exposure (at least 2000 times less actual damage level) based on accepted safety standards for thermal and photochemical mechanisms [32]. For additional safety in this sensitive group, exposure is less than 90 seconds and distance greater than 12 inches.

2.4. Statistical Methods. Unadjusted group means were compared using pooled two-sided two-sample t-tests if the folded F-test for equality of variances was not statistically significant at $\alpha = 0.05$ level; otherwise, the Satterthwaite approximation was used.

The proportion of subjects that failed to return to baseline within 5 minutes were calculated and compared between groups using Fisher's exact test. Failure rates using all qualified eyes were compared using logistic regression with a random subject factor to account for the correlation between eyes. Recovery times were analyzed using proportional hazards regression and tested using a Wald test. Proportional hazards analyses of all qualified eyes included a random subject factor. Kaplan–Meier product limit estimation was used to generate recovery time curves.

Statistical analyses were conducted using SAS 9.4, with PROC FREQ, PROC GENMOD, PROC PHREG, and PROC LIFETEST.

3. Results

3.1. Demographics and ETDRS BCVA. The mean age for the older group was 75.1 ± 4.79 years (67.0–83.3) (4M, 8F). For the young group, the mean age was 26.2 ± 4.19 years (19.5–30.0) (2M, 3F). At baseline, mean ETDRS best-corrected visual acuity for the younger group was -0.04 ± 0.055 and for the older group 0.17 ± 0.167. The group means were statistically different based on the Satterthwaite t-test ($p = 0.0017$).

3.2. Baseline Flicker Sensitivity. Mean normalized baseline flicker sensitivity (SD) was 0.11 (0.161) for the older group and 0.05 (0.026) for younger. The difference was not statistically significant, $p = 0.2077$.

3.3. Photostress Recovery. In the older group, 9 out of 12 (75%) study eyes failed to return to baseline within 5 minutes, compared to 1 out of 5 (20%) in the young group ($p = 0.1007$) (Figure 1). In the analysis of failure rates using all qualified eyes, the odds of failing to return to baseline are 1.92 in the older group compared to 0.25 in the young group (OR = 7.69; $p = 0.0203$).

The proportional hazards analysis of recovery time yielded a statistically significant difference between the older group and the young group (HR = 0.181; $p = 0.0289$). The estimated hazard ratio of 0.181 indicates that older subjects return to baseline at less than one-fifth the rate of younger subjects. Luminance ($p = 0.2093$) and frequency ($p = 0.3665$) of the stimulus were not statistically significant and were removed from the model. The hazards ratio remained statistically significant after adjusting for visual acuity (HR = 0.093; $p = 0.0424$). In the all qualified eyes analysis, the estimated hazard ratio was HR = 0.134 ($p = 0.0046$) and HR = 0.032 ($p = 0.0022$) after adjusting for visual acuity.

4. Discussion

Previous visual psychophysical-based studies of photostress recovery in both normal and AMD subjects have primarily used visual acuity recovery as an endpoint [17–26]. Various approaches have been used to apply photostress to the subject's visual system which has been identified as a significant factor in test variability [21]. The most important differentiator between these approaches has been bleaches using a photoflash stimulus of duration of several milliseconds and long-duration "equilibrium" bleach of several seconds or more [33, 34]. For bleaching cone photoreceptors, an equilibrium bleach has been shown to be preferable in order to deplete local stores of photopigment derived from the retinoid present in the Müller cells [35]. Our approach follows this methodology using a custom-designed light source (Ora Lux) to provide a bleach of at least 84% of cone photoreceptors while maintaining safe levels of exposure [31, 36].

Results of at least eight previous studies of healthy subjects over a broad range of age, based on visual psychophysical outcomes, have been published [19–26]. Six of these studies found a significantly longer mean recovery time in older subjects [19–24]. Reported recovery time of oldest to youngest subjects varied considerably from as little as 15% to over 90%. Since these studies used a recovery endpoint of visual acuity, one must be cautious in a direct comparison to the results presented here.

In early age-related macular degeneration, outer retinal metabolism is known to be compromised [37]. Since the detection of a flickering stimulus imposes a higher metabolic requirement than does a static stimulus, flicker

detects functional change at an earlier stage of the disease [38]. The variable contrast flickering stimulus investigated here was selected based on the effectiveness of showing group differences between normal and AMD subject groupings [9, 27, 28]. Based on previous results from the literature [27, 28], we have investigated several target frequencies and luminance levels. These changes are designed to provide optimal differentiation between normal and AMD groups as well as improve reliability. Sensitivity to foveal flickering stimuli has been shown to decrease with age [9]. However, in this study, mean baseline sensitivity between young and old was not found to be statistically different. Nevertheless, the addition of photostress to the baseline stimulus resulted in an increased separation between groups which was found to be significant. Since retinal changes in AMD appear to share some similarities to age-related changes, we would expect that young normal and older normal subjects should show easily detectable differences. The differences found here in this study suggest that this is the case.

5. Conclusion

In contrast to previous studies on photostress in normal subjects, in which recovery endpoints based on visual acuity were used, the recovery endpoint used here is a flickering foveal blob presented on a computer screen with mesopic luminance background. Unlike visual acuity, this endpoint is particularly useful for assessing the health of the aging retina due to its relative insensitivity to defects in the ocular media. The combination of photostress and flicker constitute a retinal stress test which also stresses the visual cycle and retinal metabolism. We find that using a mesopic flicker recovery target followed by our high bleach photostress system strongly differentiates aging macular function. Inconsistent and nonstandardization of the bleach process used in previous studies has been found to result in high variability in outcomes [21]. The use of a consistent bleaching process in this study, bleaching a high percentage of cone photoreceptors (84%), should allow for reduced variability and more efficient clinical trials. Moreover, the flicker endpoint described here extends previous work by incorporating reduced luminance background. This is in accord with well-known difficulties reported by both AMD and older normal subjects under mesopic luminance levels. This study shows that a flicker target with high bleach photostress methodology is sensitive to the retina/macular changes that occur as a result of age. Perhaps this same methodology would differentiate between age-related retinal changes and retinal changes due to AMD. In clinical trials, visual function endpoints, such as the variable contrast flickering endpoint may provide a useful supplement to current endpoints in studies of early AMD.

Data Availability

The data used in this study are contained in the supplementary data file.

Conflicts of Interest

JR, DW, DN, and MA are employees of Ora, Inc. GW is an employee of Statistics and Data Corp and has no conflicts of interest regarding the publication of this paper.

Acknowledgments

This study was funded by Ora, Inc.

Supplementary Materials

The data used in this study are contained in the supplementary data file. The data are organized with one subject eye per row. The columns are as follows: ID: subject ID number; age: subject age in years; age group: young for age <31.0 and older for age ≥60.0; gender: F for female and M for male, SEYE: subject study eye; OD or OS QEYE: subject qualifying eye(s); OD, OS, or OU EYE: subject eye tested; OD or OS lum: luminance of stimulus; 30 or 60 freq: frequency of stimulus; 4, 14, or 30 Hz baseThr: nonnormalized baseline threshold; baseline_Fflicker: normalized baseline threshold; return_time: time to return to baseline; blank for eyes that do not return to baseline within the allotted time; time_last: last stimulus time; ETDRS: ETDRS (logMAR). (*Supplementary Materials*)

References

[1] P. Bailliart, "General review of the pathology of the retina," *Bulletin Des Sociétés D'ophtalmologie de France*, vol. 6, pp. 501–509, 1954.

[2] H. Magder, "Test for central serous retinopathy based on clinical observations and trial," *American Journal of Ophthalmology*, vol. 49, no. 1, pp. 147–150, 1960.

[3] G. A. Chilaris, "Recovery time after macular illumination as a diagnostic and prognostic test," *American Journal of Ophthalmology*, vol. 53, no. 2, pp. 311–314, 1962.

[4] H. Forsius, A. W. Eriksson, and U. Krause, "The dazzling test in diseases of the retina," *Acta Acta Ophthalmologica*, vol. 42, no. 1, pp. 55–63, 1964.

[5] K. Frost-Larsen and H. W. Larsen, "Macular recovery time recorded by nyctometry—a screening method for selection of patients who are at risk of developing proliferative diabetic retinopathy. Results of a 5-year follow-up," *Acta Ophthalmologica Supplement*, vol. 173, pp. 39–47, 1985.

[6] G. Wu and J. J. Weiter, S. Santos, L. Ginsburg, R. Villalobos, The macular photostress test in diabetic retinopathy and age-related macular degeneration," *Archives of Ophthalmology*, vol. 108, no. 11, pp. 1556–1558, 1990.

[7] G. R. Jackson, C. Owsley, and G. McGwin Jr., "Aging and dark adaptation," *Vision Research*, vol. 39, no. 23, pp. 3975–3982, 1999.

[8] D. W. Kline, T. J. B. Kline, J. L. Fozard, W. Kosnik, F. Schieber, and R. Sekuler, "Vision, aging, and driving: the problems of older drivers," *Journal of Gerontology*, vol. 47, no. 1, pp. P27–P34, 1992.

[9] W. Bi, H. Gillespie-Gallery, A. Binns, and J. L. Barbur, "Flicker sensitivity in normal aging-monocular tests of retinal function at photopic and mesopic light levels," *Investigative Opthalmology & Visual Science*, vol. 57, no. 2, pp. 387–395, 2016.

[10] M. A. Sandberg and A. R. Gaudio, "Slow photostress recovery and disease severity in age-related macular degeneration," *Retina*, vol. 15, no. 5, pp. 407–412, 1995.

[11] A. M. Binns and T. H. Margrain, "Evaluating retinal function in age-related maculopathy with the ERG photostress test," *Investigative Opthalmology & Visual Science*, vol. 48, no. 6, pp. 2806–2813, 2007.

[12] E. Midena, C. Degli Angeli, M. C. Blarzino, M. Valenti, and T. Segato, "Macular function impairment in eyes with early age-related macular degeneration," *Investigative Ophthalmology & Visual Science*, vol. 38, no. 2, pp. 469–477, 1997.

[13] M. Collins and B. Brown, "Glare recovery and its relation to other clinical findings in age related maculopathy," *Clinical Vision Sciences*, vol. 4, no. 2, pp. 155–163, 1989.

[14] M. Collins and B. Brown, "Glare recovery and age related maculopathy," *Clinical Vision Sciences*, vol. 4, no. 2, pp. 145–153, 1989.

[15] C. A. Curcio, N. E. Medeiros, and C. L. Millican, "Photoreceptor loss in age-related macular degeneration," *Investigative Ophthalmology and Visual Science*, vol. 37, no. 7, pp. 1236–1249, 1996.

[16] C. A. Johnson, A. J. Adams, J. D. Twelker, and J. M. Quigg, "Age-related changes in the central visual field for short-wavelength-sensitive pathways," *Journal of the Optical Society of America A*, vol. 5, no. 12, pp. 2131–2139, 1988.

[17] D. Messenio, G. Marano, S. Gerosa, F. Iannelli, and E. M. Biganzoli, "The influence of age on the recovery of the ERG photostress test," *Documenta Ophthalmologica*, vol. 126, no. 2, pp. 87–97, 2013.

[18] S. L. Severin, C. Harper Jr., and J. F. Culver, "Photostress test for the evaluation of macular function," *Archives of Ophthalmology*, vol. 70, no. 5, pp. 593–597, 1963.

[19] H. Forsius, U. Krause, and A. Eriksson, "Dazzling test in central serous retinopathy," *Acta Ophthalmologica*, vol. 42, no. 1, pp. 25–32, 1964.

[20] J. V. Lovasik, "An electrophysiological investigation of the macular photostress test," *Investigative Ophthalmology & Visual Science*, vol. 24, no. 4, pp. 437–441, 1983.

[21] T. H. Margrain and D. Thomson, "Sources of variability in the clinical photostress test," *Ophthalmic and Physiological Optics*, vol. 22, no. 1, pp. 61–67, 2002.

[22] D. A. Newsome and M. Negreiro, "Reproducible measurement of macular light flash recovery time using a novel device can indicate the presence and worsening of macular diseases," *Current Eye Research*, vol. 34, no. 2, pp. 162–170, 2009.

[23] F. Gomez-Ulla, O. Louro, and M. Mosquera, "Macular dazzling test on normal subjects," *British Journal of Ophthalmology*, vol. 70, no. 3, pp. 209–213, 1986.

[24] S. L. Severin, R. L. Tour, and R. H. Kershaw, "Macular function and the photostress test 1," *Archives of Ophthalmology*, vol. 77, no. 1, pp. 2–7, 1967.

[25] J. S. Glaser, P. J. Savino, K. D. Sumers, S. A. Mcdonald, and R. W. Knighton, "The photostress recovery test in the clinical assessment of visual function," *American Journal of Ophthalmology*, vol. 83, no. 2, pp. 255–260, 1977.

[26] P. G. Sloan, "Clinical application of the photostress test," *American Journal of Optometry and Archives of American Academy of Optometry*, vol. 45, no. 9, pp. 617–623, 1968.

[27] P. N. Dimitrov, L. D. Robman, M. Varsamidis et al., "Visual function tests as potential biomarkers in age-related macular degeneration," *Investigative Opthalmology & Visual Science*, vol. 52, no. 13, pp. 9457–9469, 2011.

[28] P. N. Dimitrov, L. D. Robman, M. Varsamidis et al., "Relationship between clinical macular changes and retinal function in age-related macular degeneration," *Investigative Opthalmology & Visual Science*, vol. 53, no. 9, pp. 5213–5220, 2012.

[29] C. B. Y. Kim and M. J. Mayer, "Foveal flicker sensitivity in healthy aging eyes II cross-sectional aging trends from 18 through 77 years of age," *Journal of the Optical Society of America A*, vol. 11, no. 7, pp. 1958–1969, 1994.

[30] H. de Lange Dzn, "Research into the dynamic nature of the human fovea → cortex systems with intermittent and modulated light I attenuation characteristics with white and colored light," *Journal of the Optical Society of America*, vol. 48, no. 11, pp. 777–784, 1958.

[31] J. Rodriguez, K. Lane, D. Hollander et al., "Cone photoreceptor macular function and recovery after photostress in early non-exudative age-related macular degeneration," *Clinical Ophthalmology*, vol. 12, pp. 1325–1335, 2018.

[32] F. C. Delori, R. H. Webb, and D. H. Sliney, "Maximum permissible exposures for ocular safety (ANSI 2000), with emphasis on ophthalmic devices," *Journal of the Optical Society of America A*, vol. 24, no. 5, pp. 1250–1265, 2007.

[33] M. Hollins and M. Alpern, "Dark adaptation and visual pigment regeneration in human cones," *The Journal of General Physiology*, vol. 62, no. 4, pp. 430–447, 1973.

[34] A. Wood, T. Margrain, and A. Binns, "The effect of bleach duration and age on the ERG photostress test," *Graefe's Archive for Clinical and Experimental Ophthalmology*, vol. 249, no. 9, pp. 1359–1365, 2011.

[35] J.-S. Wang and V. J. Kefalov, "The cone-specific visual cycle," *Progress in Retinal and Eye Research*, vol. 30, no. 2, pp. 115–128, 2011.

[36] W. A. H. Rushton and G. H. Henry, "Bleaching and regeneration of cone pigments in man," *Vision Research*, vol. 8, no. 6, pp. 617–631, 1968.

[37] E. Stefánsson, Á. Geirsdóttir, and H. Sigurdsson, "Metabolic physiology in age related macular degeneration," *Progress in Retinal and Eye Research*, vol. 30, no. 1, pp. 72–80, 2011.

[38] J. A. Phipps, T. M. Dang, A. J. Vingrys, and R. H. Guymer, "Flicker perimetry losses in age-related macular degeneration," *Investigative Opthalmology & Visual Science*, vol. 45, no. 9, pp. 3355–3360, 2004.

Hindawi
Journal of Ophthalmology
Volume 2019, Article ID 3567813, 9 pages
https://doi.org/10.1155/2019/3567813

Research Article

Distribution of Choroidal Thinning in High Myopia, Diabetes Mellitus, and Aging: A Swept-Source OCT Study

Francisco de Asís Bartol-Puyal,[1,2] **Carlos Isanta**,[1,2] **Óscar Ruiz-Moreno**,[1,2,3] **Beatriz Abadia**,[2] **Pilar Calvo**,[1,2] **and Luis Pablo**[1,2,3]

[1]*Ophthalmology Department, Miguel Servet University Hospital, Zaragoza, Spain*
[2]*Ophthalmology Innovative and Research Group (GIMSO), Aragón Institute for Health Research (IIS Aragón), Zaragoza, Spain*
[3]*University of Zaragoza, Zaragoza, Spain*

Correspondence should be addressed to Francisco de Asís Bartol-Puyal; franbarpuy@hotmail.com

Received 26 February 2019; Accepted 29 July 2019; Published 15 August 2019

Guest Editor: Hema Radhakrishnan

Purpose. To compare the macular choroidal thinning between young healthy, aged healthy, young high myopic, and aged type 2 diabetic (T2D) patients using the Early Treatment Diabetic Retinopathy Study (ETDRS) grid and three-dimensional (3D) maps. *Methods*. A prospective study including 102 eyes of 51 healthy young subjects, 60 eyes of 30 healthy aged subjects, 24 eyes of 12 high myopic patients, and 110 eyes of 55 T2D patients. Choroidal thickness (CT) was examined with swept-source optical coherence tomography Triton DRI (Topcon Corporation, Tokyo, Japan). The choroid was automatically segmented using the software algorithm, and mean CT values of a 6×6 mm macular cube were exported. 3D maps were created to represent CT, and its values were compared using the ETDRS grid. *Results*. Mean age was 27.31 ± 3.95, 66.41 ± 7.54, 27.69 ± 3.89, and 66.48 ± 7.59 years in young healthy, aged healthy, young high myopic, and T2D patients, respectively. CT was not shown to be uniform, as superior and central zones were thicker. All ETDRS sectors were always thicker ($p < 0.05$) in young healthy individuals than in the others. It was found that the choroidal sector which got thinner was inferior in case of age (103.28 μm decrease), inferior-nasal in high myopia (86.19 μm decrease), and temporal in T2D (55.57 μm decrease). In addition, the choroid got thinner in those regions where it was thicker in healthy subjects. *Conclusions*. 3D maps allow a further comprehension of choroidal changes. The choroidal pattern in young healthy individuals resembles a mountain range; with age, a mountain peak; in high myopia, an inverted gorge; and in aged T2D, gathered hills. Not all choroidal regions are affected in a similar way, as it depends on the pathology. The thicker the zone is in healthy subjects, the thinner it becomes with any pathology.

1. Introduction

With the advent of optical coherence tomography (OCT) technology, the choroid has been precisely visualized for the past few years. It has been proved to play an important role in different retinal disorders such as myopia, central serous chorioretinopathy, and age-related macular degeneration. Quantitative assessment of the choroid has allowed new research findings to differentiate normal from pathological processes within the choroid. It is known that choroidal thickness (CT) varies with age [1–3], axial length (AL) [4–7], day time [8–10], and race [11]. A choroidal thinning has been found in pathologies such as myopia [12] and diabetes mellitus [13–15], and a relevant thickening has been found in the pachychoroid spectrum, which includes the polypoidal choroidal vasculopathy [16].

Swept-source OCT (SS-OCT) is the last generation of OCT, and it uses a laser source of a longer wavelength (1050 nm) which penetrates deeper in the retinal and choroidal tissues than conventional laser sources used in previous spectral-domain OCT devices [17].

SS-OCT provides retinal and choroidal macular thickness geographically displayed as a false-color topographic map, and it is numerically reported as averages in each of the nine regions defined by the Early Treatment Diabetic Retinopathy Study (ETDRS) [11]. The ETDRS grid includes a

central disc of 500 μm of diameter (foveal region) and an inner and an outer ring; each one was divided into four quadrants, with a diameter of 3000 μm and 6000 μm, respectively. This grid is used for quantitative evaluations of either retinal or choroidal thickness.

This study aimed to evaluate the distribution of choroidal thinning in high myopia, diabetes mellitus, and aging using the classic ETDRS grid from SS-OCT and a new different mapping.

2. Methods

2.1. Sample Selection. Over a 2-year duration (from November 2015 to November 2017), we performed a cross-sectional SS-OCT study on four different groups of patients: young healthy subjects (group 1), senior healthy subjects (group 2), young high-myopic patients (group 3), and patients with type 2 diabetes mellitus (T2D) (group 4). All patients underwent a complete ophthalmic evaluation at the Miguel Servet University Hospital in Zaragoza, Spain. The study protocol adhered to the tenets of the Declaration of Helsinki and was approved by the Institutional Review Board (Clinical Research Ethics Committee of Aragón (CEICA)).

Exclusion criteria were a race different from Caucasian, any ocular pathology or previous treatment, amblyopia, endocrine or neurological diseases, cancer history, corticosteroids, and immunosuppressive drugs.

Group 1 included young healthy volunteers between 18 and 35 years old and with an AL ≤ 25 mm. Group 2 included senior healthy volunteers between 55 and 75 years old and with an AL ≤ 25 mm. Group 3 included young healthy patients between 18 and 35 years old but with an AL ≥ 25 mm. Group 4 included T2D patients between 55 and 75 years old, with mild or moderate diabetic retinopathy (DR), without macular oedema and without any previous ophthalmological treatment. Healthy individuals' medical records were examined in order to verify that all of them had no systemic illnesses. T2D patients were diagnosed after the criteria of the American Diabetes Association, and all of them were negative for anti-glutamic acid decarboxylase antibodies.

2.2. Study Protocol. Patients underwent a deep ophthalmological examination which included best-corrected visual acuity (BCVA), refraction, slit-lamp examination, intraocular pressure (IOP) with Goldmann applanation tonometry, optical biometry (IOLMaster 500, Carl Zeiss Meditec, Jena, Germany), indirect funduscopy, and SS-OCT Triton Deep Range Image (Topcon Corporation, Tokyo, Japan).

SS-OCT scans were acquired through dilated pupils at the same day time and by an experienced technician. A macular 6 × 6 mm three-dimensional (3D) cube centered on the fovea was analysed three times, but only the best examination was selected for the analysis. Scans with low quality (<40/100), motion artifacts, or decentration were discarded. The choroidal segmentation was automatically performed using the on-board device software. In case of segmentation errors, manual corrections of individual *A*-scans were performed to fit the choroidal boundaries (from the outer edge of the hyper-reflective retinal pigment epithelial line to the inner edge of the sclera).

In every OCT image, the ETDRS grid was centered on the fovea, and measurements of the nine choroidal subfields were obtained and compared between groups.

Besides the classic ETDRS grid, a fovea-centered map composed of 30 × 30 cubes was generated with automatic measurements of CT. This map comprised 900 200 × 200 μm cubes. Mean CT in every cube was exported and analysed. The left eyes were converted into the right eye format.

As a reference, young healthy subjects' choroid (group 1) was divided into different zones according to the mean CT in every macular cube (Figure 1). Zone 1 included those macular points with a CT between 215 and 239 μm, zone 2 between 240 and 264 μm, zone 3 between 265 and 290 μm, zone 4 between 290 and 314 μm, and zone 5 between 315 and 340 μm. The 5 zones were then divided into nasal and temporal, obtaining a total of 10 measurements. The mean CT of equivalent zones was calculated and compared between groups.

The two-dimensional (2D) maps of the four study groups were created with Microsoft Word (Microsoft Corporation), and Microsoft Excel (Microsoft Corporation) was used for the three-dimensional (3D) maps.

2.3. Statistical Analysis. Statistical analyses were performed using IBM SPSS (version 23.0; IBM Corporation, Somers, NY, USA) statistical software. All variables followed a normal distribution as verified by the Kolmogorov–Smirnov test. A two-tailed Student's *t*-test was used to compare CT between groups using both the classic ETDRS grid (9 regions) and the new choroidal distribution (10 regions). In case of comparisons involving group 3, a Mann–Whitney *U* test was performed due to the insufficient number of cases. For all analyses, $p < 0.05$ was considered as statistically significant.

2.4. Demographics. We enrolled 102 eyes of 51 healthy young subjects (group 1), 60 eyes of 30 healthy aged subjects (group 2), 24 eyes of 12 high-myopic patients (group 3), and 110 eyes of 55 aged patients with diabetes mellitus type 2 (group 4) with mild or moderate diabetic retinopathy and without macular oedema. Mean age outcomes in the four study groups are displayed in Table 1. There were no differences between mean ages of groups 1 (young healthy) and 3 (young myopic) ($p = 0.79$) and between groups 2 (aged healthy) and 4 (aged diabetic) ($p = 0.09$). There were no differences between the best-corrected visual acuity between groups 1 and 3 ($p = 0.97$), but there were between groups 2 and 4 ($p < 0.001$). There were no differences regarding intraocular pressure between groups 1 and 3 ($p = 0.83$), between 2 and 4 ($p = 0.14$), and between 1 and 2 ($p = 0.08$). There were differences in AL between groups 1 and 3 ($p < 0.001$), but

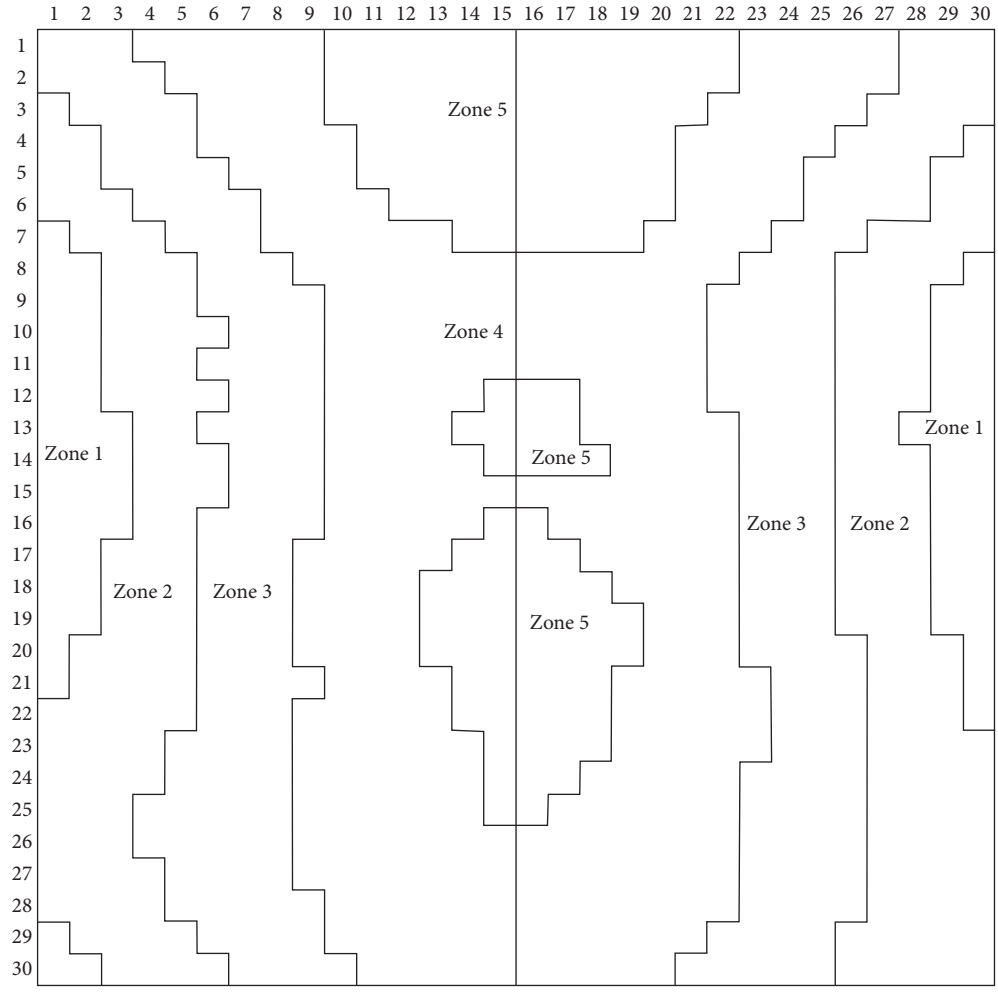

Zone 1	Choroidal thickness: 215–239 μm
Zone 2	Choroidal thickness: 240–264 μm
Zone 3	Choroidal thickness: 265–289 μm
Zone 4	Choroidal thickness: 290–314 μm
Zone 5	Choroidal thickness: 315–340 μm

Figure 1: Choroidal zones in group 1 (young healthy individuals).

Table 1: Demographic and general ophthalmological factors.

	Group 1 (young healthy)	Group 2 (senior healthy)	Group 3 (young high myopic)	Group 4 (senior T2 DM)
Age (years)	27.31 ± 3.95	66.41 ± 7.54	27.69 ± 3.89	66.48 ± 7.59
BCVA (decimal scale)	0.99 ± 0.07	0.89 ± 0.13	0.99 ± 0.03	0.75 ± 0.23
IOP (mmHg)	16.07 ± 2.38	16.09 ± 2.56	16.81 ± 3.01	16.76 ± 2.96
AL (mm)	23.68 ± 0.73	23.97 ± 1.39	25.83 ± 0.70	23.21 ± 0.92
Number of eyes (patients)	102 (51)	60 (30)	24 (12)	110 (55)

BCVA = best-corrected visual acuity; IOP = intraocular pressure; AL = axial length.

there were not between groups 1 and 2 ($p = 0.33$) and between groups 2 and 4 ($p = 0.17$).

3. Results

3.1. Choroidal Measurements. Average CT values are displayed in Table 2. When evaluating choroid with the ETDRS grid, the thickest choroid was found in the inner temporal (317.65 ± 72.30 μm), inner superior (240.35 ± 62.92 μm), outer superior (247.78 ± 61.79 μm), and inner superior (191.68 ± 76.31 μm) sectors in groups 1, 2, 3, and 4, respectively. When evaluating choroid with the new choroidal division, the thickest choroid was found in zone 5 nasal (320.93 ± 67.90 μm), zone 5 temporal (236.51 ± 60.98 μm), zone 5 temporal (250.50 ± 56.96 μm), and zone 5 temporal (189.76 ± 66.24 μm) in groups 1, 2, 3, and 4, respectively.

Table 2: Choroidal thickness using the ETDRS grid.

ETDRS sector	Young healthy (group 1)		Aged healthy (group 2)		Young myopic (group 3)		Aged diabetic (group 4)	
	Mean (μm)	SD	Mean (μm)	SD	Mean (μm)	SD	Mean (μm)	SD
Center	315.73	37.12	237.75	68.57	239.00	60.30	186.24	69.89
Inner temporal	317.65	72.30	231.30	62.62	246.10	60.85	175.73	67.17
Inner superior	309.11	68.58	240.35	62.92	240.79	60.04	191.68	76.31
Inner nasal	285.95	70.71	218.63	70.19	201.57	59.60	173.82	75.09
Inner inferior	317.22	73.91	219.31	65.44	231.03	62.13	174.61	68.70
Outer temporal	300.63	70.89	212.80	56.27	240.70	58.47	160.24	59.38
Outer superior	312.02	67.68	235.46	63.92	247.78	61.79	185.55	68.34
Outer nasal	224.53	68.67	169.29	70.70	150.73	51.19	137.06	71.78
Outer inferior	302.42	74.12	199.13	62.81	228.59	56.20	160.28	63.21
Sector of the new division								
Zone 1 nasal	234.71	93.06	169.33	73.10	175.31	77.57	137.57	71.43
Zone 1 temporal	232.19	80.77	170.32	66.48	184.43	79.29	137.93	62.21
Zone 2 nasal	255.33	87.33	178.05	66.33	189.50	69.62	142.66	64.57
Zone 2 temporal	253.88	75.41	181.00	63.64	196.54	70.98	141.28	59.14
Zone 3 nasal	279.29	70.04	196.30	62.86	206.77	64.19	154.60	64.39
Zone 3 temporal	277.77	71.42	198.19	62.05	214.47	62.26	155.73	60.61
Zone 4 nasal	304.85	71.60	217.00	59.71	229.41	57.96	172.11	64.49
Zone 4 temporal	303.68	66.63	218.29	60.37	235.26	56.23	174.23	62.90
Zone 5 nasal	320.93	67.90	234.10	59.93	246.21	58.39	185.62	66.61
Zone 5 temporal	320.92	67.37	236.51	60.98	250.50	56.96	189.76	66.24

Table 3: Choroidal thickness comparison between groups.

ETDRS region	Groups 1-2		Groups 1–3		Groups 2–4	
	CT reduction (μm)	p	CT reduction (μm)	p	CT reduction (μm)	p
Center	77.98	<0.001	76.73	<0.001	51.52	<0.001
Inner temporal	86.36	<0.001	71.54	<0.001	55.57	<0.001
Inner superior	68.77	<0.001	68.32	<0.001	48.66	<0.001
Inner nasal	67.30	<0.001	84.38	<0.001	44.81	<0.001
Inner inferior	97.89	<0.001	86.19	<0.001	44.70	<0.001
Outer temporal	87.83	<0.001	52.93	<0.001	52.56	<0.001
Outer superior	76.58	<0.001	64.25	<0.001	49.91	<0.001
Outer nasal	55.25	<0.001	73.80	<0.001	32.22	<0.001
Outer inferior	103.28	<0.001	73.83	<0.001	38.85	<0.001
Sector of the new division						
Zone 1 nasal	65.38	<0.001	59.40	<0.001	31.76	<0.001
Zone 1 temporal	61.88	<0.001	47.76	<0.001	32.38	<0.001
Zone 2 nasal	77.27	<0.001	65.83	<0.001	35.39	<0.001
Zone 2 temporal	72.89	<0.001	57.34	<0.001	39.72	<0.001
Zone 3 nasal	82.99	<0.001	72.52	<0.001	41.69	<0.001
Zone 3 temporal	79.57	<0.001	63.29	<0.001	42.47	<0.001
Zone 4 nasal	87.85	<0.001	75.44	<0.001	44.89	<0.001
Zone 4 temporal	85.39	<0.001	68.42	<0.001	44.05	<0.001
Zone 5 nasal	86.83	<0.001	74.71	<0.001	48.48	<0.001
Zone 5 temporal	84.40	<0.001	70.42	<0.001	46.76	<0.001

Table 3 shows the CT comparison between groups using ETDRS and the new division. CT was always significantly thicker ($p < 0.01$) in group 1 (young healthy) than in groups 2 and 3. Group 2 (aged healthy) always showed to have a thicker choroid ($p < 0.02$) than group 4 (aged diabetic). p values are shown in Table 3 too.

For a better understanding, Figure 2 shows a visual representation of the thinning using the ETDRS grid. In this figure, the darker, the more the choroid gets thinned.

3.2. Choroidal Maps Using the New Choroidal Division. Figure 3 shows a colored 2D representation of CT in the four study groups. Black lines were drawn following the results in group 1 (young healthy) to allow an easier comparison. Figure 4 shows a 3D representation of CT in the four study groups. It does not represent the real choroidal shape, as it is just a mathematical representation of its thickness on a flat surface. Nevertheless, the combination of these 2D and 3D maps allows better and easier understanding and visual comparison.

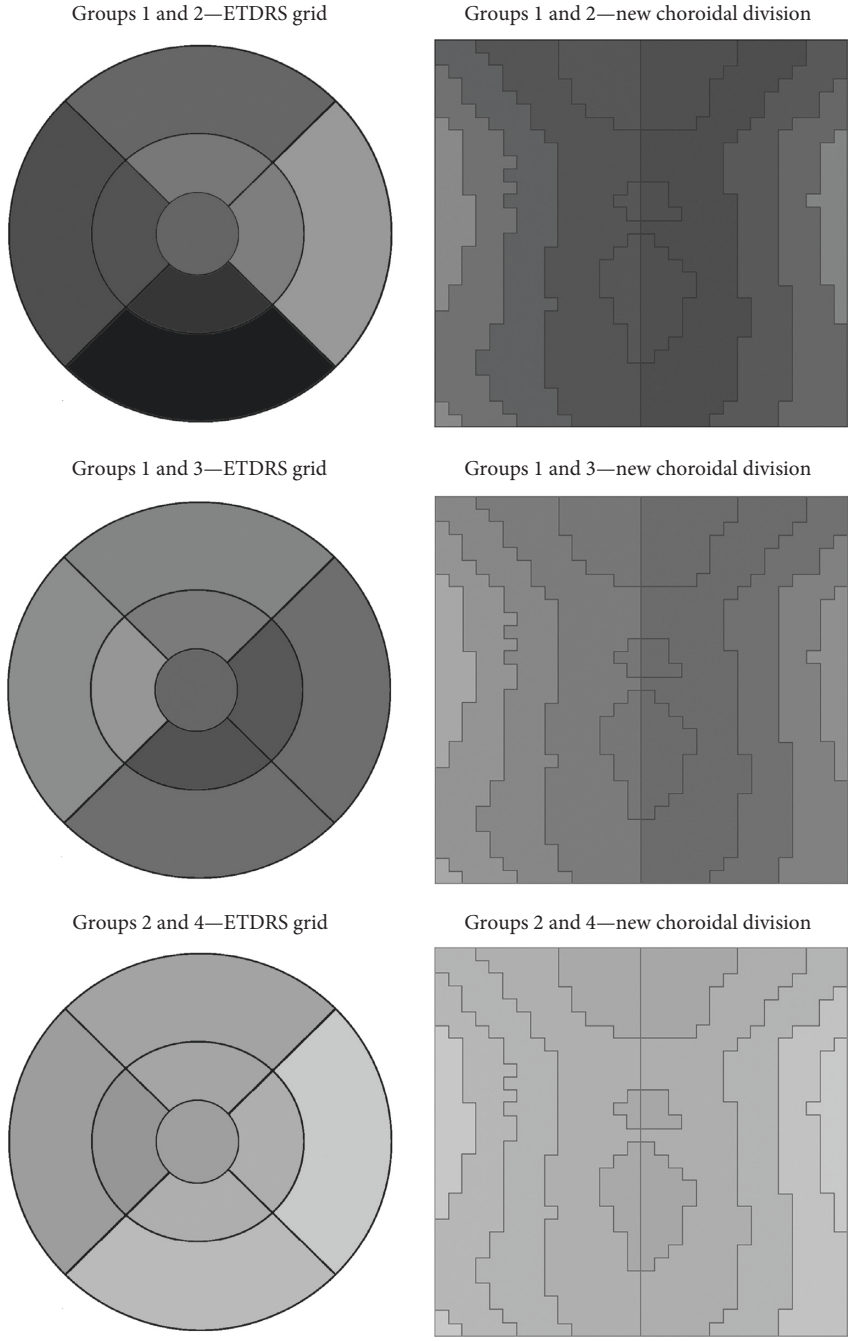

Figure 2: Mean choroidal thinning.

The thickest choroidal region was always superocentral to the fovea, showing a kind of ellipsoid shape. In young healthy individuals (group 1), it resembled a mountain range with its peaks and the valleys at both sides. In case of the other groups, the choroid tended to be flatter and the pattern was not always preserved. The aged healthy group (number 2) showed a higher reduction of CT in the inferior side, resulting in a choroidal pattern which resembled a single mountain peak. Something different happened with the young myopic patients (group 3), whose CT pattern stayed similar to the young healthy patients (group 1) but with a remarkable choroidal thinning on nasal and temporal sides. It resembled an inverted gorge. Finally, aged diabetic patients (group 4) showed to have the flattest choroid and its pattern was close to aged healthy patients' one (group 2), but instead of mountain peak, it was more similar to gathered hills.

4. Discussion

A thin choroid has been associated with ocular and systemic disorders, and sometimes can be useful in the differential diagnostic of some pathologies, such as between age-related macular degeneration and polypoidal choroidal vasculopathy

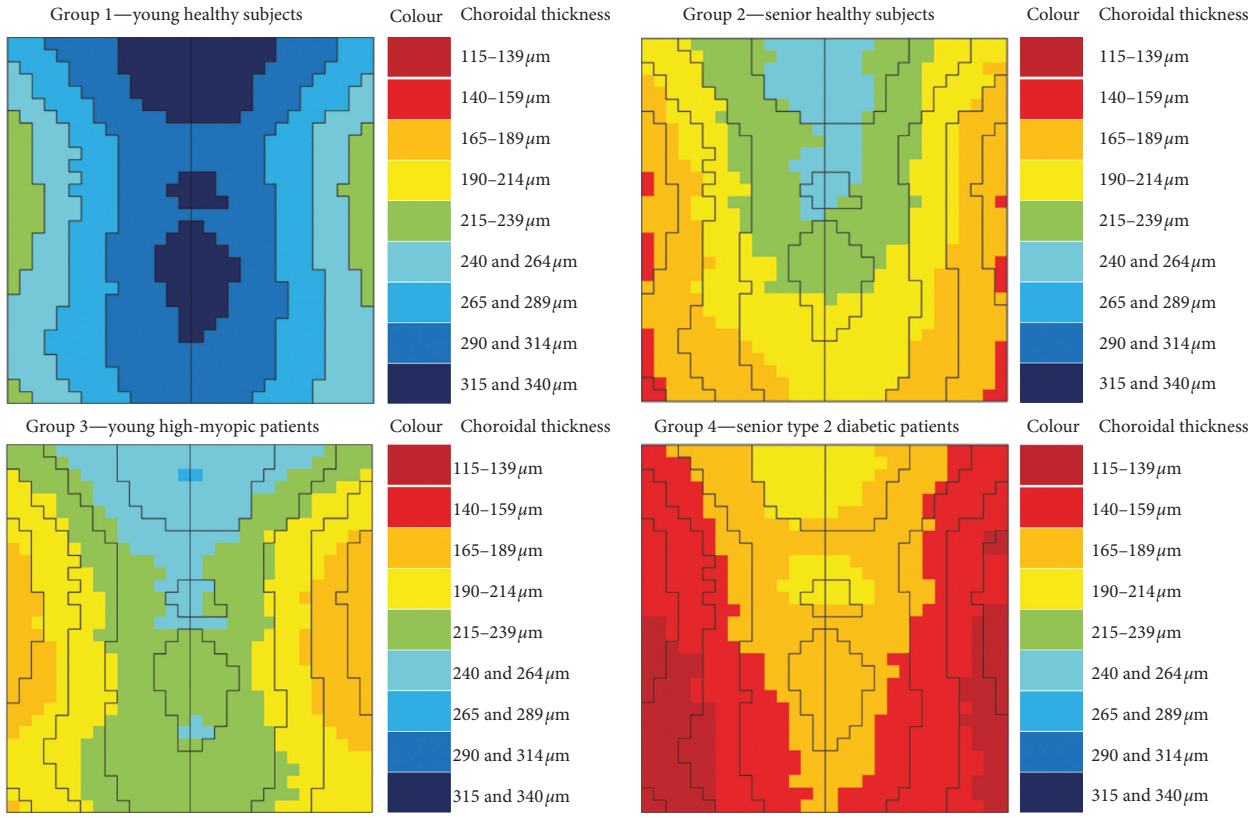

Figure 3: Two-dimensional representation of choroidal thickness.

[16]. One of the SS-OCT used so far for a deep comprehensive choroidal study has been Triton DRI. Its repeatability and reliability have been proved in healthy patients [18, 19] and in choroid-thickness thinning pathologies [20]. It gives similar measurements to the Zeiss Cirrus HD-OCT [21] (Carl Zeiss) although results should not be interchangeable [18]. It has been stated that automatic measurements reduce variability [22] although there is still little possibility of scan artifacts [23].

The most commonly used pattern is the ETDRS grid, as it is in retina, too. Nevertheless, the composition and functions of choroid has nothing to do with the ones of retina and its thickness does not follow the same pattern [5, 6, 12]. Although retinal thickness is not the same among ETDRS sectors, it does not differ too much [24], and that is why the ETDRS grid is an adequate useful pattern, whereas it might not be for choroid. However, no choroidal division has been proposed so far.

Choroid has usually been analysed with the ETDRS grid or with horizontal lines. At a first glance, the overall thickness map does not differ too much from the ones already published and mean CT values are similar, too. Some authors have described higher values of CT in superior parts [5, 6, 25] and the lowest in the outer macula area [5, 6, 26, 27], as well as we have. The fact of having analysed together right and left eyes should not have biased our study, as already stated by Chen et al. [28].

Shin et al. tried to make a choroidal map using radial OCT scans of the choroid and with the ETDRS grid, but they used a SD-OCT [26], and so the exact thickness values may differ. In our study, we found that the thickest choroid was always located in the superocentral area and the thinnest in temporal and nasal zones. With choroidal-thinning pathologies, the resulting CT map tends to be rather flat. However, the choroidal pattern differs depending on the pathology. Young healthy individuals show a mountain range pattern; aged healthy subjects, a mountain peak pattern; young high myopic, an inverted gorge pattern; and aged diabetic patients a gathered hills pattern, as displayed in Figures 3 and 4. This is why a 3D representation of CT has an importance, as it gives more information than ETDRS values alone.

The thickness range of 25 μm for every color range in our maps is acceptable, as it is higher than the possible internal variation of the OCT but not so high that it remained unaltered with affecting pathologies. Rahman et al. stated that a manually measured change greater than 23 μm in the subfoveal field may represent choroidal change when using SD-OCT with enhanced depth imaging (EDI) and manual measuring [22].

Although all the choroid and its sectors get significantly thinner with age, not all the sectors become equally affected. Bafiq et al. studied CT variation with age using manual measurements, and they found that the central choroidal thickness increased with age, the most thinned sector was the nasal outer one, and the second most thinned was the inferior ones, what differs to some extent to our results [11]. The outer inferior ETDRS grid sector is the most thinned, and the outer nasal one is the less

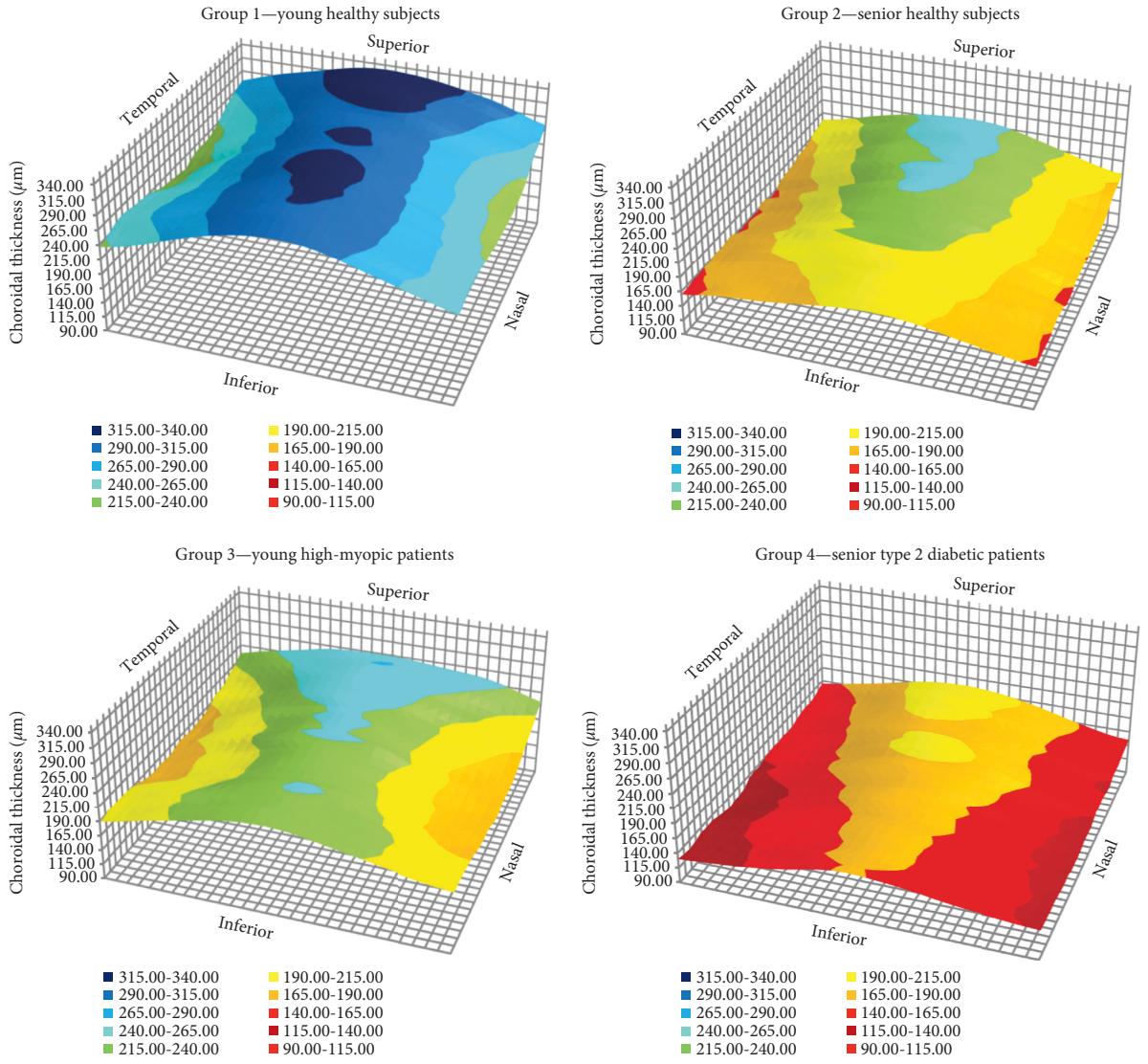

Figure 4: 3D maps of choroidal thickness.

thinned. As the latter has already been described as the thinnest choroidal zone even in healthy subjects, it is easy to understand that it is more difficult to achieve an even higher thinning.

On the contrary, high-myopic patients' choroid does not experience the same kind of thinning as with age. Their most thinned ETDRS sectors are the inferior and the nasal. Zhang et al. already found that the temporal choroid becomes less thinned than nasal, but they did not examine the superior or inferior choroid [12].

Finally, aged patients with mild and moderate DR suffer from a choroidal thinning which is softer in the outer nasal ETDRS sector. Their outer inferior ETDRS sector is affected from little thinning as well, but we should consider that this sector was already thinned because of age and then an even higher choroidal thinning would be rather difficult to achieve.

Thus, it is noticeable that, under these pathologies, there is a considerable flattening, and in those zones where CT was higher, choroidal thinning is also greater.

The strengths of this study include study-naïve patients and SS-OCT automatic measurements performed at the same day time. Furthermore, thickness maps seem easier to evaluate the choroid than manual measurements or ETDRS numerical values.

The main limitations of this study are a low number of young high-myopic patients and the small quantity of choroidal-thinning pathologies evaluated. It would be of interest how the whole macular choroid changes in other situations.

In conclusion, choroidal-thinning pathologies affect choroidal regions in a different way. This fact gains relevance especially in choroidal measurements because not all regions are interchangeable and CT should be measured in the proper place depending on the particular pathology. Therefore, lineal OCT examinations are inadequate for choroidal evaluation as superior and inferior macular regions remain unanalyzed. Second, choroidal thinning follows the following rule: the thicker the zone is in healthy subjects, the thinner it becomes when affected by any

pathology. Third, 3D representations of CT provide us with visual information which helps us to make an easier and faster general valuation. In general lines, the choroid in young healthy individuals follows a mountain range pattern; in aged healthy subjects, it follows a mountain peak pattern; in young high-myopic patients, it follows an inverted gorge pattern; and in aged diabetic patients, it follows a gathered hills pattern. All these pathologies tend to make a flat uniform choroid.

Data Availability

All data of this study has been collected and stored at the Miguel Servet University Hospital in Zaragoza, Spain.

Conflicts of Interest

The authors declare that they have no conflicts of interest.

References

[1] J. Ruiz-Medrano, I. Flores-Moreno, P. Peña-García, J. A. Montero, J. S. Duker, and J. M. Ruiz-Moreno, "Macular choroidal thickness profile in a healthy population measured by swept-source optical coherence tomography," *Investigative Opthalmology & Visual Science*, vol. 55, no. 6, pp. 3532–3542, 2014.

[2] S. Ozdogan Erkul, Z. Kapran, and O. Murat Uyar, "Quantitative analysis of subfoveal choroidal thickness using enhanced depth imaging optical coherence tomography in normal eyes," *International Ophthalmology*, vol. 34, no. 1, pp. 35–40, 2014.

[3] Y. Wakatsuki, A. Shinojima, A. Kawamura, and M. Yuzawa, "Correlation of aging and segmental choroidal thickness measurement using swept source optical coherence tomography in healthy eyes," *PLoS One*, vol. 10, no. 12, Article ID e0144156, 2015.

[4] M. Esmaeelpour, B. Považay, B. Hermann et al., "Three-dimensional 1060-nm OCT: choroidal thickness maps in normal subjects and improved posterior segment visualization in cataract patients," *Investigative Opthalmology & Visual Science*, vol. 51, no. 10, pp. 5260–5266, 2010.

[5] M. Hirata, A. Tsujikawa, A. Matsumoto et al., "Macular choroidal thickness and volume in normal subjects measured by swept-source optical coherence tomography," *Investigative Opthalmology & Visual Science*, vol. 52, no. 8, pp. 4971–4978, 2011.

[6] C. S. H. Tan, K. X. Cheong, L. W. Lim, and K. Z. Li, "Topographic variation of choroidal and retinal thicknesses at the macula in healthy adults," *British Journal of Ophthalmology*, vol. 98, no. 3, pp. 339–344, 2014.

[7] C. S. H. Tan and K. X. Cheong, "Macular choroidal thicknesses in healthy adults-relationship with ocular and demographic factors," *Investigative Opthalmology & Visual Science*, vol. 55, no. 10, p. 6452, 2014.

[8] M. Gabriel, M. Esmaeelpour, F. Shams-Mafi et al., "Mapping diurnal changes in choroidal, Haller's and Sattler's layer thickness using 3-dimensional 1060-nm optical coherence tomography," *Graefe's Archive for Clinical and Experimental Ophthalmology*, vol. 255, no. 10, pp. 1957–1963, 2017.

[9] M. Zhao, X. F. Yang, X. Jiao et al., "The diurnal variation pattern of choroidal thickness in macular region of young healthy female individuals using spectral domain optical coherence tomography," *International Journal of Ophthalmology*, vol. 9, no. 4, pp. 561–566, 2016.

[10] S. Usui, Y. Ikuno, M. Akiba et al., "Circadian changes in subfoveal choroidal thickness and the relationship with circulatory factors in healthy subjects," *Investigative Opthalmology & Visual Science*, vol. 53, no. 4, p. 2300, 2012.

[11] R. Bafiq, R. Mathew, E. Pearce et al., "Age, sex, and ethnic variations in inner and outer retinal and choroidal thickness on spectral-domain optical coherence tomography," *American Journal of Ophthalmology*, vol. 160, no. 5, pp. 1034–1043, 2015.

[12] Q. Zhang, M. Neitz, J. Neitz, and R. K. Wang, "Geographic mapping of choroidal thickness in myopic eyes using 1050-nm spectral domain optical coherence tomography," *Journal of Innovative Optical Health Sciences*, vol. 8, no. 4, article 1550012, 2015.

[13] D. Melancia, A. Vicente, J. P. Cunha, L. Abegão Pinto, and J. Ferreira, "Diabetic choroidopathy: a review of the current literature," *Graefe's Archive for Clinical and Experimental Ophthalmology*, vol. 254, no. 8, pp. 1453–1461, 2016.

[14] S. Kase, H. Endo, M. Yokoi et al., "Choroidal thickness in diabetic retinopathy in relation to long-term systemic treatments for diabetes mellitus," *European Journal of Ophthalmology*, vol. 26, no. 2, pp. 158–162, 2016.

[15] S. Galgauskas, G. Laurinavičiūtė, D. Norvydaitė, S. Stech, and R. Ašoklis, "Changes in choroidal thickness and corneal parameters in diabetic eyes," *European Journal of Ophthalmology*, vol. 26, no. 2, pp. 163–167, 2016.

[16] K. K. Dansingani, C. Balaratnasingam, J. Naysan, and K. B. Freund, "En face imaging of pachychoroid spectrum disorders with swept-source optical coherence tomography," *Retina*, vol. 36, no. 3, pp. 499–516, 2016.

[17] S. M. Waldstein, H. Faatz, M. Szimacsek et al., "Comparison of penetration depth in choroidal imaging using swept source vs spectral domain optical coherence tomography," *Eye*, vol. 29, no. 3, pp. 409–415, 2015.

[18] Y. Matsuo, T. Sakamoto, T. Yamashita, M. Tomita, M. Shirasawa, and H. Terasaki, "Comparisons of choroidal thickness of normal eyes obtained by two different spectral-domain OCT instruments and one swept-source OCT instrument," *Investigative Opthalmology & Visual Science*, vol. 54, no. 12, pp. 7630–7636, 2013.

[19] S. Y. Lee, H. W. Bae, H. J. Kwon, G. J. Seong, and C. Y. Kim, "Repeatability and agreement of swept source and spectral domain optical coherence tomography evaluations of thickness sectors in normal eyes," *Journal of Glaucoma*, vol. 26, no. 2, p. 1, 2016.

[20] J. K. Min, S. Lee, J. S. Kim, J. M. Woo, and H. S. Yang, "Effects of diabetic macular edema on repeatability of retinal nerve fiber layer thickness measurements at the macular and peripapillary area using swept-source optical coherence tomography," *Current Eye Research*, vol. 42, no. 2, pp. 307–314, 2017.

[21] C. S. H. Tan, W. K. Ngo, and K. X. Cheong, "Comparison of choroidal thicknesses using swept source and spectral domain optical coherence tomography in diseased and normal eyes," *British Journal of Ophthalmology*, vol. 99, no. 3, pp. 354–358, 2015.

[22] W. Rahman, F. K. Chen, J. Yeoh, P. Patel, A. Tufail, and L. Da Cruz, "Repeatability of manual subfoveal choroidal thickness measurements in healthy subjects using the technique of enhanced depth imaging optical coherence tomography," *Investigative Opthalmology & Visual Science*, vol. 52, no. 5, pp. 2267–2271, 2011.

[23] K. Mansouri, F. A. Medeiros, A. J. Tatham, N. Marchase, and R. N. Weinreb, "Evaluation of retinal and choroidal thickness by swept-source optical coherence tomography: repeatability and assessment of artifacts," *American Journal of Ophthalmology*, vol. 157, no. 5, pp. 1022–1032, 2014.

[24] J. Wang, X. Gao, W. Huang et al., "Swept-source optical coherence tomography imaging of macular retinal and choroidal structures in healthy eyes," *BMC Ophthalmology*, vol. 15, no. 1, p. 122, 2015.

[25] Y. Ouyang, F. M. Heussen, N. Mokwa et al., "Spatial distribution of posterior pole choroidal thickness by spectral domain optical coherence tomography," *Investigative Opthalmology & Visual Science*, vol. 52, no. 9, pp. 7019–7026, 2011.

[26] J. W. Shin, Y. U. Shin, and B. R. Lee, "Choroidal thickness and volume mapping by a six radial scan protocol on spectral-domain optical coherence tomography," *Ophthalmology*, vol. 119, no. 5, pp. 1017–1023, 2012.

[27] V. Manjunath, M. Taha, J. G. Fujimoto, and J. S. Duker, "Choroidal thickness in normal eyes measured using cirrus HD optical coherence tomography," *American Journal of Ophthalmology*, vol. 150, no. 3, pp. 325–329, 2010.

[28] F. K. Chen, J. Yeoh, W. Rahman, P. J. Patel, A. Tufail, and L. Da Cruz, "Topographic variation and interocular symmetry of macular choroidal thickness using enhanced depth imaging optical coherence tomography," *Investigative Opthalmology & Visual Science*, vol. 53, no. 2, pp. 975–985, 2012.

Hindawi
Journal of Ophthalmology
Volume 2019, Article ID 1698967, 8 pages
https://doi.org/10.1155/2019/1698967

Research Article

Outer Retinal Layers' Thickness Changes in relation to Age and Choroidal Thickness in Normal Eyes

Mona Kamal Abdellatif, Yasser Abdelmaguid Mohamed Elzankalony, Ahmed Abdelmonsef Abdelhamid Ebeid, and Weam Mohamed Ebeid

Department of Ophthalmology, Faculty of Medicine, Ain Shams University, Cairo, Egypt

Correspondence should be addressed to Weam Mohamed Ebeid; weam.ebeid@med.asu.edu.eg

Received 1 March 2019; Revised 22 May 2019; Accepted 1 July 2019; Published 31 July 2019

Guest Editor: Rune Brautaset

Purpose. To identify and correlate age-related changes in outer retinal layers' thickness and choroidal thickness (CT) in the normal eyes using spectral-domain optical coherence tomography (SD-OCT) and to investigate factors affecting these changes. *Study Design*. Observational cross-sectional study. *Subjects and Methods*. We studied 125 healthy Egyptians between 20 and 79 years old. Patients were divided into 3 groups: group 1 (20–40 years), group 2 (40–60 years), and group 3 (>60 years). All patients had full ophthalmic examination. SD-OCT was done to measure the 9 ETDRS macular grid sectors of retinal pigment epithelium and photoreceptor outer segment (RPE-OS), outer nuclear layer and photoreceptor inner segment (ONL-IS), and choroidal thickness (CT) (by enhanced depth imaging). *Results*. RPE-OS was significantly thinner in group 3 than in the other 2 groups (central: $P < 0.001$). Moreover, the 3 groups were significantly different from each other regarding the CT (central: $P < 0.001$); significant thinning was noticed in the choroid with age. The 3 groups did not show significant difference concerning the ONL-IS thickness. RPE-OS and CT showed statistically significant negative correlation with age (central RPE-OS: $r = -0$ C.345, $P < 0.001$, and central CT: $r = -0.725$, $P < 0.001$) while ONL-IS showed statistically nonsignificant correlation with age (central ONL-IS: $r = -0.08$, $P = 0.376$). Multiple regression analysis revealed that the most important determinant of central 1 mm RPE-OS thickness in this study was age ($\beta = -0.087$, $P = 0.010$) rather than choroidal thinning ($\beta = 0.001$, $P = 0.879$). *Conclusion*. RPE-OS layer thickness shows significant thinning with increasing age, and with decrease in CT, however, age is the most determinant factor of this thinning.

1. Introduction

The new optical coherence tomography (OCT) devices provide high-resolution images of the retinal layers [1, 2]. This allows precise segmentation of individual retinal layers and provides thickness maps that could help in studying diseases affecting specific retinal layers [3].

Recently, the introduction of the enhanced depth imaging (EDI) technique to spectral-domain OCT by Spaide has added the advantage of detailed choroidal imaging [4].

Previous reports have indicated that total retinal thickness shows variations with age, but it is not well understood whether the differences in total retinal thickness may be explained by variations in thickness of the inner or outer retinal layers [5].

Earlier histological studies have suggested that there is a decrease in cone pigment with age [6], which indicates a loss and displacement of photoreceptors with age [7, 8].

Moreover, many studies have proved significant choroidal thinning with age [5, 9, 10], which could be of great importance since the outer retinal layers do not have a vascular network and rely on choriocapillaris, which exhibits a slow blood velocity, in supplying the retinal pigment epithelium (RPE) and outer retina with oxygen and nutrients, thus maintaining normal retinal function [11, 12].

Accordingly, variation in outer retinal layers' thickness with age could be either due to vascular insufficiency as a result of choroidal thickness change or direct effect due to the aging process itself [6].

Selective outer retinal degeneration (photoreceptor cells) occurs in various retinal degenerative processes such as age-related macular degeneration (AMD) and hereditary retinal dystrophies, and different therapeutic strategies have been proposed to slow the progression of photoreceptor cell loss in these cases [2]. Hence, studying the different factors that may affect photoreceptor thickness in normal eyes (including age) may help to understand the pathology and treatment response of these conditions.

The aim of our study was to identify and correlate age-related changes in outer retinal layers' thickness and choroidal thickness in normal eyes using spectral-domain optical coherence tomography (SD-OCT) and to investigate factors affecting these changes.

2. Patients and Methods

This cross-sectional observational clinical study was conducted between July 2018 and February 2019 in the Ophthalmology Department, Ain Shams University. It included 125 eyes of 125 healthy Egyptian individuals, and their ages ranged from 20 to 79 years.

The study was approved by the Research Ethical Committee at the Faculty of Medicine-Ain Shams University, with informed consent obtained from every patient.

All patients had full ophthalmic examination including best-corrected visual acuity testing with Snellen's charts, refraction, slit lamp biomicroscopy, dilated fundus ophthalmoscopy, axial length measurement using an A-scan device (Echo Scan US-800, Nidek, Aichi, Japan), and intraocular pressure measurement by using a Goldmann applanation tonometer at the outpatient clinic of the Ophthalmology Department of Ain Shams University. Only the right eye of every patient was examined.

Exclusion criteria included patients with systemic diseases that would affect the retina or choroid as diabetes, hypertension, renal diseases, infections, autoimmune diseases, and degenerative neuro-ophthalmological diseases. Patients with any known ocular pathology and history of previous ocular surgery, patients with glaucoma or intraocular pressure >18 mmHg, and patients with refractive error >+4 or <−4 were all excluded from the study.

3. Spectral-Domain Optical Coherence Tomography (SD-OCT)

Optical coherence tomography was performed by using the Nidek RS-3,000 Advance SD-OCT (Retinascan RS-3000 Advance, Nidek Co. Ltd., Gamagori, Japan), with scan speed 53,000 A-scan/s. All patients were examined between 10 am and 12 pm after mydriasis using Mydriacyl 0.5% eye drops. Radial lines scan was used to measure the retinal pigment epithelium and photoreceptor outer segment (RPE-OS) layer thickness (extending from the inner segment/outer segment (IS/OS) layer to the outer surface of RPE) and the outer nuclear layer and photoreceptor inner segment (ONL-IS) thickness (measured from the interface between the outer plexiform layer (OPL) and the outer nuclear layer (ONL) extending to the IS/OS layer). Macular thickness measurements were derived from the software (NAVIS-EX Image Filing software, RS-3,000 OCT, NIDEK, Gamagori, Japan) provided by the manufacturer; no manual manipulation of OCT data was performed in the calculation. ETDRS chart was obtained, and the 9 ETDRS subfields were measured. The ETDRS map standard retinal subfields are central, inner (superior, inferior, nasal, and temporal), and outer (superior, inferior, nasal, and temporal). The central subfield is bounded by the innermost 1 mm diameter circle. The inner and outer subfields are bounded by the 3 mm and 6 mm diameter circles, respectively (Figure 1).

The choroid was imaged using the enhanced depth imaging technique (EDI) by positioning the SD-OCT closer to the eye to create an inverted image bringing the choroid to the zero delay line, which is the point of maximum sensitivity on SD-OCT. The image colors were made white on black to make the interface between the choroid and the sclera more distinct. The sclerochoroidal interface was drawn in the twelve radial lines manually. Choroidal thickness (CT) was measured from the outer surface of RPE to the manually drawn line. A CT map was automatically obtained with an ETDRS chart including the central CT in the innermost 1 mm circle and other ETDRS subfields (Figure 2). Drawing sclerochoroidal interface was performed by two independent expert investigators, and the average was taken. Only OCT scans with good signal quality were included (signal-to-noise ratio ≥7).

4. Statistical Analysis

All data analyses were performed using the Statistical Package for Social Sciences version 16.0 (SPSS© v. 16.0, SPSS Inc., Chicago, IL, USA). Quantitative data were presented as mean ± standard deviation (SD). Multiple group means were compared using the ANOVA test. Tukey's honestly significant difference (HSD) post hoc test was performed if an overall significance was found. Linear correlation coefficient was used for detection of correlation between two quantitative variables in one group. Regression analyses were done to assess the different factors that can affect ONL-IS and RPE-OS thickness in patients. The reliability and reproducibility of manual choroidal thickness measurements between the two investigators were measured using the interclass correlation coefficient (ICC). P values were considered statistically significant if <0.05.

5. Results

This study included 125 participants, with age ranged between 20 and 79 years old, with mean 47.32 ± 15.68 years old. Subjects were divided into 3 age groups: group 1 (45 participants, 20–40 years old), group 2 (43 participants, 40–60 years old), and group 3 (37 participants, age >60 years). There were 58 males (46.4%) and 67 females (53.6%) (Table 1).

Central 1 mm thickness as well as other 8 ETDRS subfields of the RPE-OS, the ONL-IS, and the choroid was measured in the three groups as shown in Table 2.

Interclass correlation coefficients (ICC) for CT measurements between the two investigators in the central 1 mm and the 8 ETDRS subfields (upper, lower, nasal and temporal

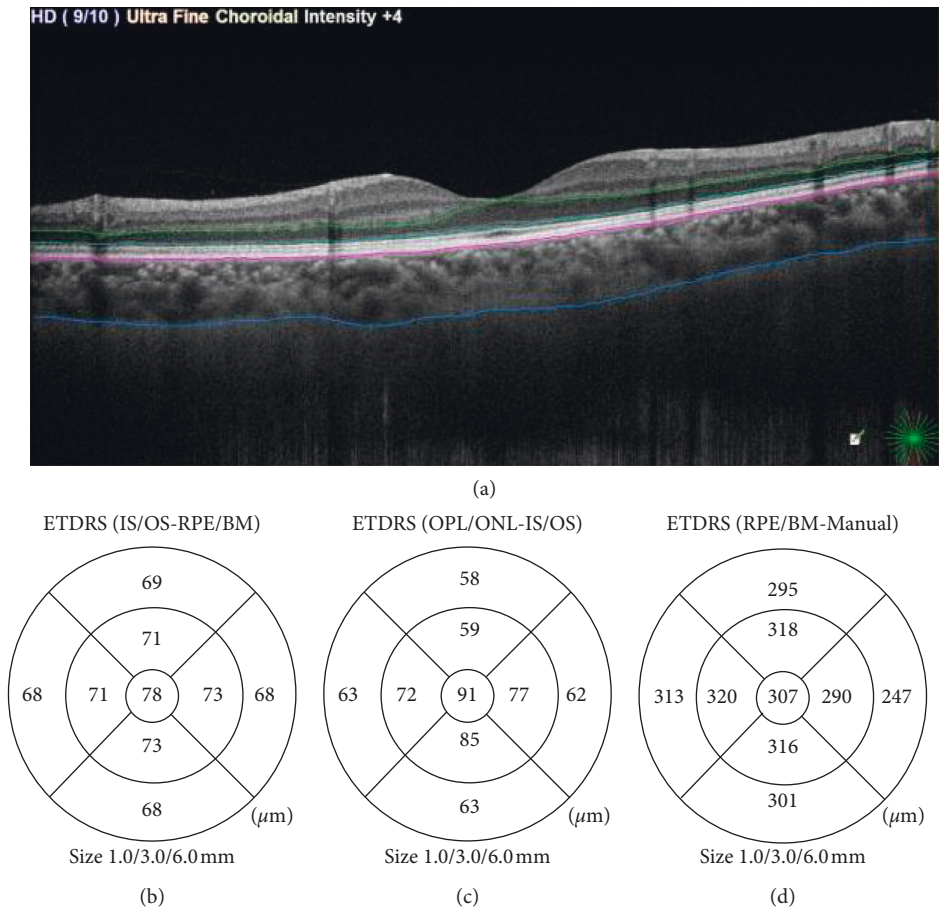

Figure 1: (a) OCT radial scan. ETDRS map: (b) retinal pigment epithelium and photoreceptor outer segment (RPE-OS) layer thickness (extending from the inner segment/outer segment (IS/OS) layer to the outer surface of RPE); (c) the outer nuclear layer and photoreceptor inner segment (ONL-IS) thickness (measured from the interface between the outer plexiform layer (OPL) and the outer nuclear layer (ONL) extending to the IS/OS layer); (d) choroidal thickness (CT) measured from the outer surface of RPE to the manually drawn sclerochoroidal interface.

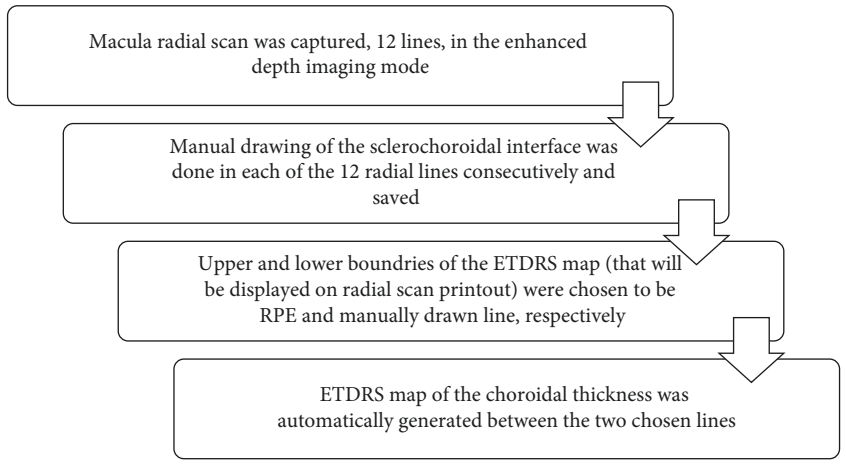

Figure 2: Schematic diagram showing the different steps performed to obtain the choroidal thickness map.

quadrants in the inner and outer rings) were 0.994, 0.985, 0.964, 0.984, 0.988, 0.979, 0.982, 0.987, and 0.986 consecutively, denoting excellent reliability of manual CT measurements.

On comparing the 3 groups, central RPE-OS as well as other 8 ETDRS RPE-OS subfields was significantly thinner in group 3 than in the other 2 groups ($P < 0.001$). Moreover, a progressive significant choroidal thinning was evident in the 9 ETDRS subfields among the 3 groups along with aging ($P < 0.001$). The 3 groups did not show significant difference concerning the ONL-IS thickness (Table 2).

Table 1: Demographic and ocular characteristics of the 3 studied groups' participants.

	Group 1 (mean ± SD)	Group 2 (mean ± SD)	Group 3 (mean ± SD)	P	G1 vs G2	G1 vs G3	G2 vs G3
Age, years	29.85 ± 4.9	49.22 ± 6.1	66.35 ± 4.1	**<0.001**	**<0.001**	**<0.001**	**<0.001**
Gender, M : F (N)	26 : 19	16 : 27	21 : 16	$X^2 = 1.33$ $P = 0.514$	—	—	—
Refraction (spherical equivalent), diopters	−0.69 ± 0.61	−0.80 ± 0.59	−0.65 ± 0.62	0.640	0.530	0.744	0.358
Axial length (mm)	22.91 ± 0.37	23.02 ± 0.35	22.91 ± 0.28	0.251	0.141	0.994	0.164

Bold numbers refer to statistically significant values.

Table 2: Comparison of mean thickness (in μm) of 9 ETDRS subfields for RPE-OS, ONL-IS, and choroid in the 3 studied groups.

	Group 1 (mean ± SD)	Group 2 (mean ± SD)	Group 3 (mean ± SD)	P	G1 vs G2	G1 vs G3	G2 vs G3
RPE-OS							
Central RPE-OS	74.76 ± 3.0	74.63 ± 3.33	71.05 ± 4.81	**<0.001**	0.87	**<0.001**	**<0.001**
Inner ring							
Superior	67.62 ± 2.71	68.05 ± 3.28	65.19 ± 3.65	**<0.001**	0.54	**0.001**	**<0.001**
Inferior	67.73 ± 3.28	68.07 ± 3.48	64.84 ± 3.33	**<0.001**	0.64	**<0.001**	**<0.001**
Nasal	67.98 ± 2.77	67.56 ± 4.45	64.78 ± 4.11	**<0.001**	0.61	**<0.001**	**0.002**
Temporal	68.16 ± 2.99	68.98 ± 3.61	65.32 ± 3.57	**<0.001**	0.26	**<0.001**	**<0.001**
Outer ring							
Superior	65.04 ± 2.20	65.79 ± 3.44	62.46 ± 3.35	**<0.001**	0.25	**<0.001**	**<0.001**
Inferior	64.44 ± 2.34	64.256 ± 2.84	61.0 ± 3.46	**<0.001**	0.76	**<0.001**	**<0.001**
Nasal	64.91 ± 2.60	63.69 ± 4.46	61.24 ± 2.96	**<0.001**	0.10	**<0.001**	**0.002**
Temporal	64.60 ± 1.95	64.72 ± 3.62	61.54 ± 3.70	**<0.001**	0.86	**<0.001**	**<0.001**
ONL-IS							
Central ONL-IS	83.98 ± 10.3	84.00 ± 24.57	88.16 ± 11.51	0.45	0.99	0.27	0.27
Inner ring							
Superior	69.69 ± 7.44	71.86 ± 8.68	69.29 ± 8.88	0.321	0.223	0.83	0.17
Inferior	69.16 ± 8.89	70.69 ± 9.218	71.51 ± 9.58	0.497	0.434	0.25	0.69
Nasal	70.62 ± 10.48	73.09 ± 10.88	68.57 ± 10.12	0.160	0.273	0.38	0.06
Temporal	69.38 ± 8.73	70.58 ± 8.79	75.00 ± 9.05	0.014	0.525	**0.005**	**0.03**
Outer ring							
Superior	61.13 ± 7.55	62.26 ± 8.46	61.621 ± 8.795	0.816	0.525	0.790	0.732
Inferior	57.18 ± 7.37	58.86 ± 8.55	59.540 ± 8.102	0.383	0.327	0.186	0.706
Nasal	58.53 ± 6.74	59.26 ± 9.53	58.757 ± 10.712	0.930	0.708	0.911	0.806
Temporal	60.51 ± 8.29	62.23 ± 8.77	64.324 ± 8.913	0.143	0.352	**0.049**	0.283
CT							
Central CT	356.16 ± 59.88	296.21 ± 41.26	255.14 ± 33.61	**<0.001**	**<0.001**	**<0.001**	**<0.001**
Inner ring							
Superior	352.69 ± 56.17	291.442 ± 32.22	257.49 ± 33.04	**<0.001**	**<0.001**	**<0.001**	**0.001**
Inferior	345.73 ± 63.77	279.48 ± 32.06	254.97 ± 35.44	**<0.001**	**<0.001**	**<0.001**	**0.021**
Nasal	316.73 ± 50.67	263.14 ± 32.13	231.03 ± 33.68	**<0.001**	**<0.001**	**<0.001**	**0.001**
Temporal	338.80 ± 54.55	280.51 ± 35.21	243.70 ± 32.05	**<0.001**	**<0.001**	**<0.001**	**<0.001**
Outer ring							
Superior	338.07 ± 52.29	276.05 ± 28.84	244.86 ± 36.59	**<0.001**	**<0.001**	**<0.001**	**0.001**
Inferior	324.16 ± 61.13	258.49 ± 33.55	229.46 ± 51.99	**<0.001**	**<0.001**	**<0.001**	**0.011**
Nasal	273.18 ± 46.56	235.49 ± 36.32	207.73 ± 35.19	**<0.001**	**<0.001**	**<0.001**	**0.002**
Temporal	322.47 ± 52.19	261.88 ± 39.01	229.19 ± 31.94	**<0.001**	**<0.001**	**<0.001**	**0.001**

CT: choroidal thickness. Bold numbers refer to statistically significant values.

The nine ETDRS subfields of RPE-OS and CT showed statistically significant negative correlation with age (central RPE-OS: $r = -0$ C.345, $P < 0.001$, and central T: $r = -0.725$, $P < 0.001$), while ETDRS subfields of ONL-IS did not show any significant correlation with age except the inner temporal subfield (central ONL-IS: $P = 0.376$) (Table 3).

RPE-OS showed positive statistically significant correlation with CT in all sectors of the ETDRS (central subfield: $r = 0.273$, $P = 0.002$); however, ONL-IS showed insignificant correlation with CT (central subfield: $P = 0.409$). No statistically significant correlation was found either with refraction or with axial length or gender in the three layers (Table 3).

Multiple regression analysis was carried out to detect factors more likely associated with thinning of RPE-OS layer. It revealed that the most important determinant of

Table 3: Correlation of the 9 ETDRS subfields mean thickness of RPE-OS, ONL-IS, and CT with age, gender, refraction, axial length, and CT.

	Correlation with age		Correlation with gender		Correlation with CT		Correlation with refraction		Correlation with axial length	
	r	*P* value	*r*	*P* value	*r*	*P* value	*r*	*P* value	*r*	*P* value
RPE-OS										
Central RPE-OS	−0.345	**<0.001**	−0.049	0.590	0.273	**0.002**	0.092	0.306	0.027	0.767
Inner ring										
Superior	−0.253	**0.004**	−0.119	0.186	0.182	**0.042**	0.069	0.446	−0.025	0.779
Inferior	−0.280	**0.002**	−0.100	0.268	0.227	**0.011**	−0.034	0.710	0.102	0.256
Nasal	−0.287	**0.001**	−0.062	0.492	0.339	**<0.001**	0.109	0.224	−0.047	0.601
Temporal	−0.260	**0.003**	−0.058	0.523	0.283	**0.001**	0.091	0.310	<0.001	0.997
Outer ring										
Superior	−0.264	**0.003**	−0.107	0.236	0.175	0.051	0.103	0.252	0.010	0.915
Inferior	−0.396	**<0.001**	−0.040	0.655	0.352	**0.001**	0.053	0.555	0.076	0.397
Nasal	−0.366	**<0.001**	−0.075	0.407	0.479	**<0.001**	0.164	0.068	−0.087	0.336
Temporal	−0.311	**<0.001**	−0.030	0.743	0.325	**<0.001**	0.071	0.429	0.010	0.915
ONL-IS										
Central ONL-IS	0.08	0.376	0.019	0.833	−0.075	0.409	0.136	0.130	−0.124	0.167
Inner ring										
Superior	0.062	0.495	−0.173	0.054	−0.024	0.791	−0.012	0.893	−0.001	0.994
Inferior	0.143	0.111	−0.185	0.039	−0.047	0.599	0.005	0.953	0.017	0.853
Nasal	−0.046	0.614	−0.132	0.142	0.114	0.207	0.094	0.297	0.123	0.171
Temporal	0.294	**0.001**	−0.095	0.292	−0.237	**0.008**	−0.037	0.681	−0.047	0.604
Outer ring										
Superior	0.073	0.417	−0.099	0.271	−0.039	0.665	0.027	0.766	−0.016	0.861
Inferior	0.164	0.068	−0.144	0.109	−0.124	0.168	−0.032	0.725	0.066	0.463
Nasal	0.057	0.530	−0.082	0.361	−0.114	0.206	0.004	0.962	−0.030	0.739
Temporal	0.222	**0.013**	−0.014	0.120	−0.135	0.133	−0.071	0.433	−0.014	0.880
CT										
Central CT	−0.725	**<0.001**	−0.013	0.255	—	—	0.166	0.064	−0.015	0.868
Inner ring										
Superior	−0.727	**<0.001**	−0.101	0.260	0.865	**<0.001**	−0.003	0.976	0.054	0.547
Inferior	−0.669	**<0.001**	−0.120	0.183	0.837	**<0.001**	0.015	0.871	0.057	0.528
Nasal	−0.672	**<0.001**	−0.119	0.186	0.784	**<0.001**	−0.030	0.744	0.017	0.853
Temporal	−0.683	**<0.001**	−0.110	0.224	0.781	**<0.001**	−0.018	0.840	−0.024	0.790
Outer ring										
Superior	−0.729	**<0.001**	−0.072	0.424	0.817	**<0.001**	−0.003	0.976	0.065	0.470
Inferior	−0.651	**<0.001**	−0.142	0.114	0.772	**<0.001**	0.045	0.621	0.075	0.403
Nasal	−0.566	**<0.001**	−0.177	0.048	0.700	**<0.001**	0.000	0.998	0.054	0.549
Temporal	−0.658	**<0.001**	−0.094	0.296	0.704	**<0.001**	0.020	0.822	−0.047	0.601

CT: choroidal thickness. Bold numbers refer to statistically significant values.

central 1 mm RPE-OS thickness in this study was age ($\beta = -0.087$, $P = 0.010$) rather than choroidal thinning ($\beta = 0.001$, $P = 0.879$) (Table 4).

Regarding other RPE-OS layer ETDRS sectors, regression analysis revealed that upper and lower zones thickness showed significant regression with age rather than CT (Table 4).

6. Discussion

New OCT technology has provided valuable quantitative information that could greatly enhance our understanding of outer retinal layers' diseases and allow clinicians to confirm their improvement or progression [13, 14]. Moreover, OCT may aid in evaluating the efficacy of new therapies by quantifying the photoreceptor cell layer in a reliable and reproducible way [2, 15]. For instance, previous studies using ultrahigh resolution OCT showed that the severity of photoreceptor loss is associated with visual loss in retinitis pigmentosa, [13] while other studies using SD-OCT showed that by measuring the thickness of the outer nuclear layer in the fovea, we can predict visual prognosis in retinal diseases such as central serous chorioretinopathy [16], polypoidal choroidal vasculopathy [17], and epiretinal membrane [15].

Earlier studies using SD-OCT [18–21] in healthy eyes reported changes in the macular profile in relation to factors such as age, sex, and axial length [15]. Thickness of different retinal layers has shown variation according to age in variable studies as well [8, 14, 21, 22]. Studying this expected variation in individual retinal layers using the new OCT technology would be of great help in distinguishing pathological retinal changes from age-related ones.

Table 4: Multiple regression analysis of different factors affecting the thickness of 9 ETDRS subfields of RPE-OS and ONL-IS.

	Regression with age		Regression with gender		Regression with CT		Regression with refraction		Regression with axial length	
	B-coefficient	*P* value	*B*-coefficient	*P* value	*B*-coefficient	*P* value	*B*-coefficient	*P* value	*B*-coefficient	*P* value
RPE-OS										
Central RPE-OS	−0.087	**0.010**	−0.664	0.355	0.001	0.879	0.691	0.218	0.213	0.838
Inner ring										
Superior	−0.065	**0.023**	−1.059	0.088	−0.003	0.716	0.472	0.327	−0.304	0.729
Inferior	−0.060	**0.031**	−0.793	0.227	0.002	0.777	−0.067	0.895	0.926	0.319
Nasal	−0.032	0.297	−0.452	0.525	0.019	**0.033**	0.778	0.161	−0.561	0.578
Temporal	−0.033	0.256	−0.438	0.510	0.012	0.135	0.610	0.240	0.070	0.941
Outer ring										
Superior	−0.070	**0.011**	−0.989	0.095	−0.005	0.547	0.658	0.158	0.088	0.918
Inferior	−0.064	**0.007**	−0.307	0.586	0.007	0.230	0.310	0.479	0.557	0.483
Nasal	−0.036	0.120	−0.284	0.641	0.031	**<0.001**	0.960	**0.042**	−1.107	0.196
Temporal	−0.039	0.128	−0.212	0.727	0.012	0.081	0.404	0.396	0.182	0.834
ONL-IS										
Central ONL-IS	0.083	0.568	0.204	0.948	0.001	0.985	3.383	0.169	−5.519	0.227
Inner ring										
Superior	0.022	0.753	−2.866	0.067	−0.001	0.939	0.112	0.926	−0.059	0.979
Inferior	0.090	0.211	−3.189	0.063	0.005	0.786	0.390	0.769	0.481	0.786
Nasal	−0.181	**0.027**	−4.218	**0.029**	−0.063	**0.010**	2.045	0.171	3.819	0.160
Temporal	0.127	0.075	−1.601	0.329	−0.016	0.418	−0.483	0.705	−1.234	0.597
Outer ring										
Superior	0.037	0.604	−1.622	0.291	0.001	0.965	0.492	0.683	−0.320	0.884
Inferior	0.052	0.401	−2.344	0.119	−0.011	0.493	−0.063	0.957	1.685	0.424
Nasal	−0.023	0.721	−2.065	0.226	−0.029	0.174	0.241	0.854	−0.649	0.786
Temporal	0.116	0.085	−2.082	0.192	−0.001	0.943	−0.811	0.515	−0.368	0.943

CT: choroidal thickness. Bold numbers refer to statistically significant values.

In our study, we studied age-related changes in outer retinal layers' thickness and choroidal thickness in normal eyes aiming to identify the most influential factor on outer retinal layers' thickness.

Our results showed that macular CT was negatively correlated with age; this is in accordance with previous studies using EDI-OCT in normal eyes that have reported that macular choroidal thickness is negatively correlated with age [1, 5, 10, 23, 24].

Moreover, in our study, the thickness of RPE-OS showed a statistically significant negative correlation with age in the central foveal zone and also in the parafoveal and perifoveal rings, with a decline of 0.8 μm per decade in the central 1 mm, when the entire cohort was compared. However, this number is just an impression of the theoretical speed of age-related changes based on the found linear relationship between thickness measurements and age and can only be verified with a longitudinal study. Regarding the ONL-IS, no statistically significant thinning was noticed with aging. This variable effect of aging on foveal layers may give a clue why earlier studies found no statistically significant correlations between age and overall central foveal retinal thickness, which is composed primarily of outer retinal layers [20, 21, 25].

Our findings are supported by earlier histological studies using fundus reflectometry that demonstrated loss of foveal cone visual pigment in the human retinae with aging [6, 26].

Our results are in concordance with a previous study by Abdolrahimzadeh et al. [22] who reported that, in all ETDRS grid zones, outer retinal layer thickness correlated positively with CT and negatively with age, also with Nieves-Moreno et al. [27] as they found negative correlation of the photoreceptor layer (measured as the thickness between the outer limiting membrane and Burch's membrane) with age in 3 ETDRS rings, and with Demirkaya et al. [8] who demonstrated a significant decrease in foveal outer segment layer (OSL) thickness with increasing age; however, they found that this decrease was nonsignificant in the perifoveal and parafoveal rings [8].

On the contrary, Bafik and his colleagues [5] reported that the outer retina did not show any age or sex-related differences; however, in their study, the outer retinal thickness was measured from the inner nuclear layer/outer plexiform layer (INL/OPL) junction to the outer border of the RPE layer; i.e., their measurement included RPE-OS and ONL-IS layers. This is unlike our study, where, we segregated the outer retina into layers, the outer one (RPE-OS) correlated with age while the inner one (ONL-IS) did not show any correlation with age. Won and coworkers [14] demonstrated that PHL, ONL, and foveal RPE thickness showed no significant differences with increasing age; however, their study only included 50 subjects which is a rather small sample, and the segmentation protocol they used is different from the one used in the present study since ONL, photoreceptors, and RPE are considered separately in the former which might be a possible reason for discrepancy.

By contrast, Ooto et al. [28] reported a thickening of the OS layer in all macular zones, unlike our results that showed a thinning in RPE-OS with aging. However, the RPE was not

included in their segmentation algorithms. Worth mentioning that they stated in their discussion that RPE and OS tip lines were difficult to identify independently in some subjects; this ambiguity in the definition of the OS tips might have led to the different results. According to our device segmentation algorithm, we defined the RPE-OS layer as the layer between the IS/OS transition and outer surface of RPE, which are relatively clear transitions. Moreover, all subjects included in their study were Japanese adults, whereas foveal thickness differences between different ethnic groups have been previously reported [28].

Flores-Moreno et al. [29] did not find any correlation between age and photoreceptors-RPE layer thickness (measured from the hyper-reflective line corresponding to the ELM to the outer border of the RPE); this result may be due to the smaller number of patients (60) in their study, the selected group of highly myopic eyes (≥−6D) as opposed to our cohort where subjects with refractive error >+4 or <−4 were all excluded from the study, and also the different device used (Topcon 3D-2000 OCT).

Kenmochi et al. [30] stated that the RPE-COST thickness and the IS/OS-ELM thickness at the fovea were significantly associated with age. Conversely, they found that the COST-IS/OS thickness, which incorporates the outer segments of the photoreceptor cells, was not significantly associated with age. However, in their study, the RPE line and the COST line were sometimes not completely separated, as they described, and all their measurements relied on manual segmentation. In addition, all their measurements were taken from a single-line OCT scan and were reported as a single-point thickness, unlike our study where all measurements of outer retinal layers were done automatically in 12 radial lines and reported as thickness maps in the 9 ETDRS macular map sectors which reduce our measurements variability.

In this study, we found statistically significant positive correlation of RPE-OS with CT in all ETDRS macular grid zones, which agree with Abdolrahimzadeh et al. [22]. This was expected since the photoreceptor layer in the foveal region depends mainly in its nourishment on the underlying choroid. Furthermore, it has been previously reported that choroidal alterations and thinning in pathological conditions can lead to outer retinal layer thinning [29, 31].

In view of the fact that photoreceptor age-related loss might either be a consequence of age-related choriocapillary rarefaction (choroidal thinning) or age-related neural tissue loss, we performed a multiple regression analysis, in an attempt to understand the effects of age, choroid thickness, and other variables including gender, refraction, and axial length on the outer retinal layer thickness.

The multiple regression analysis revealed that the central foveal zone of RPE-OS as well as superior and inferior parafoveal and perifoveal zones was independently affected by age rather than choroidal thinning. This might suggest that the photoreceptor age-related neural tissue loss has more prominent impact than vascular supply diminution due to choroidal thinning on outer retinal layer thickness. Thus, it is essential to consider age when outer retinal layer thickness is evaluated in the context of monitoring the progression of outer retinal layer diseases like retinitis pigmentosa, evaluating the efficacy of various therapeutic modalities that target the photoreceptor layer and predicting visual prognosis in various macular diseases.

It is noteworthy that there is no general consensus on where to set the boundaries between retinal layers. This may partially explain the contrasting results obtained in different studies. In our study, we measured the RPE-OS layer (from the IS/OS junction to the outer aspect of RPE); however, thickening of the RPE with age has been previously reported [12, 27]. Accordingly, photoreceptors outer-segment thinning with age might be even greater than that reported in this study.

The strengths of the current study include our robust measurements of different layers. Measurements of outer retinal layers were based on automatic segmentation done by the device software (NAVIS-EX Image Filing software, RS3000-OCT, NIDEK, Gamagori, Japan) with no manual correction done which ensures the accuracy of the measurements. In addition, we measured thickness maps in 9 areas of 6 mm ETDRS macular grid rather than single-point foveal measurements on single-line OCT scans done in previous reports; where this central foveal zone is just a little portion of the retina and the information obtained from this area cannot be extended to all the other macular subfields. Even in other studies which measured parafoveal thickness, they relied on single-point thickness using single-line OCT scan which would be less accurate than the map we constructed. Regarding choroidal thickness, sclerochoroidal interface was manually drawn but with very good reliability measures, and the interface was drawn in each of the 12 radial lines of macular radial scan, and based on this, choroidal thickness map was generated; hence, our measurements are much more precise and show less variability. Finally, we had an appropriate group of normal individuals of wide-ranging age and properly distributed age groups.

Limitations of the present study include the cross-sectional design rather than the longitudinal design. Further studies with longitudinal data on a larger cohort are warranted and would aid in building up a normative database against which thickness maps of individual retinal layers in diseased eyes can be compared, which may advance our understanding of pathological mechanisms in various retinal degenerative diseases.

Data Availability

The data used to support the findings of this study are available from the corresponding author upon request.

Conflicts of Interest

The authors certify that they have no affiliations with any organization or entity with any financial or nonfinancial interest in the subject matter or materials discussed in this manuscript.

References

[1] S. Ooto, M. Hangai, and N. Yoshimura, "Effects of sex and age on the normal retinal and choroidal structures on optical coherence tomography," *Current Eye Research*, vol. 40, no. 2, pp. 213–225, 2015.

[2] A. Chan, J. S. Duker, H. Ishikawa, T. H. Ko, J. S. Schuman, and J. G. Fujimoto, "Quantification of photoreceptor layer thickness in normal eyes using optical coherence tomography," *Retina*, vol. 26, no. 6, pp. 655–660, 2006.

[3] A. L. Loduca, C. Zhang, R. Zelkha, and M. Shahidi, "Thickness mapping of retinal layers by spectral-domain optical coherence tomography," *American Journal of Ophthalmology*, vol. 150, no. 6, pp. 849–855, 2010.

[4] R. F. Spaide, H. Koizumi, and M. C. Pozonni, "Enhanced depth imaging spectral-domain optical coherence tomography," *American Journal of Ophthalmology*, vol. 146, no. 4, pp. 496–500, 2008.

[5] R. Bafiq, R. Mathew, E. Pearce et al., "Age, sex, and ethnic variations in inner and outer retinal and choroidal thickness on spectral-domain optical coherence tomography," *American Journal of Ophthalmology*, vol. 160, no. 5, pp. 1034–1043, 2015.

[6] T. C. Nag and S. Wadhwa, "Ultrastructure of the human retina in aging and various pathological states," *Micron*, vol. 43, no. 7, pp. 759–781, 2012.

[7] G. R. Jackson, C. Owsley, and C. A. Curcio, "Photoreceptor degeneration and dysfunction in aging and age-related maculopathy," *Ageing Research Reviews*, vol. 1, no. 3, pp. 381–396, 2002.

[8] N. Demirkaya, H. W. van Dijk, S. M. van Schuppen et al., "Effect of age on individual retinal layer thickness in normal eyes as measured with spectral-domain optical coherence tomography," *Investigative Opthalmology & Visual Science*, vol. 54, no. 7, pp. 4934–4940, 2013.

[9] M. Kim, S. S. Kim, H. J. Koh, and S. C. Lee, "Choroidal thickness, age, and refractive error in healthy Korean subjects," *Optometry and Vision Science*, vol. 91, no. 5, pp. 491–496, 2014.

[10] R. Margolis and R. F. Spaide, "A pilot study of enhanced depth imaging optical coherence tomography of the choroid in normal eyes," *American Journal of Ophthalmology*, vol. 147, no. 5, pp. 811–815, 2009.

[11] A. A. E.-F. El-Shazly, R. S. Elkitkat, W. M. Ebeid, and M. R. Deghedy, "Correlation between subfoveal choroidal thickness and foveal thickness in thalassemic patients," *Retina*, vol. 36, no. 9, pp. 1767–1772, 2016.

[12] P. Rutkowski and C. A. May, "Nutrition and vascular supply of retinal ganglion cells during human development," *Frontiers in Neurology*, vol. 7, 2016.

[13] A. J. Witkin, T. H. Ko, J. G. Fujimoto et al., "Ultra-high resolution optical coherence tomography assessment of photoreceptors in retinitis pigmentosa and related diseases," *American Journal of Ophthalmology*, vol. 142, no. 6, pp. 945–952.e1, 2006.

[14] J. Y. Won, S. E. Kim, and Y. H. Park, "Effect of age and sex on retinal layer thickness and volume in normal eyes," *Medicine*, vol. 95, no. 46, article e5441, 2016.

[15] S. Ooto, M. Hangai, K. Takayama et al., "High-resolution imaging of the photoreceptor layer in epiretinal membrane using adaptive optics scanning laser ophthalmoscopy," *Ophthalmology*, vol. 118, no. 5, pp. 873–881, 2011.

[16] H. Matsumoto, T. Sato, and S. Kishi, "Outer nuclear layer thickness at the fovea determines visual outcomes in resolved central serous chorioretinopathy," *American Journal of Ophthalmology*, vol. 148, no. 1, pp. 105–110.e1, 2009.

[17] S. Ooto, A. Tsujikawa, S. Mori, H. Tamura, K. Yamashiro, and N. Yoshimura, "Thickness of photoreceptor layers in polypoidal choroidal vasculopathy and central serous chorioretinopathy," *Graefe's Archive for Clinical and Experimental Ophthalmology*, vol. 248, no. 8, pp. 1077–1086, 2010.

[18] J. E. Legarreta, O. S. Punjabi, G. Gregori, R. W. Knighton, G. Lalwani, and C. A. Puliafito, "Macular thickness measurements in normal eyes using spectral-domain optical coherence tomography," *Investigative Ophthalmology & Visual Science*.vol. 48, no. 13, p. 2595, 2007.

[19] S. Grover, R. K. Murthy, V. S. Brar, and K. V. Chalam, "Normative data for macular thickness by high-definition spectral-domain optical coherence tomography (spectralis)," *American Journal of Ophthalmology*, vol. 148, no. 2, pp. 266–271, 2009.

[20] W. K. Song, S. C. Lee, E. S. Lee, C. Y. Kim, and S. S. Kim, "Macular thickness variations with sex, age, and axial length in healthy subjects: a spectral domain-optical coherence tomography study," *Investigative Opthalmology & Visual Science*, vol. 51, no. 8, pp. 3913–3918, 2010.

[21] S. Ooto, M. Hangai, A. Sakamoto et al., "Three-dimensional profile of macular retinal thickness in normal Japanese eyes," *Investigative Opthalmology & Visual Science*, vol. 51, no. 1, pp. 465–473, 2010.

[22] S. Abdolrahimzadeh, F. Parisi, V. Scavella, and S. M. Recupero, "Optical coherence tomography evidence on the correlation of choroidal thickness and age with vascularized retinal layers in normal eyes," *Retina*, vol. 36, no. 12, pp. 2329–2338, 2016.

[23] M. Hirata, A. Tsujikawa, A. Matsumoto et al., "Macular choroidal thickness and volume in normal subjects measured by swept-source optical coherence tomography," *Investigative Opthalmology & Visual Science*, vol. 52, no. 8, pp. 4971–4978, 2011.

[24] Y. Ikuno, K. Kawaguchi, T. Nouchi, and Y. Yasuno, "Choroidal thickness in healthy Japanese subjects," *Investigative Opthalmology & Visual Science*, vol. 51, no. 4, pp. 2173–2176, 2010.

[25] K. R. Sung, G. Wollstein, R. A. Bilonick et al., "Effects of age on optical coherence tomography measurements of healthy retinal nerve fiber layer, macula, and optic nerve head," *Ophthalmology*, vol. 116, no. 6, pp. 1119–1124, 2009.

[26] P. E. Kilbride, L. P. Hutman, M. Fishman, and J. S. Read, "Foveal cone pigment density difference in the aging human eye," *Vision Research*, vol. 26, no. 2, pp. 321–325, 1986.

[27] M. Nieves-Moreno, J. M. Martínez-de-la-Casa, L. Morales-Fernández, R. Sánchez-Jean, F. Sáenz-Francés, and J. García-Feijoó, "Impacts of age and sex on retinal layer thicknesses measured by spectral domain optical coherence tomography with spectralis," *PLoS One*, vol. 13, no. 3, Article ID e0194169, 2018.

[28] S. Ooto, M. Hangai, A. Tomidokoro et al., "Effects of age, sex, and axial length on the three-dimensional profile of normal macular layer structures," *Investigative Opthalmology & Visual Science*, vol. 52, no. 12, pp. 8769–8779, 2011.

[29] I. Flores-Moreno, J. Ruiz-Medrano, J. S. Duker, and J. M. Ruiz-Moreno, "The relationship between retinal and choroidal thickness and visual acuity in highly myopic eyes," *British Journal of Ophthalmology*, vol. 97, no. 8, pp. 1010–1013, 2013.

[30] J. Kenmochi, Y. Ito, and H. Terasaki, "Changes of outer retinal thickness with increasing age in normal eyes and in normal fellow eyes of patients with unilateral age-related macular degeneration," *Retina*, vol. 37, no. 1, pp. 47–52, 2017.

[31] S. Abdolrahimzadeh, L. Felli, R. Plateroti et al., "Morphologic and vasculature features of the choroid and associated choroid-retinal thickness alterations in neurofibromatosis type 1," *British Journal of Ophthalmology*, vol. 99, no. 6, pp. 789–793, 2015.

Hindawi
Journal of Ophthalmology
Volume 2019, Article ID 8787149, 4 pages
https://doi.org/10.1155/2019/8787149

Research Article

CLU Polymorphisms in Patients with Pseudoexfoliation Syndrome in Polish Population

Hanna Lesiewska,[1] **Katarzyna Linkowska**,[2] **Joanna Stafiej**,[1] **Tomasz Grzybowski**,[2] **Jacek Swobodziński**,[2] **and Grażyna Malukiewicz**[1]

[1]*Department of Ophthalmology, The Nicolaus Copernicus University, Ludwik Rydygier's Collegium Medicum in Bydgoszcz, Skłodowskiej Curie 9, 85-094 Bydgoszcz, Poland*
[2]*Department of Molecular and Forensic Genetics, Institute of Forensic Medicine, The Nicolaus Copernicus University, Ludwik Rydygier's Collegium Medicum Ludwik Rydygier, Skłodowskiej Curie 9, 85-094 Bydgoszcz, Poland*

Correspondence should be addressed to Hanna Lesiewska; hanjot@op.pl

Received 24 January 2019; Accepted 15 April 2019; Published 1 July 2019

Academic Editor: Alejandro Cerviño

Purpose. To evaluate *CLU* polymorphisms in patients with pseudoexfoliation syndrome. *Materials and Methods*. We studied 81 patients (23 males and 58 females, the median age 76 years) and 91 control subjects (27 males and 64 females, the median age 75 years). Genotypes of the *CLU* polymorphisms (SNPs), rs3087554 and rs2279590, were determined using a commercially available validated genotyping assays. The χ^2 test was performed to compare patient and control groups for possible associations between SNP genotype/allele frequency and disease state. *Results*. There were no significant differences for both allele and genotype frequencies between PEX patients and controls for rs3087554 and rs2279590 polymorphisms. The haplotypes distribution shows statistically significant difference between groups ($p = 0.03$). The haplotype (CT) more often was found in controls than in PEX patients, conferring an 18-fold decreased risk to the disease. *Conclusion*. Our results indicate that CLU variants may contribute to the risk of PEX in the Polish population.

1. Introduction

Pseudoexfoliation syndrome (PEX) is a form of age-related elastosis resulting from the overproduction or over-aggregation of elastic microfibrillar components [1]. There is an increasing prevalence of PEX as the mean age of the general population increases. The role of inheritance in PEX is still unclear. Several studies demonstrated an increased prevalence of pseudoexfoliation in relatives of family members affected with pseudoexfoliation compared to the general population [2–5]. These findings encouraged other investigators to identify possible genetic factors which could be involved. The genome-wide study conducted in populations of Iceland and Sweden showed the strong association between two single-nucleotide polymorphisms (SNPs) in the lysyl oxidase-like gene and PEX syndrome [6]. This association was then confirmed in many populations worldwide, including our present group of PEX patients [7–13]. The gene expression analyses revealed several genes that may play a role in PEX syndrome pathology, where clusterin was one among them (CLU) [14]. As the results of the studies on CLU association with PEX syndrome were inconclusive, we decided to determine this possible association in the Polish population.

2. Materials and Methods

We studied 81 patients (23 males and 58 females, the median age 76 years, $Q_1 = 72.0$; $Q_3 = 82.0$) and 91 control subjects (27 males and 64 females, the median age 75 years, $Q_1 = 70.0$; $Q_3 = 80.0$), who presented to the Department of Ophthalmology, Collegium Medicum UMK in Bydgoszcz, Poland, for cataract surgery. This work has been approved by the local bioethical committee. All patients gave their informed

consent for this study. Patients were enrolled into the study if they had no other ocular or general diseases e.g., glaucoma, age-related macular degeneration (AMD), diabetes, dislipidemia, and arterial hypertension, except cataract and PEX. Glaucoma was defined based on measurements of IOP consistently >21 mmHg without glaucoma medication and the presence of typical glaucomatous optic nerve and visual field changes or previously diagnosed glaucoma under treatment. AMD was diagnosed on the basis of the presence of hard and soft drusen, changes in the retinal pigment epithelium (RPE), geographic atrophy, choroidal neovascular membrane, or disciform scar. In every patient, the diagnosis of PEX was confirmed by slit-lamp examination after pupil dilation. Pseudoexfoliation changes were identified as the presence of typical PEX material on the anterior lens surface, iris, or corneal endothelium. The individuals without any evidence of pseudoexfoliation deposits on intraocular tissues were taken as the control group.

2.1. Genotyping. DNA extracts obtained from patients' blood by using the Gene Matrix Bio-Trace DNA Purification Kit (Eurx Ltd., Gdańsk) as part of previous PEX research were reused. The DNA concentration was measured using a spectrophotometer (DeNovix). Genotypes of the *CLU* SNPs, rs3087554, and rs2279590 were determined using a commercially available validated genotyping assay, TaqMan SNP genotyping assay (assay ID: C___1187215_10 i C___1842470_20) (Applied Biosystems) with the ViiA™ 7 real-time PCR system (Applied Biosystems) in accordance with the manufacturer's instructions. The DNA concentration in PCR reaction was 1 ng/μl in total volume 10 μl. Due to the small amount of the material, we were not able to determine both SNPs in all patients.

2.2. Statistical Analysis. The χ^2 test was performed to compare patient and control groups for possible associations between SNP genotype/allele frequency and disease state. The Arlequin software version 3.1 was used to determine the Hardy–Weinberg equilibrium and to estimate haplotype frequencies. Odds ratios were also calculated. The significance level for all statistical tests was 0.05. Statistical analysis was performed using Statistica software (version 12).

3. Results

Two SNPs of *CLU* were assessed: rs3087554 in 81 PEX patients and 91 controls and rs2279590 in 67 PEX patients and 50 controls. Due to the small amount of material, both SNPs were determined only in some probes. Allelic frequencies of SNPs rs3087554 and rs2279590 were in the Hardy–Weinberg equilibrium in both groups.

Allele and genotype frequencies of rs3087554 polymorphism are presented in Tables 1 and 2. There were no significant differences for both allele and genotype frequencies between PEX patients and controls; $p = 0.94$ and $p = 0.83$, respectively.

Allele and genotype frequencies of rs2279590 polymorphism are presented in Tables 3 and 4. Also for this polymorphism, there were no statistically significant differences in the frequency of alleles and genotypes between the groups; $p = 0.54$ and $p = 0.41$, respectively.

Table 1: Allele frequencies of rs3087554 polymorphisms in Polish population.

Allele	PEX patients		Controls		p
	$n = 162$	Frequency	$n = 182$	Frequency	
C	46	0.28	51	0.28	0.9388
T	116	0.72	131	0.72	

Table 2: Genotype frequencies of rs3087554 polymorphisms in Polish population.

Genotype	PEX patients		Controls		p
	$n = 81$	Frequency	$n = 91$	Frequency	
CC	7	0.09	6	0.07	
CT	32	0.40	39	0.43	0.8315
TT	42	0.52	46	0.51	

Table 3: Allele frequencies of rs2279590 polymorphisms in Polish population.

Allele	PEX patients		Controls	
	$n = 134$	Frequency	$n = 100$	Frequency
C	86	0.64	68	0.68
T	48	0.36	32	0.32

Table 4: Genotype frequencies of rs2279590 polymorphisms in Polish population.

Genotype	PEX patients		Controls	
	$n = 67$	Frequency	$n = 50$	Frequency
CC	29	0.43	21	0.42
CT	28	0.42	26	0.52
TT	10	0.15	3	0.06

The frequencies of *CLU* haplotypes are presented in Table 5.

The haplotypes distribution shows statistically significant difference between groups ($p = 0.03$). The haplotype (CT) more often was found in controls than in PEX patients ($p = 0.0484$), conferring an 18-fold decreased risk to the disease. The risk of patients with haplotype (CT) for developing PEX is 0.0545. The haplotype (TT) nearly doubles the risk of pseudoexfoliation, but this result was not statistically significant ($p = 0.0687$).

4. Discussion

Several lines of evidence, including regional clustering, transmission in two-generation families, familial aggregation, twin studies, and genetic linkage analyses, support a genetic predisposition to PEX [2–5, 15, 16]. The underlying genetic mechanisms are thought to be due to the disruption of regulatory genes that are involved in both the production and the breakdown of extracellular material in PEX. The results of several studies suggest that the cross-linking

Table 5: Frequencies of *CLU* haplotypes in PEX patients and controls.

Haplotype*	Estimated haplotype frequencies (%)		p value (test X^2)	OR (95% CI)	p value
	PEX patients ($n = 130$)	Controls ($n = 98$)			
TT	48 (37)	25 (26)	**0.0300**	1.7093 (0.9597–3.0443)	0.0687
TC	45 (35)	43 (44)		0.6772 (0.3953–1.1600)	0.1557
CC	37 (28)	24 (24)		1.2267 (0.6749–2.2298)	0.5028
CT	0 (0)	6 (6)		0.0545 (0.0030–0.9799)	**0.0484**

*Order of the alleles is as follows: rs308755 and rs2279590.

enzyme lysyl oxidase-like 1 (LOXL1) participates in the stabilization of newly synthesized elastic proteins and finally in the stable accumulation of this material [17–19]. Clusterin (CLU) has been supposed to potentially influence the manifestation of the PEX syndrome [20–22]. Clusterin is a multifunctional protein which plays a role in many cellular processes ranging from lipid transport, acting as extracellular chaperone, to cellular proliferation and death and was found in most tissues and body liquids. The gene encoding this protein is induced by heat and oxidative and mechanical stress. It was found to be present in exfoliation deposits on anterior lens capsules, but the iris is the tissue where CLU was the most abundantly expressed gene [23, 24]. Studies on clusterin have also indicated that its deficiency may result in PEX material accumulation [25]. In PEX eyes, a significant downregulation of clusterin mRNA was seen in all anterior segment tissues, when compared to normal eyes. Clusterin aqueous humour levels were also significantly reduced in PEX eyes [26]. The clusterin presence in PEX deposits and reduced amounts in aqueous humour of PEX patients led to an investigation of the genetic variants of the CLU gene and its association with PEX syndrome. Nine SNPs of the CLU gene in 86 cases of PEX and 2422 controls from the Blue Mountains Eye Study Cohort were genotyped by Burdon et al. [27]. They found that variants of CLU gene do not strongly modify the risk of PEX in this population, but one SNP (rs3087554) haplotype with a frequency of 7% may confer some increased risk. The significant age difference between cases and controls makes the power of this study lower; the mean age of cases was six years greater than that of the controls. When the age of controls was restricted to 73 years or older, the association between SNP rs3087554 and PEX was not found ($p = 0.072$). Krumbiegel et al. observed the association between PEX and SNP rs2279590 in intron 8 of the CLU gene in two German cohorts ($p = 0.0347$, $p = 0.0244$) [28]. This association was not confirmed in Italian patients ($p = 0.7173$). None of the other evaluated SNPs of CLU were associated with PEX in both populations. The results of Burdon et al. and Krumbiegel et al. indicate that common genetic variation of *CLU* is not a strong genetic modifier of the risk of PEX, but may confer some increased risk in some populations [27, 28]. Padhy et al. revealed a genetic association between CLU SNP rs2279590 and PEX in Indian population with a p value of 0.004 [29]. The high risk allele "G" at rs2279590 has an effect on clusterin mRNA expression. There was a two-fold higher clusterin mRNA level in "GG" genotyped individuals in comparison to "AA" genotyped individuals ($p = 0.039$). Five CLU SNPs (rs11136000, rs2279590, rs9331888, rs9331931, and rs3087554) were evaluated in the study of Dubey et al. [30]. These authors did not find any significant differences in the distributions of genotype and allele frequencies between PEX patients and control subjects in Indian population. The CLU SNP rs2279590 was evaluated in both aforementioned studies and their results were contradictory.

In our study, the possible association between two CLU SNPs, rs3087554 and rs2279590, and PEX syndrome in Polish population was assessed. There were no significant differences in the distributions of genotype and allele frequencies between PEX patients and controls. However, the distribution of haplotype frequencies differs between groups with p value equal 0.03. The haplotype (CT) was more common in control group than in PEX patients ($p = 0.0484$), conferring an 18-fold decreased risk to the disease. The risk of patients with this haplotype (CT) for developing PEX is equal 0.0545. Due to the small groups studied and the fact that haplotype (CT) was not found at all in the PEX group, the results should be quantified with caution. The haplotype (TT) almost doubles the risk of PEX, but this result was not statistically significant ($p = 0.0687$).

5. Conclusions

Our results indicate that CLU variants may contribute to the risk of PEX in Polish population.

Data Availability

The data used to support the findings of this study are available from the corresponding author upon request.

Conflicts of Interest

The authors declare that there are no conflicts of interest.

References

[1] R. Ritch and U. Schlotzer-Schrehardt, "Exfoliation (pseudoexfoliation) syndrome: toward a new understanding. Proceedings of the first international think tank," *Acta Ophthalmologica Scandinavica*, vol. 79, no. 2, pp. 213–217, 2001.

[2] R. R. Allingham, M. Loftsdottir, M. S. Gottfredsdottir et al., "Pseudoexfoliation syndrome in Icelandic families," *British Journal of Ophthalmology*, vol. 85, no. 6, pp. 702–707, 2001.

[3] J. M. Teikari, "Genetic factors in open angle (simple and capsular) glaucoma: a population based twin study," *Acta Ophthalmologica*, vol. 65, no. 6, pp. 715–720, 1987.

[4] M. S. Gottfredsdottir, T. Sverrisson, D. C. Musch, and E. Stefansson, "Chronic open-angle glaucoma and associated ophthalmic findings in monozygotic twins and their spouses in Iceland," *Journal of Glaucoma*, vol. 8, no. 2, pp. 134–139, 1999.

[5] J. G. Hardie, F. Mercieca, T. Fenech, and A. Cuschieri, "Familial pseudoexfoliation in gozo," *Eye*, vol. 19, no. 12, pp. 1280–1285, 2005.

[6] G. Thorleifsson, K. P. Magnusson, P. Sulem et al., "Common sequence variants in the LOXL1 gene confer susceptibility to exfoliation glaucoma," *Science*, vol. 317, no. 5843, pp. 1397–1400, 2007.

[7] J. A. Aragon-MartinR. Ritch et al., "Evaluation of LOXL1 gene polymorphisms in exfoliation syndrome and exfoliation glaucoma," *Molecular Vision*, vol. 4, pp. 533–541, 2008.

[8] B. J. Fan, L. Pasquale, C. L. Grosskreutz et al., "DNA sequence variants in the LOXL1 gene are associated with pseudoexfoliation glaucoma in a U.S. clinic-based population with broad ethnic diversity," *BMC Medical Genetics*, vol. 9, no. 1, p. 5, 2008.

[9] W. F. Gong, S. W. Chiang, L. J. Chen et al., "Evaluation of LOXL1 polymorphisms in primary open-angle glaucoma in southern and northern Chinese," *Molecular Vision*, vol. 14, pp. 2381–2389, 2008.

[10] R. K. Lee, "The molecular pathophysiology of pseudoexfoliation glaucoma," *Current Opinion in Ophthalmology*, vol. 19, no. 2, pp. 95–101, 2008.

[11] G. Malukiewicz, H. Lesiewska-Junk, K. Linkowska, M. Mielnik, T. Grzybowski, and N. Sulima, "Analysis of LOXL1 single nucleotide polymorphisms in polish population with pseudoexfoliation syndrome," *Acta Ophthalmologica*, vol. 89, pp. 64–66, 2010.

[12] V. L. Ramprasad, R. George, N. Soumittra, F. Sharmila, L. Vijaya, and G. Kumaramanickavel, "Association of non-synonymous single nucleotide polymorphisms in the LOXL1 gene with pseudoexfoliation syndrome in India," *Molecular Vision*, vol. 14, pp. 318–322, 2008.

[13] M. Tanito, M. Minami, M. Akahori et al., "LOXL1 variants in elderly Japanese patients with exfoliation syndrome/glaucoma, primary open-angle glaucoma, normal tension glaucoma, and cataract," *Molecular Vision*, vol. 14, pp. 1898–1905, 2008.

[14] M. Zenkel, E. Po¨schl, K. von der Mark et al., "Differential gene expression in pseudoexfoliation syndrome," *Investigative Opthalmology & Visual Science*, vol. 46, no. 10, pp. 3742–3752, 2005.

[15] K. F. Damji, H. S. Bains, E. Stefansson et al., "Is pseudoexfoliation syndrome inherited? A review of genetic and nongenetic factors and a new observation," *Ophthalmic Genetics*, vol. 19, no. 4, pp. 175–185, 1998.

[16] U. Schlotzer-Schrehardt, "Genetics and genomics of pseudoexfoliation syndrome/glaucoma," *Middle East African Journal of Ophthalmology*, vol. 18, no. 1, pp. 30–36, 2011.

[17] C. M. Kielty, T. J. Wess, L. Haston, J. L. Ashworth, M. J. Sherratt, and C. A. Shuttleworth, "Fibrillin-rich microfibrils: elastic biopolymers of the extracellular matrix," *Journal of Muscle Research and Cell Motility*, vol. 23, no. 5-6, pp. 581–596, 2002.

[18] X. Liu, Y. Zhao, J. Gao et al., "Elastic fiber homeostasis requires lysyl oxidase-like 1 protein," *Nature Genetics*, vol. 36, no. 2, pp. 178–182, 2004.

[19] L. Thomassin, C. C. Werneck, T. J. Broekelmann et al., "The pro-regions of lysyl oxidase and lysyl oxidase-like 1 are required for deposition onto elastic fibers," *Journal of Biological Chemistry*, vol. 280, no. 52, pp. 42848–42855, 2005.

[20] J. Sein, A. Galor, A. Sheth, J. Kruh, L. R. Pasquale, and C. L. Karp, "Exfoliation syndrome," *Current Opinion in Ophthalmology*, vol. 24, no. 2, pp. 167–174, 2013.

[21] M. Zenkel, A. Krysta, F. Pasutto, A. Juenemann, F. E. Kruse, and U. Schlötzer-Schrehardt, "Regulation of lysyl oxidase-like 1 (LOXL1) and elastin-related genes by pathogenic factors associated with pseudoexfoliation syndrome," *Investigative Opthalmology & Visual Science*, vol. 52, no. 11, pp. 8488–8495, 2011.

[22] M. Zenkel, "Extracellular matrix regulation and dysregulation in exfoliation syndrome," *Journal of Glaucoma*, vol. 1, pp. 24–28, 2018.

[23] T. Borrás, "The cellular and molecular biology of the Iris, an overlooked tissue," *Journal of Glaucoma*, vol. 23, pp. S39–S42, 2014.

[24] M. R. Wilson and S. B. Easterbrook-Smith, "Clusterin is a secreted mammalian chaperone," *Trends in Biochemical Sciences*, vol. 25, no. 3, pp. 95–98, 2000.

[25] E. Elhawy, G. Kamthan, C. Q. Dong, and J. Danias, "Pseudoexfoliation syndrome, a systemic disorder with ocular manifestations," *Human Genomics*, vol. 6, no. 1, p. 22, 2012.

[26] M. Zenkel, F. E. Kruse, A. G. Ju¨nemann, G. O. H. Naumann, and U. Schlo¨tzer-Schrehardt, "Clusterin deficiency in eyes with pseudoexfoliation syndrome may be implicated in the aggregation and deposition of pseudoexfoliative material," *Investigative Opthalmology & Visual Science*, vol. 47, no. 5, pp. 1982–1990, 2006.

[27] K. P. Burdon, S. Sharma, A. W. Hewitt et al., "Genetic analysis of the clusterin gene in pseudoexfoliation syndrome," *Molecular Vision*, vol. 14, pp. 1727–1736, 2008.

[28] M. Krumbiegel, F. Pasutto, C. Y. Mardin et al., "Exploring functional candidate genes for genetic association in German patients with pseudoexfoliation syndrome and pseudoexfoliation glaucoma," *Investigative Opthalmology & Visual Science*, vol. 50, no. 6, pp. 2796–2801, 2009.

[29] B. Padhy, G. G. Nanda, M. Chowdhury, D. Padhi, A. Rao, and D. P. Alone, "Role of an extracellular chaperone, clusterin in the pathogenesis of pseudoexfoliation syndrome and pseudoexfoliation glaucoma," *Experimental Eye Research*, vol. 127, pp. 69–76, 2014.

[30] S. K. Dubey, J. F. Hejtmancik, S. R. Krishnadas, R. Sharmila, A. Haripriya, and P. Sundaresan, "Evaluation of genetic polymorphisms in clusterin and tumor necrosis factor-alpha genes in South Indian individuals with pseudoexfoliation syndrome," *Current Eye Research*, vol. 40, no. 12, pp. 1218–1224, 2015.

Hindawi
Journal of Ophthalmology
Volume 2019, Article ID 7604396, 11 pages
https://doi.org/10.1155/2019/7604396

Research Article

Repressed Wnt Signaling Accelerates the Aging Process in Mouse Eyes

Yujin Zhang,[1] Joseph Jeffrey,[2] Fei Dong,[2] Jianhua Zhang,[2] Winston W.-Y. Kao,[2] Chia-Yang Liu,[1] and Yong Yuan[2]

[1]*School of Optometry, Indiana University, 800 East Atwater Avenue, Bloomington, IN 47405, USA*
[2]*Crawley Vision Research Laboratory, Department of Ophthalmology, College of Medicine, University of Cincinnati, Cincinnati, OH, USA*

Correspondence should be addressed to Chia-Yang Liu; liuchia@iu.edu and Yong Yuan; yuany@ucmail.uc.edu

Received 26 February 2019; Accepted 26 May 2019; Published 17 June 2019

Academic Editor: Alejandro Cerviño

Purpose. Ocular aging is a natural process of functional decline in vision. When the process reaches a point that compromised vision affects normal daily activity, it manifests as age-related ocular diseases, such as age-related macular degeneration, cataracts, glaucoma, and pseudoexfoliation syndrome. We previously reported that repressed Wnt signaling accelerated the maturation of corneal epithelium during tissue development. Here, we explore the hypothesis that repressed Wnt signaling is associated with accelerated aging in mouse eyes. *Methods*. Wnt ligand antagonist secreted frizzled-related protein 1 (sFRP1) was expressed in the corneal stroma by a tissue-specific, inducible, bitransgenic system. Tissue structure was analyzed for signs of aging. Signal transduction analysis was performed to determine the cellular response to sFRP1. *Results*. Mouse eyes with sFRP1 expression showed signs of accelerated aging, resembling those found in pseudoexfoliation (PEX) syndrome, a known age-related disease. Specific findings include granular deposition on the surface of the anterior lens capsule, pigment loss from the anterior surface of the iris, the presence of fibrillary material in the anterior chamber, and changes in cell size (polymegethism) and shape (pleomorphism) of the corneal endothelial cells. *In vitro* studies demonstrated that sFRP1 did not inhibit Wnt5a function and that cells responded to sFRP1 and Wnt5a in a very similar manner. *Conclusion*. The expression of sFRP1 accelerates the aging process in mouse eyes and future studies are warranted to elucidate the underlying mechanisms.

1. Introduction

Aging is a natural process that affects the function of many organs, including eyes. Patients usually experience the first sign of ocular aging when they have difficulty reading fine print. This age-related condition, called presbyopia, is caused by gradual hardening of the lens [1]. Like cataracts, the defect can be corrected by corrective lens, either inside the eyes or in front of the eyes. Other age-related conditions will manifest into debilitating eye diseases, such as age-related macular degeneration, cataracts, diabetic eye disease, glaucoma, and pseudoexfoliation (PEX) syndrome. These age-related eye diseases account for most cases of permanent vision loss and blindness. Determining the mechanism behind these conditions can provide new lifestyle and treatment guidelines that delay the onset of diseases as well as treat them.

Several signaling pathways have been implicated in aging. The first one is the target of rapamycin (mTOR) pathway. Inhibition of mTOR activity with rapamycin doubled the lifespan of simple organisms like yeast. Rapamycin treatment also extended the life of mice by about 15% percent [2]. Because mTOR serves as the master nutrient and energy sensor, this may also explain the effect of calorie restriction on aging. The second pathway is the Wnt signaling pathway. Data from *C. elegans* studies indicate that Wnt signaling plays a dual role in aging. Specifically, mom-2/Wnt and cwn-2/Wnt mutants live 35% and 18% longer compared to wild-type controls. In contrast, lin-44/Wnt and egl-20/Wnt mutants live 30% and 25% shorter than their

wild-type controls [3]. Further examination of the Wnt signaling pathway may provide information on the processes involved in ocular aging.

Previously, we reported that loss of canonical Wnt function during corneal development accelerated the maturation of corneal epithelium [4]. Wnt signaling is involved in organogenesis and homeostasis. There are several Wnt signaling pathways, including canonical Wnt signaling and noncanonical Wnt signaling. A delicate balance between the two Wnt signaling pathways is key to achieving normal tissue structure and function. Canonical Wnt signaling is activated through the binding of Wnt ligands (such as Wnt3a and Wnt7) to their coreceptors (LRP5 and LRP6) [5]. This releases beta-catenin from a destruction complex and subsequently allows it to drive the expression of target genes by binding to TCF/LEF transcription factors. On the other hand, noncanonical Wnt signaling is activated through the binding of Wnt ligands (mainly Wnt5a and Wnt4) to their receptors (ROR2 or VANGL2) [6]. This triggers the activation of a panel of small GTPases, such as RhoA, Rac1, and CDC42 [7]. Subsequently, Rho-associated kinase (ROCK) is activated and transduces the signal to myosin light chain to modulate cytoskeleton structure. There have been numerous findings that the two Wnt signaling pathways inhibit each other in different tissues [8, 9]. Wnt signaling has been implicated in the development and aging process of many organs. Because loss of canonical Wnt signaling, or on the other hand increased noncanonical Wnt signaling, is associated with aging [10, 11], we set out to explore if repressed canonical Wnt signaling in adult mice can accelerate the aging process.

In our study, canonical Wnt signaling was repressed by the expression of a Wnt ligand antagonist called secreted frizzled-related protein 1 (sFRP1) in the corneal stroma. In this model, we found signs consistent with pseudoexfoliation (PEX) syndrome, an age-related disease that affects the eyes and many other organs [12]. Hallmarks of PEX syndrome observed in this model include granular deposition on the surface of the anterior lens capsule, iris stromal atrophy, accumulation of fibrillary material in the anterior chamber, and disorganized ciliary zonules. Furthermore, *in vitro* findings demonstrated that sFRP1 can stimulate the activation of noncanonical Wnt signaling. These results suggest that disruption of Wnt signaling homeostasis in the eye is associated with accelerated aging.

2. Methods

2.1. Animal Experiments. To express sFRP1 in mouse corneal stroma, bitransgenic mice (KR-sFRP1) were generated by breeding keratocan/rtTA knock-in (KR/rtTA) mice [13] with tetracycline-On promoter-driven sFRP1 (Tet-O-sFRP1) [14]. Tet-O-sFRP1 mice were a gift from Dr. Thierry Couffinhal (Hospital Haut-Leveque, Pessac, France). The knock-in $Kera^{RT}$ mice were crossed with an enhanced GFP (EGFP) reporter mouse line, *tet-o-Hist1H$_{2B}$-EGFP* (*TH$_{2B}$-EGFP*, Stock number: 005104; Jackson Laboratories) [15] to obtain the double transgenic mice $Kera^{RT}$/*TH$_{2B}$-EGFP*. Genotyping of double transgenic mice was accomplished by PCR. The knock-in $Kera^{RT}$ mice were identified by PCR using the following primers:

(i) Kera-F1, 5′-TGGTGGCTTGCTTCAAGCTTCT-TC-3′

(ii) Kera-R1, 5′-TATCCAACTCACAACGTGGCAC-TG-3′

(iii) Kera-R2, 5′-GGAGTCTGCACTACCAGTACTC-AT-3′

The Tet-O-sFRP1 mice were genotyped with the following primers:

(i) SFRP1F: 5′-TGT GTC CTC CAT GTG ACA ACG AGC-3′

(ii) SFRP1R: 5′-TGA GAT GAG TTT TTG TTC GGG C-3′

Animal care and use conformed to the ARVO Statement for the Use of Animals in Ophthalmic and Vision Research. All animal protocols were approved by the Institutional Animal Care and Use Committee (IACUC) of the University of Cincinnati. The mice used in this project were housed in AALAC-approved animal facilities within the University of Cincinnati, College of Medicine. Programs of animal husbandry, preventive medicine, and pre- and postsurgical care have been developed to assure that adequate veterinary care is provided at all times. Complete veterinary, diagnostic, and clinical support services are available.

KR-sFRP1 bitransgenic mice ($n = 8$) and their single transgenic control littermates ($n = 8$) were housed in the same cage. At the age of 4 months, all mice were fed with Dox chow (1 g/kg; Custom Animal Diets, Bangor, PA, USA) for 2 months. At the age of 6 months, all mice were anesthetized by intraperitoneal injection of ketamine hydrochloride (0.1 mg/gm body weight) and xylazine (0.02 mg/gm body weight) and examined by slit lamp and stereomicroscopy.

2.2. Slit-Lamp Examination. Slit-lamp examinations were performed on a modified Topcon slit lamp. A beam splitter (BS7030-TOPCON) was installed in front of the eyepieces. An AccuBeam Video Adapter was attached to the beam splitter. A high-definition digital camera was mounted on the Video Adapter. Animals were anesthetized and pupils were dilated. A vertical broad slit-lamp beam was placed on the pupillary margin, and still images were taken under the same beam intensity and exposure time.

2.3. Stereomicroscopy and Iris Angiography. Fluorescein Ak-Fluor (10%; Akorn Pharmaceuticals), diluted with sterile 1 × DPBS (final concentration 10 mg/mL), was administered by bolus injection (50 μL) into the peritoneum of anesthetized mice. For iris angiography, the nondilated eyes were observed using Zeiss Axio Zoom.V16 stereo fluorescence microscope (Oberkochen, Germany).

2.4. Histology and Immunostaining. Enucleated eyes were fixed in Davidson's fixation overnight and dehydrated

through ethanol steps. Dehydrated eyes were immersed in paraffin overnight, then embedded and cut into sections after 24 hours. The sections were deparaffinized and rehydrated in a graded ethanol series (95%, 75% ethanol, and PBS for 3 minutes each). Rehydrated slides underwent either hematoxylin and eosin (H&E) staining, periodic acid-Schiff (PAS) staining, or immunofluorescence staining. For immunofluorescence staining, an antigen retrieval step was performed by boiling the slides in citrate buffer for 10 minutes. The following antibodies were used in the study: rabbit anti-LOXL1 (Novus Biologicals, NBP182827), rabbit anti-sFRP1 (Novus Biologicals, NBP1-02432), and Cy5-labeled goat anti-rabbit IgG secondary antibody (Invitrogen, A10523). Fluorescent images were taken with a Leica confocal microscope under 63x oil objective lens. For corneal whole-mount staining, mice were euthanatized, and the eyeball was fixed in 4% paraformaldehyde in 0.1 M phosphate buffer, pH 7.4, at 4°C overnight. After removal of the iris, lens, and posterior tissues, the cornea was incubated with 0.1% Triton X-100 in PBS for 1 hour and stained with Alexa Fluor 555 Phalloidin (ThermoFisher, A34055) at room temperature and counterstained with DAPI. Images were taken in the central region of the cornea by a Leica confocal microscope. The images were analyzed by CellProfiler software [16]. Two pipelines were developed to determine the size of the cells and the stress fiber distribution within each cell.

2.5. Cell Culture and Adenovirus-Mediated Gene Expression. Primary human corneal stromal cells were established from a donor cornea that was not suitable for transplantation. The primary cells were maintained in SF-1 hMSC medium (United Healthcare Inc., Taiwan). Full-length mouse Wnt5a cDNA (pLNC Wnt-5aHA) was a gift from Jan Kitajewski (Addgene plasmid #18032) [17], and mouse sFRP1 cDNA XE141 sFRP-1-CS2+ was a gift from Randall Moon (Addgene plasmid #16693; http://n2t.net/addgene:16693; RRID : Addgene_16693). These cDNA constructs were used to generate the recombinant adenovirus vector according to a published protocol [18]. Another recombinant adenovirus coding GFP alone (AdGFP) was used as a control. AdGFP, AdsFRP1, and AdWnt5a viruses were amplified and purified according to the protocol.

Cells were seeded into Corning™ 96-Well Half Area High Content Imaging Film Bottom Microplate and were infected with AdGFP or AdsFRP1 after 24 hours. 72 hours after infection, the cells were fixed for 20 minutes in 1% glutaraldehyde. Cells were permeabilized with 0.2% Triton X-100 in PBS and were stained with an antibody against sFRP1 (Novus Biologicals, NBP1-02432), CHOP (Cell Signaling, 5554S), and ROR2 (Cell Signaling, 88639S). The images were taken with an epifluorescence microscope (Axioscop2, Carl Zeiss, München-Hallbergmoos, Germany) and were photographed with a digital camera system (Axiocam, Carl Zeiss).

2.6. Real-Time qRT-PCR. Total RNA was isolated from cultured cells with the RNeasy Mini Kit (Qiagen). 5 μg of total RNA was reverse transcribed with Maxima First Strand cDNA Synthesis Kit for qRT-PCR (Fermentas). qRT-PCRs were performed using the CFX96™ real-time PCR system (Bio-Rad) operated by CFX Manager™ software. Primer sequences used in the study were as follows:

(i) hCHOPf: TGGATCAGTCTGGAAAAGCA
(ii) hCHOPr: AGCCAAAATCAGAGCTGGAA
(iii) hMMP1f: TTGTGGCCAGAAAACAGAAA
(iv) hMMP1r: TTCGGGGAGAAGTGATGTTC

A panel of 8 housekeeping genes (Real Time Primers, Cat#HKK1) was used to normalize the expression levels.

2.7. Statistical Analysis. Unpaired Student's *t*-test was used to determine the statistical significance (*P* value) of the mean values for 2-sample comparisons. Values shown on the graphs represent the mean ± SD (standard derivation). A difference between average means where $P < 0.05$ was deemed to be statistically significant.

3. Results

3.1. Macroscopic Signs of Accelerated Aging. To express sFRP1 in mouse corneal stroma, bitransgenic mice were generated by breeding keratocan/rtTA knock-in (KR/rtTA) mice with tetracycline-On promoter-driven sFRP1 (Tet-O-sFRP1). Bitransgenic mice (KR/sFRP1) expressed sFRP1 in the corneal stroma upon doxycycline induction (Figure 1(a)). To verify that the target gene can be expressed in the corneal stroma in a doxycycline-dependent manner, we bred the driver mouse KR/rtTA with a reporter mouse (Tet-O-histone GFP). One week after doxycycline induction, GFP-positive cells were found in the corneas (Figure 1(b)). Two months after doxycycline induction, KR/sFRP1 mice and their control littermates were used to examine the expression of sFRP1. As shown in Figures 1(c) and 1(d), the control eyes did not express sFRP1 while there were strong sFRP1-positive cells in the corneal stroma of KR/sFRP1 eyes, confirming the expression of sFRP1 in the corneal stroma of our doxycycline-induced bitransgenic mice.

Two months after doxycycline induction, KR/sFRP1 mice and their control littermates were examined. Using qualitative levels of grey hair as a readout for aging, we set out to examine the amount of grey hair present on the backs of mice. At the age of six months, control mice had few grey hairs on their back (Figure 2(a), while KR/sFRP1 mice had apparently more grey hairs (Figure 2(b)). Under the slit lamp, the anterior lens capsule of the control mice appeared smooth and uniform (Figures 2(c) and 2(e)). In the KR/sFRP1 eyes, surface roughness was revealed by side illumination (Figure 2(a)). The granular characteristics presented as bright reflections and dark shadows, which were more easily appreciated in higher magnification image (Figure 2(f)). These macroscopic features are consistent with our previous findings in mouse eyes with pseudoexfoliation syndrome-like phenotypes [19].

Finally, iris atrophy was observed by live stereoscopy. Figure 3(a) represents the normal structure of the anterior

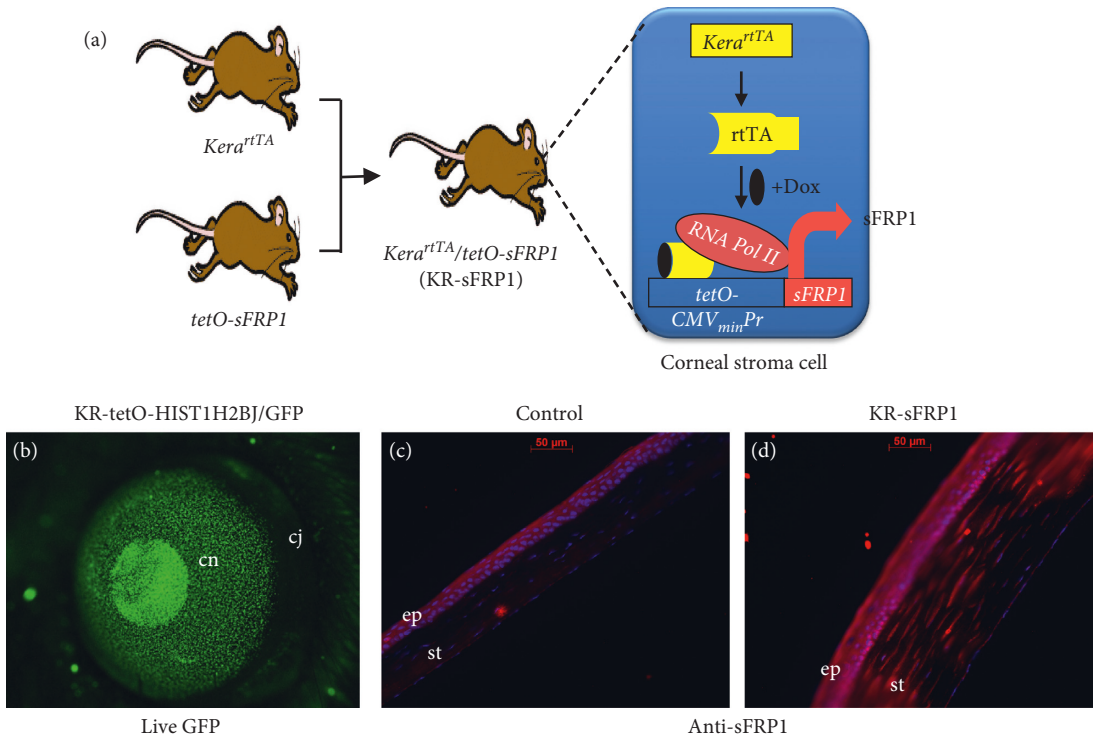

Figure 1: Inducible expression of sFRP1 in corneal stroma. (a) Diagram showing the generation of bitransgenic mouse strain keratocan rtTA/Tet-O-sFRP1 (KR/sFRP1). Bitransgenic mice were generated by breeding keratocan/rtTA knock-in (KR/rtTA) mice with tetracycline-On promoter-driven sFRP1 (Tet-O-sFRP1). Bitransgenic mice expressed sFRP1 in corneal stroma upon doxycycline induction. (b) Corneal stromal expression of reporter gene GFP in adult KR/GFP mice. (c, d) Immunostaining verified that only bitransgenic KR/sFRP1 mice were positive for sFRP1 in the corneal stroma. Abbreviations: cn = cornea, cj = conjunctiva, ep = epithelium, and st = stroma.

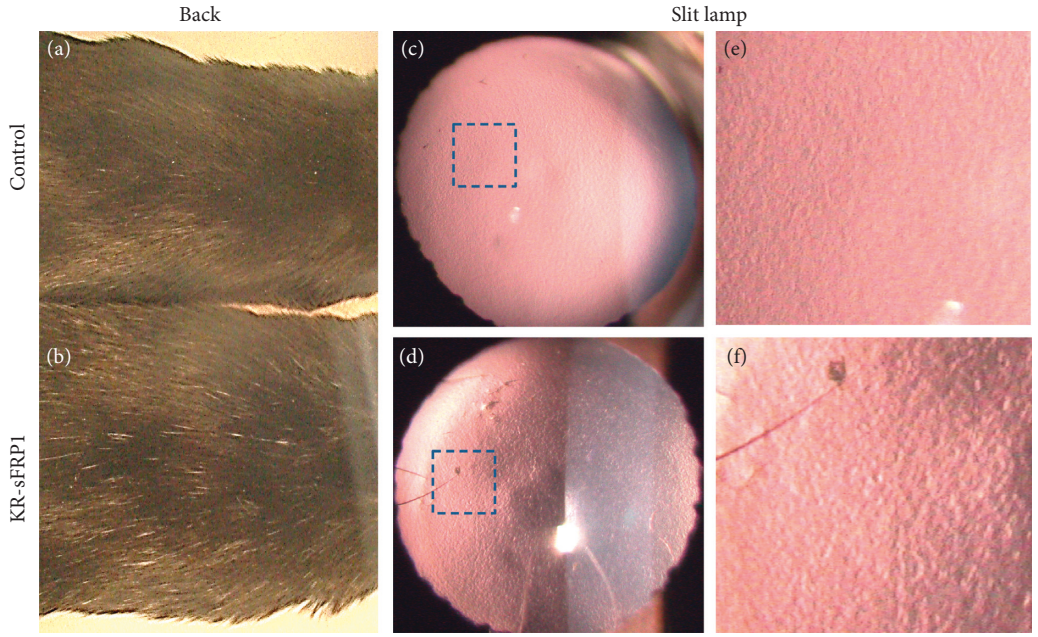

Figure 2: Signs of aging in KR/sFRP1 mice. (a, b) KR/sFRP1 mice had more grey hairs on the back than their control littermates, serving as a qualitative readout of aging. (c, d) KR/sFRP1 mouse eyes exhibited a rough surface on the anterior lens capsule. The granular deposits were more apparent in high-magnification images (e, f).

iris surface, as seen in control eyes: large radial vessels were half-buried in the stroma while networks of smaller vessels were mostly buried. The surface area between vessels was smooth and uniform. In the KR/sFRP1 eyes, the blood vessels were bulging and tortuous (Figure 3(b)). A higher degree of stromal degeneration was apparent in pupillary

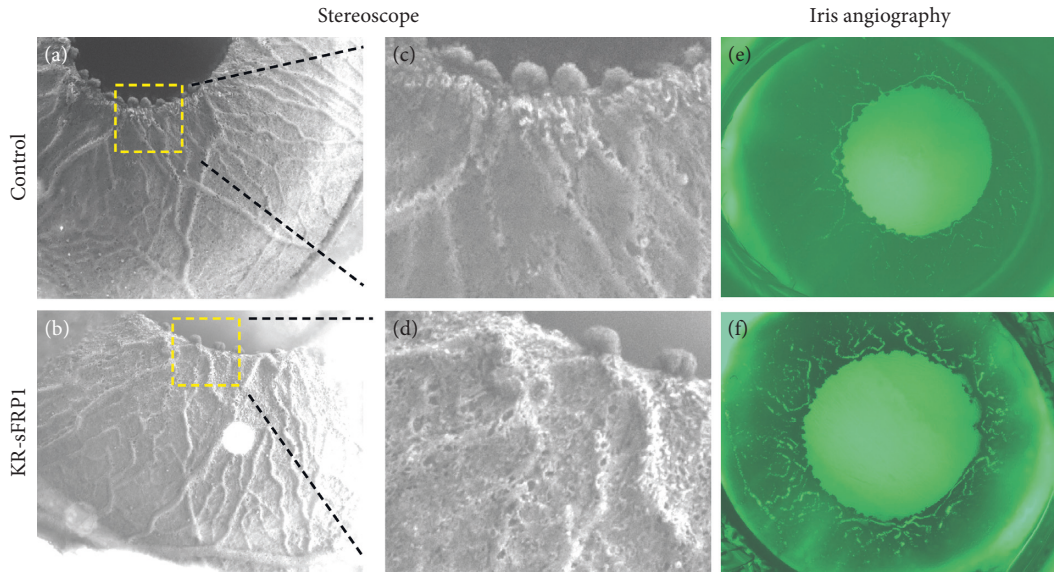

Figure 3: Signs of iris stromal atrophy in KR/sFRP1 mice. Overall surface texture of irises for control (a) and KR/sFRP1 (b) mice. High-magnification images revealed the difference between the two (c, d). In the control eyes, the surface area between vessels was smooth and uniform. In the KR/sFRP1 eyes, the blood vessels were bulging and tortuous. Iris angiography images of the control (e) and KR/sFRP1 (f) mice further demonstrate tortuous vessels. The atrophic findings of the KR/sFRP1 irises further demonstrate ocular findings consistent with aging.

margins. High-magnification images showed a few small holes along the blood vessels on the iris surface of the control eyes (Figure 3(c)). In the KR/sFRP1 eyes, the size and the number of the holes increased, forming a sponge-like surface texture (Figure 3(d)). Additionally, the loss of anterior iris surface material was verified by angiography. In normal control eyes, the iris blood vessels were buried in the heavily pigmented stroma, making them invisible under fluorescent microscope (Figure 3(e)). The only visible signals were in the pupillary margin, where the vessels were exposed to the surface. In KR/sFRP1 eyes, tortuous vasculature structures were clearly visible in the middle region of the iris (Figure 3(f)). The atrophic findings of the KR/sFRP1 irises further demonstrate ocular findings consistent with aging.

3.2. Microscopic Signs of Accelerated Aging. Microscopic features of aging were examined by histological examination. The macroscopic features of the KR/sFRP1 eyes, such as granular deposition and iris atrophy, indicated signs of pseudoexfoliation (PEX) syndrome, an age-related disease. Microscopic studies were conducted to further document signs of PEX syndrome. As shown in Figure 4, the anterior chamber of the control eyes was free of aggregates (Figure 4(a)), while the KR/sFRP1 eyes contained fibrillar material (Figure 4(b)). Clumps of abnormal fibrillar material were found adhering to the apical surface of the endothelial cells and more were found floating just beneath the corneal endothelium. Another feature of PEX is the weakness of zonules [20]. The structure of zonules was revealed by overexposing the H&E images. In the control eyes, the main zonular bundles were straight and compact (Figure 4(c)). In the KR/sFRP1 eyes, the zonular bundles were curly, loose, disorganized, and decorated with granular material. Periodic acid-Schiff (PAS) staining verified the presence of proteoglycans in the zonule. Scanning of PAS-positive zonular fibers confirmed the structural difference of zonules between the control and KR/sFRP1 eyes (Figures 4(e) and 4(f)). These histological findings correlate with PEX phenotypes and indicate evidence of ocular aging.

Further microscopic examination was conducted to analyze the expression of lysyl oxidase-like 1 (LOXL1). LOXL1 is a member of the lysyl oxidase family of enzymes that catalyze cross-linking in the extracellular matrix (ECM). LOXL1 is a known component of ECM and therefore also of PEX material [21]. As shown in Figure 5(a), LOXL1 was weakly stained within the corneal epithelial cells in control eyes. LOXL1 formed a dense, uniform layer in Descemet's membrane (Figure 5(a)). In the KR/sFRP1 eyes, however, LOXL1 expression was increased in the corneal epithelium with a perinuclear distribution pattern (Figures 5(c) and 5(d)). The well-organized LOXL1-positive layer was not seen in Descemet's membrane. Strong positive staining was found between as well as on the apical side of the endothelial cells. The LOXL1-positive aggregates can also be found detaching from the endothelium and floating in the anterior chamber. These data further confirmed that the KR/sFRP1 eyes had some ocular features of PEX syndrome.

Another sign of aging eyes, as well as sign of PEX syndrome, is the change in cell size (polymegethism) and shape (pleomorphism) of the corneal endothelial cells [22]. Whole-mount staining was performed on two control corneas and four KR/sFRP1 corneas. The corneas were stained with phalloidin to reveal the cytoskeleton structure. In control corneas, endothelial cytoskeleton was arranged in linear circumferential strands that formed a hexagonal array (Figure 6(a)). In KR/sFRP1 corneas, circumferential strands were loosely arranged, resulting in increased bandwidth with

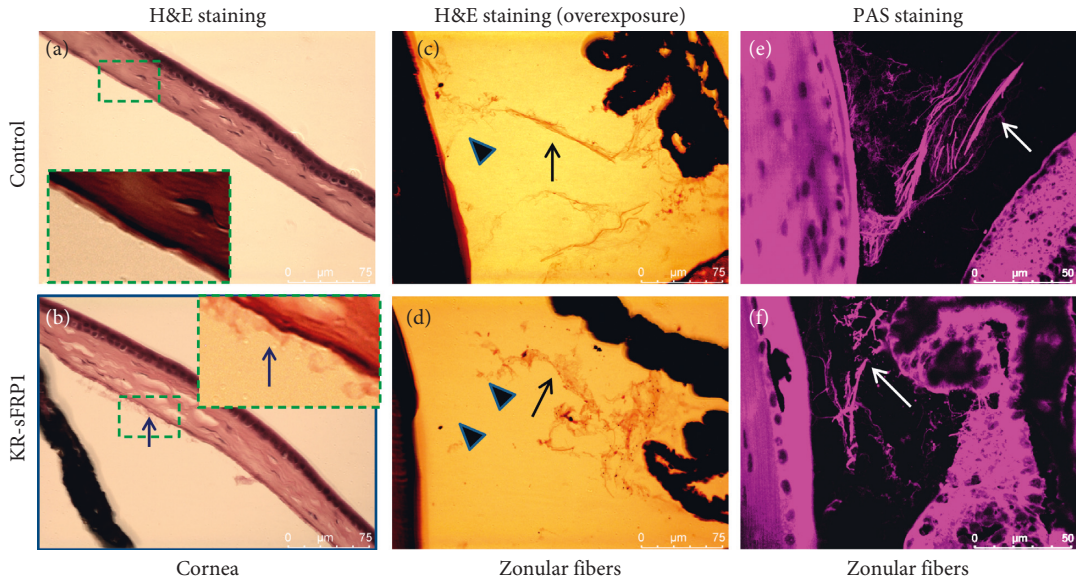

Figure 4: sFRP1 causes fibrillary accumulation in the anterior chamber and weakened zonules. (a, b) H&E staining of the control and KR/sFRP1 eyes. Arrow in the highlighted box indicates the fibrillary material in the anterior chamber, as evidenced in KR/sFRP1 eyes but not controls. (c) and (d) are overexposure images to reveal zonular structure (arrows). In the control eyes, the main zonular bundles were straight and compact. In the KR/sFRP1 eyes, the zonular bundles were curly, loose, disorganized, and decorated with granular material. (e) and (f) are confocal scanning images of PAS staining, which confirmed the presence of proteoglycans. Arrows indicate the differences in zonular structure.

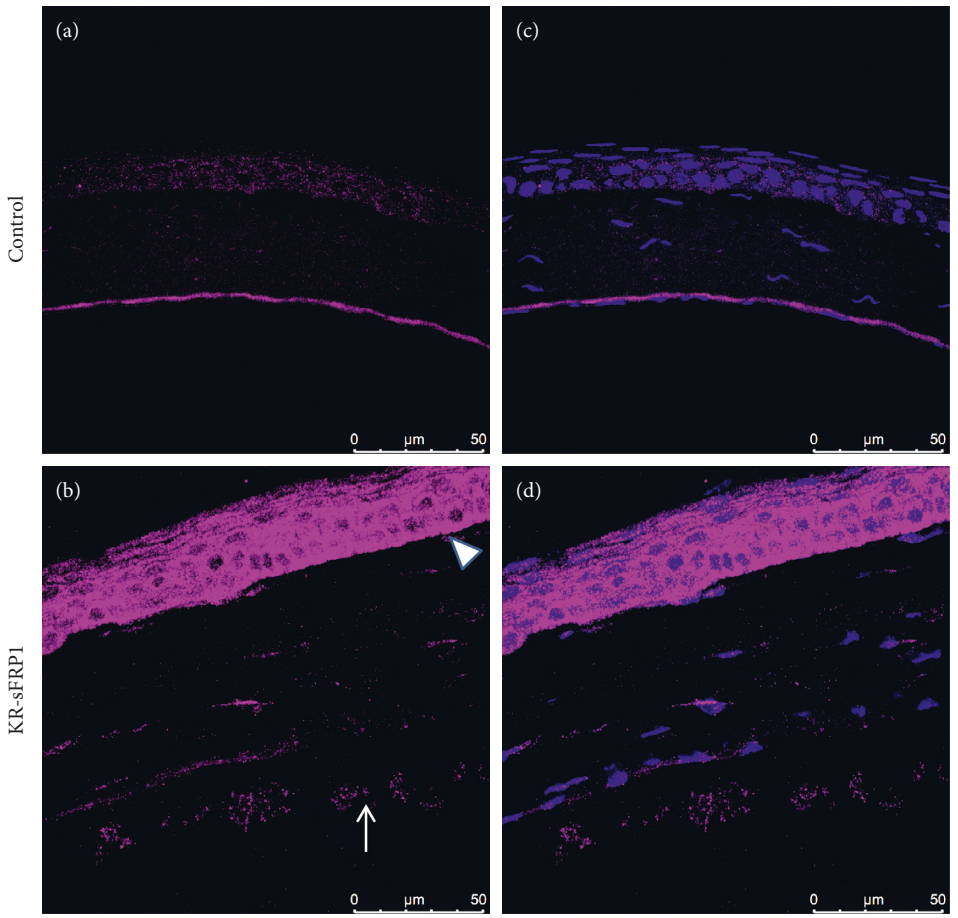

Figure 5: Exfoliation-like material is LOXL1-positive. LOXL1 immunostaining of control corneas (a) revealed LOXL1-positive bands on the corneal endothelium (a, c). KR/sFRP1 corneas exhibited increased LOXL1 expression in the corneal epithelium. LOXL1-positive aggregates can be found in the anterior chamber (arrow in b). These findings are highly consistent with PEX syndrome phenotypes.

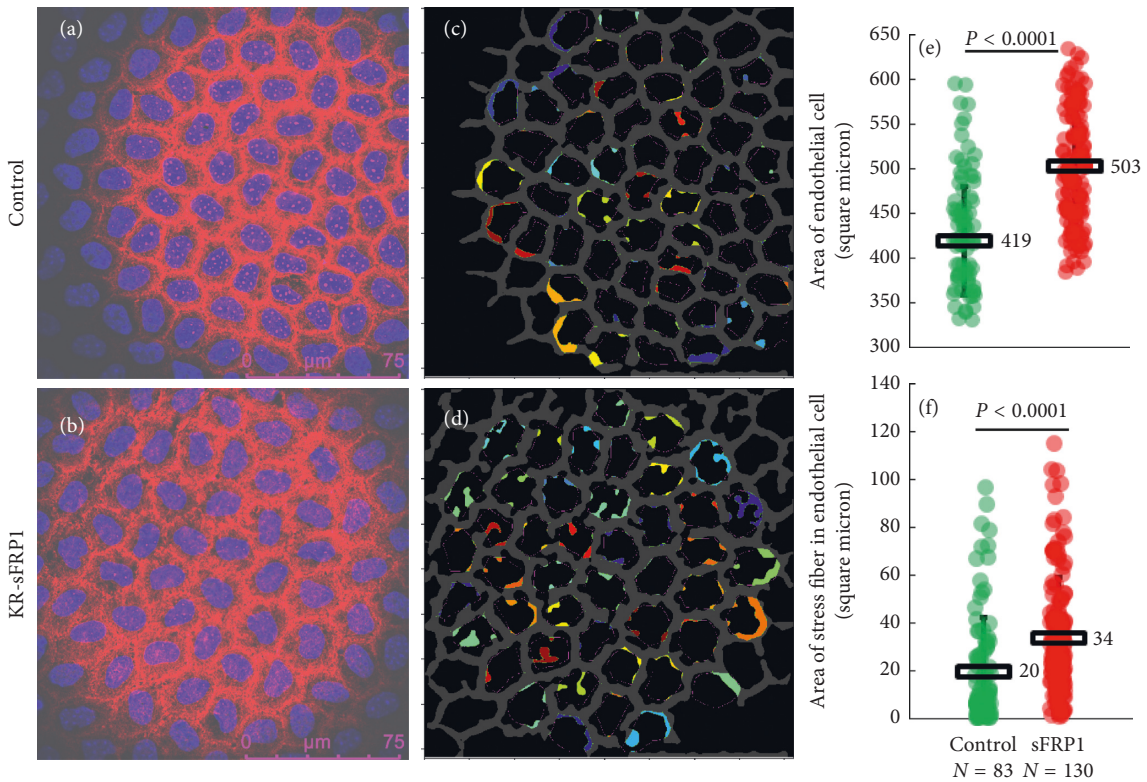

Figure 6: sFRP1 induces polymegethism and pleomorphism in the corneal endothelium. Original (a, b) and processed (c, d) images of the corneal endothelium of the control and KR/sFRP1 mice. Colored nodules represent the stress fibers (c, d). The structure from the control corneas was uniform with very few broken strands, while the thickness of the intercellular cytoskeleton bands varied greatly in KR/sFRP1 corneas with many broken strands. The size of the cells and the stress fibers is summarized in (e) and (f). The average size of corneal endothelial cells was 419 ± 60 square microns ($n = 83$) vs. 503 ± 63 square microns ($n = 130$) in KR/sFRP1 eyes ($P < 0.0001$). The average size of stress fiber per cell was also significantly increased in KR/sFRP1 eyes (20 ± 23 square microns ($n = 83$) vs. 34 ± 25 square microns ($n = 130$); $P < 0.0001$). These findings demonstrate polymegethism and pleomorphism consistent with aging eyes.

some stress fibers extending towards the nuclei (Figure 6(b)). CellProfiler software identified the overall structure of the apical cytoskeleton networks of the endothelium and presented it as a grey "fishnet-like" structure. The structure from the control corneas was uniform with very few broken strands (Figure 6(c)), while the thickness of the intercellular cytoskeleton bands varied greatly in KR/sFRP1 corneas with many broken strands (Figure 6(d)). The colored nodules next to the intercellular cytoskeleton structure represented the stress fibers extending toward the center of the cell (Figures 6(c) and 6(d)). This stress fiber formation was more apparent in KR/sFRP1 eyes. Figures 6(e) and 6(f) summarize the size of the cells and the size of stress fibers, respectively. In control eyes, the average size of corneal endothelial cells was 419 ± 60 square microns, $n = 83$. In KR/sFRP1 eyes, the average size of corneal endothelial cells was 503 ± 63 square microns, $n = 130$. The difference between the means was statistically different ($P < 0.0001$). In control eyes, the average size of stress fiber per cell was 20 ± 23 square microns, $n = 83$. In KR/sFRP1 eyes, the average size of stress fiber per cell was 34 ± 25 square microns, $n = 130$. Again, the difference between the means was statistically different ($P < 0.0001$). These findings demonstrate polymegethism and pleomorphism consistent with aging eyes.

3.3. Potential Mechanisms for sFRP1-Induced Aging. sFRP1 was discovered as a naturally occurring secreted antagonist of Wnt signaling [23]. Later studies uncovered more complicated roles of sFRP1 in modulation of Wnt signaling: it acts as a biphasic modulator of Wnt signaling, counteracting Wnt-induced effects at high concentrations and promoting them at lower concentrations [24]. Because there are several Wnt signaling pathways, the balance between the canonical and noncanonical Wnt signaling is carefully regulated. Most studies show that at high concentrations, sFRP1 can inhibit canonical Wnt signaling [25, 26], which in turn favors heightened noncanonical Wnt signaling. We performed an *in vitro* study to determine if sFRP1 can also inhibit noncanonical Wnt signaling. Primary human corneal stromal cells were infected with adenovirus coding sFRP1 and Wnt5a either separately or together. Noncanonical signaling was evaluated by measuring several downstream targets: CHOP, MMP1, and ROR2 [27]. Compared with control AdGFP-infected cells, cells infected with AdWnt5a exhibited an increase in CHOP and MMP1 expression (red bar in Figure 7(a)). AdsFRP1-infected cells also exhibited increased expression of CHOP and MMP1 (purple bar in Figure 7(a)). The combination of AdWnt5a and AdsFRP1 yielded a greater degree of increased

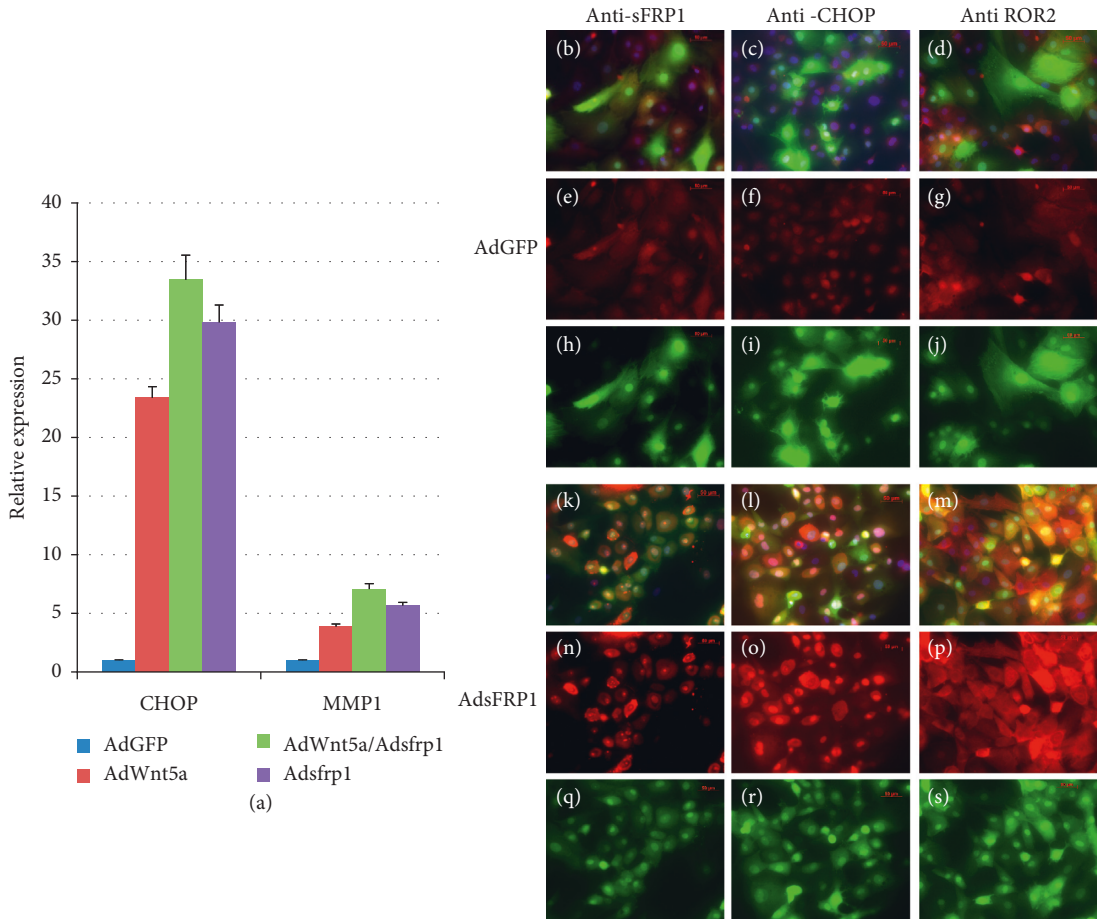

Figure 7: sFRP1 activates the noncanonical Wnt signaling. (a) Real-time RT-PCR demonstrated that both Wnt5a and sFRP1 can stimulate the expression of CHOP and MMP1 (red and purple bars). Stronger effects were observed when cells were treated with Wnt5a and sFRP1 together (green bar). Immunostaining demonstrated that sFRP1 stimulates the expression of CHOP and ROR2 (red channel) ((k)–(s)). Upper panels were cells infected with AdGFP control virus, and lower panels were cells infected with AdsFRP1 virus. All adenoviruses also expressed GFP. Combined channels revealed the expression of protein of interest (red) in adenovirus-infected cells (green) ((b)–(d) and (k)–(m)). Red channel signaling clearly demonstrated the increased signals from cells infected with AdsFRP1 (compare (e)–(g) with (n)–(p)). Green channel signaling revealed the adenovirus-infected cells ((h)–(j) and (q)–(s)).

expression of CHOP and MMP1 than either treatment alone (green bar in Figure 7(a)). This result indicates that sFRP1 did not inhibit Wnt5a function and sFRP1 alone can activate noncanonical Wnt signaling. This observation was confirmed at the protein level shown in Figures 7(b)–7(s). Compared to control AdGFP-infected cells (7(b)–7(j)), AdsFRP1-infected cells exhibited higher levels of sFRP1, CHOP, and ROR2 protein (7(k)–7(s)). ROR2 is a noncanonical Wnt receptor whose expression level can be stimulated by noncanonical Wnt signaling through a feed-forward mechanism [28]. Overall, the expression of sFRP1 appears to favor noncanonical Wnt signaling, either by indirect inhibition of canonical Wnt or by direct stimulation of noncanonical Wnt signaling.

4. Discussion

The exact mechanisms that underlie the process of aging are currently unclear. Two theories have been proposed to be the major contributors for aging [29]. The first one is the programmed theory, and the second is the damage-related theory. The programmed theory considers aging as pre-programmed genetic events, just as were embryonic development and early childhood development. The gene expression driving these events is programmed in the DNA and is unfolded in a precisely controlled manner. Evidence supporting this theory includes the steady shortening of telomeres during the lifetime of dividing cells. Also, a decreased growth hormone/insulin-like growth factor 1 signaling pathway or nutrient-sensing mTOR signaling has been associated with increased lifespan [30]. Overactivation of mTOR signaling is also considered a major factor for stem cell depletion [31]. The damage-related theory regards aging as the consequence of a loss of cells due to accumulative damages beyond repair. We consider both theories depending on the tissue context. For tissues that can regenerate, such as skin and blood, keeping a healthy pool of stem cells is critical and therefore may relate to the programmed theory. For tissues mainly dependent on their differentiated cells to function, such as heart muscle and neurons, preventing damage-related

cell loss is the best strategy in concordance with the damage-related theory.

If we consider aging as a programmed process, we can also consider it to be a developmental process destined towards self-destruction. The fate is inevitable, but the process can be prolonged and delayed. The basic premise behind our study takes into account these ideas: if a factor can accelerate the development of a tissue during early development, this factor may also accelerate the aging process later in life. This idea draws upon the facets of developmental drift [32]. According to this theory, selection pressure is the highest in early development. Evolution selects pathways that provide an early selective advantage to the animals. These pathways may also accelerate other biological processes, such as aging. We previously reported that knockout beta-catenin, a key canonical Wnt signaling mediator, from the corneal stroma accelerated the maturation of corneal epithelium [4]. Here we report signs of accelerated aging in mice expressing the Wnt antagonist sFRP1. The first sign we noticed was the increased number of grey hairs on the back of the KR/sFRP1 mice. Grey hair is a documented sign of aging, caused by oxidative stress in pigment-producing cells [33]. The KR driver mice were designed to express genes in corneal stromal cells, but a low level of expression may also occur in other tissues of neural crest origin, such as melanocytes and cartilage precursors. Because the expression pattern of the KR driver has not been fully characterized in adult mice, we can only speculate that the increased number of grey hairs is caused by sFRP1 expression in the melanocytes of hair follicles.

The signs of accelerated aging presented in the KR/sFRP1 resemble those of PEX syndrome. PEX syndrome is an age-related systemic disease characterized by the accumulation of an extracellular fibrillar material in the eyes, skin, lungs, heart, kidneys, and other organs. About 30% of patients with PEX syndrome will progress to glaucoma within 7 years [34]. Further associated clinical signs and potential complications include angle-closure glaucoma, cataracts, phacodonesis, and lens subluxation due to weakened ciliary zonules, insufficient mydriasis, saw-tooth structure of the iris pigment epithelium, peripupillary transillumination defects due to dispersion of pigment, iris stromal atrophy, iris vasculopathy associated with blood-aqueous barrier defects, and formation of posterior synechiae as well as corneal endothelial decompensation [35]. Within two months of sFRP1 expression (mice chronological age of six months), the following signs of PEX syndrome were observed: granular deposition on the surface of the anterior lens capsule, pigment loss from the anterior surface of the iris, presence of fibrillary material in the anterior chamber, and weakened ciliary zonules. We did also observe some of those signs in the much older control mice (over twelve months old, data not shown), further suggesting that sFRP1 accelerated the aging process. Currently, we do not know if the ocular alterations are directly caused by diffusible sFRP1 expressed by the keratocyte or by secondary factors due to the expression of sFRP1. Diffusible factors are critical in the homeostasis of this part of the eyes which does not have an extensive vascular network.

In addition to mTOR signaling, Wnt signaling has been implicated in the aging process [10]. The consensus is that canonical Wnt signaling delays the aging process by preserving a healthy pool of stem cell population, while non-canonical Wnt signaling accelerates the aging process by depleting the stem cell pool. The detrimental role of non-canonical Wnt signaling in aging is supported by the longevity studies in *C. elegans* of which mom-2/Wnt and cwn-2/Wnt mutants live 35% and 18% longer compared to wild-type controls. *cwn-2* is an ortholog of human *Wnt5a*, a known noncanonical Wnt ligand. On the other hand, lin-44/Wnt and egl-20/Wnt mutants live 30% and 25% shorter than their wild-type controls. Both lin-44 and egl-20 are orthologs of human *Wnt7*, a known canonical Wnt ligand [36]. This connection provides the foundation for the role of non-canonical Wnt signaling in the processes of ocular aging.

It is well documented that sFRP1 can inhibit canonical Wnt signaling by sequestering the Wnt ligands. If the only function of sFRP1 is binding and sequestering the Wnt ligands, it should also bind and sequester noncanonical Wnt ligands, such as Wnt5a. However, our data demonstrated that this is not the case. sFRP1 does not inhibit Wnt5a-mediated signal transduction, but rather it behaves like Wnt5a. This notion is supported by genetic studies that sFRP1 knockout mice have the same phenotypes as Wnt5a knockout mice in male sexual development [37]. Eyes expressing Wnt5a also exhibit PEX-like phenotypes just as do sFRP1 eyes [19]. So, we suggest that it is possible that sFRP1 can directly stimulate noncanonical Wnt signaling. To prove that, endogenous Wnt5a or other noncanonical Wnt ligands must be knocked out in order to rule out the possibility that sFRP1 indirectly activates noncanonical Wnt signaling by facilitating a Wnt5a feed-forward cycle. Further studies will be conducted to tease out the relationship between sFRP1 and noncanonical Wnt ligands such as Wnt5a.

In our study, we did not examine the potential important role of sFRP1 in glaucoma, another age-related eye disease. Evidence indicates that there may be a relationship between sFRP1 and glaucoma: sFRP1 is upregulated in the trabecular meshwork cells from primary open-angle glaucoma patients [38]. Also, adenovirus-mediated sFRP1 expression elicits ocular hypertension in mice [39]. Based on these reports, KR/sFRP1 should have glaucoma-related retinal ganglion cell loss. If KR/sFRP1 mice do have such retinal ganglion cell loss, it could serve as an animal model for glaucoma. We aim to further analyze the potential relationship between sFRP1 mice and glaucoma, ideally determining features that could prove beneficial to an animal model.

In summary, we found signs of accelerated aging in eyes with exogenous sFRP1 expression. The effects found were determined to be associated with increased noncanonical Wnt signaling. Further proving this connection may provide therapeutic benefits, as noncanonical Wnt inhibitors, like ROCK inhibitor Rhopressa, have been approved to ameliorate symptoms of glaucoma. Such therapeutic agents may also be very useful in preventing the accelerated aging process in eyes caused by over-activated noncanonical Wnt signaling. Further work is needed to establish sFRP1 expression as a model useful in studying phenotypes of ocular

aging before any therapeutic considerations can be made. However, this study provides clues as to how noncanonical Wnt signaling in the eye may lead to accelerated ocular aging, with phenotypes consistent with other age-related ocular manifestations such as PEX syndrome.

Data Availability

The imaging data used to support the findings of this study are included within the article. The CellProfiler Pipeline files data used to support the findings of this study are available from the corresponding author upon request.

Conflicts of Interest

The authors declare that there are no conflicts of interest regarding the publication of this paper.

Acknowledgments

This study was supported in part by grants from the Glaucoma Foundation (YY), Ohio Lions Eye Research Foundation and NIH-EY013755 (WWK), and R01EY029071 (CYL).

References

[1] A. Glasser and M. C. W. Campbell, "Biometric, optical and physical changes in the isolated human crystalline lens with age in relation to presbyopia," *Vision Research*, vol. 39, no. 11, pp. 1991–2015, 1999.

[2] D. E. Harrison, R. Strong, Z. D. Sharp et al., "Rapamycin fed late in life extends lifespan in genetically heterogeneous mice," *Nature*, vol. 460, no. 7253, pp. 392–395, 2009.

[3] M. Lezzerini and Y. Budovskaya, "A dual role of the Wnt signaling pathway during aging in *Caenorhabditis elegans*," *Aging Cell*, vol. 13, no. 1, pp. 8–18, 2014.

[4] Y. Zhang, L.-K. Yeh, S. Zhang et al., "Wnt/β-catenin signaling modulates corneal epithelium stratification via inhibition of Bmp4 during mouse development," *Development*, vol. 142, no. 19, pp. 3383–3393, 2015.

[5] J. Behrens, J. P. von Kries, M. Kühl et al., "Functional interaction of β-catenin with the transcription factor LEF-1," *Nature*, vol. 382, no. 6592, pp. 638–642, 1996.

[6] L. Grumolato, G. Liu, P. Mong et al., "Canonical and noncanonical Wnts use a common mechanism to activate completely unrelated coreceptors," *Genes & Development*, vol. 24, no. 22, pp. 2517–2530, 2010.

[7] R. Habas, I. B. Dawid, and X. He, "Coactivation of rac and rho by Wnt/Frizzled signaling is required for vertebrate gastrulation," *Genes & Development*, vol. 17, no. 2, pp. 295–309, 2003.

[8] L. Topol, X. Jiang, H. Choi, L. Garrett-Beal, P. J. Carolan, and Y. Yang, "Wnt-5a inhibits the canonical Wnt pathway by promoting GSK-3-independent β-catenin degradation," *Journal of Cell Biology*, vol. 162, no. 5, pp. 899–908, 2003.

[9] V. Bryja, E. R. Andersson, A. Schambony et al., "The extracellular domain of Lrp5/6 inhibits noncanonical Wnt signaling in vivo," *Molecular Biology of the Cell*, vol. 20, no. 3, pp. 924–936, 2009.

[10] M. J. Nemeth, L. Topol, S. M. Anderson, Y. Yang, and D. M. Bodine, "Wnt5a inhibits canonical Wnt signaling in hematopoietic stem cells and enhances repopulation," *Proceedings of the National Academy of Sciences*, vol. 104, no. 39, pp. 15436–15441, 2007.

[11] M. C. Florian, K. J. Nattamai, K. Dörr et al., "A canonical to non-canonical Wnt signalling switch in haematopoietic stem-cell ageing," *Nature*, vol. 503, no. 7476, pp. 392–396, 2013.

[12] U. M. Schlötzer-Schrehardt, M. R. Koca, G. O. Naumann, and H. Volkholz, "Pseudoexfoliation syndrome ocular manifestation of a systemic disorder?," *Archives of Ophthalmology*, vol. 110, no. 12, pp. 1752–1756, 1992.

[13] Y. Zhang, W. W.-Y. Kao, Y. Hayashi et al., "Generation and characterization of a novel mouse line, keratocan-rtTA (KeraRT), for corneal stroma and tendon research," *Investigative Opthalmology & Visual Science*, vol. 58, no. 11, pp. 4800–4808, 2017.

[14] L. Barandon, P. Dufourcq, P. Costet et al., "Involvement of FrzA/sFRP-1 and the Wnt/frizzled pathway in ischemic preconditioning," *Circulation Research*, vol. 96, no. 12, pp. 1299–1306, 2005.

[15] T. Kanda, K. F. Sullivan, and G. M. Wahl, "Histone-GFP fusion protein enables sensitive analysis of chromosome dynamics in living mammalian cells," *Current Biology*, vol. 8, no. 7, pp. 377–385, 1998.

[16] A. E. Carpenter, T. R. Jones, M. R. Lamprecht et al., "CellProfiler: image analysis software for identifying and quantifying cell phenotypes," *Genome Biology*, vol. 7, no. 10, p. R100, 2006.

[17] H. Shimizu, M. A. Julius, M. Giarre, Z. Zheng, A. M. Brown, and J. Kitajewski, "Transformation by Wnt family proteins correlates with regulation of beta-catenin," *Cell Growth and Differentiation*, vol. 8, pp. 1349–1358, 1997.

[18] J. Luo, Z.-L. Deng, X. Luo et al., "A protocol for rapid generation of recombinant adenoviruses using the AdEasy system," *Nature Protocols*, vol. 2, no. 5, pp. 1236–1247, 2007.

[19] Y. Yuan, U. Schlötzer-Schrehardt, R. Ritch et al., "Transient expression of Wnt5a elicits ocular features of pseudoexfoliation syndrome in mice," *PLoS One*, vol. 14, no. 3, Article ID e0212569, 2019.

[20] U. Schlötzer-Schrehardt and G. O. H. Naumann, "A histopathologic study of zonular instability in pseudoexfoliation syndrome," *American Journal of Ophthalmology*, vol. 118, no. 6, pp. 730–743, 1994.

[21] S. Sharma, T. Chataway, K. P. Burdon et al., "Identification of LOXL1 protein and apolipoprotein E as components of surgically isolated pseudoexfoliation material by direct mass spectrometry," *Experimental Eye Research*, vol. 89, no. 4, pp. 479–485, 2009.

[22] R. W. Yee, M. Matsuda, R. O. Schultz, and H. F. Edelhauser, "Changes in the normal corneal endothelial cellular pattern as a function of age," *Current Eye Research*, vol. 4, no. 6, pp. 671–678, 1985.

[23] Q. Xu, P. A. D'Amore, and S. Y. Sokol, "Functional and biochemical interactions of Wnts with FrzA, a secreted Wnt antagonist," *Development*, vol. 125, no. 23, pp. 4767–4776, 1998.

[24] A. Üren, F. Reichsman, V. Anest et al., "Secreted frizzled-related protein-1 binds directly to wingless and is a biphasic modulator of Wnt signaling," *Journal of Biological Chemistry*, vol. 275, no. 6, pp. 4374–4382, 2000.

[25] Y. Matsuda, T. Schlange, E. J. Oakeley, A. Boulay, and N. E. Hynes, "WNT signaling enhances breast cancer cell motility and blockade of the WNT pathway by sFRP1 suppresses MDA-MB-231 xenograft growth," *Breast Cancer Research*, vol. 11, no. 3, p. R32, 2009.

[26] L. M. Galli, T. Barnes, T. Cheng et al., "Differential inhibition of Wnt-3a by Sfrp-1, Sfrp-2, and Sfrp-3," *Developmental Dynamics*, vol. 235, no. 3, pp. 681–690, 2006.

[27] B. Ohkawara and C. Niehrs, "An ATF2-based luciferase reporter to monitor non-canonical Wnt signaling in xenopus embryos," *Developmental Dynamics*, vol. 240, no. 1, pp. 188–194, 2011.

[28] I. I. Pacheco and R. J. MacLeod, "CaSR stimulates secretion of Wnt5a from colonic myofibroblasts to stimulate CDX2 and sucrase-isomaltase using Ror2 on intestinal epithelia," *American Journal of Physiology-Gastrointestinal and Liver Physiology*, vol. 295, no. 4, pp. G748–G759, 2008.

[29] K. Jin, "Modern biological theories of aging," *Aging and Disease*, vol. 1, no. 2, pp. 72–74, 2010.

[30] T. Vellai, K. Takacs-Vellai, Y. Zhang, A. L. Kovacs, L. Orosz, and F. Müller, "Influence of TOR kinase on lifespan in *C. elegans*," *Nature*, vol. 426, no. 6967, 620 pages, 2003.

[31] J. Y. Lee, D. Nakada, O. H. Yilmaz et al., "mTOR activation induces tumor suppressors that inhibit leukemogenesis and deplete hematopoietic stem cells after pten deletion," *Cell Stem Cell*, vol. 7, no. 5, pp. 593–605, 2010.

[32] M. Lezzerini, R. L. Smith, and Y. Budovskaya, "Developmental drift as a mechanism for aging: lessons from nematodes," *Biogerontology*, vol. 14, no. 6, pp. 693–701, 2013.

[33] P. C. Arck, R. Overall, K. Spatz et al., "Towards a "free radical theory of graying": melanocyte apoptosis in the aging human hair follicle is an indicator of oxidative stress induced tissue damage," *FASEB Journal*, vol. 20, no. 9, pp. 1567–1569, 2006.

[34] P. Puska, "Unilateral exfoliation syndrome: conversion to bilateral exfoliation and to glaucoma: a prospective 10-year follow-up study," *Journal of Glaucoma*, vol. 11, no. 6, pp. 517–524, 2002.

[35] G. Naumann, U. Schlötzer-Schrehardt, and M. Küchle, "Pseudoexfoliation syndrome for the comprehensive ophthalmologist intraocular and systemic manifestations historical image," *Ophthalmology*, vol. 105, no. 6, pp. 951–968, 1998.

[36] E. Posokhova, A. Shukla, S. Seaman et al., "GPR124 functions as a WNT7-specific coactivator of canonical β-catenin signaling," *Cell Reports*, vol. 10, no. 2, pp. 123–130, 2015.

[37] N. Warr, P. Siggers, D. Bogani et al., "Sfrp1 and Sfrp2 are required for normal male sexual development in mice," *Developmental Biology*, vol. 326, no. 2, pp. 273–284, 2009.

[38] W. H. Wang, L. G. McNatt, I. H. Pang et al., "Increased expression of the WNT antagonist sFRP-1 in glaucoma elevates intraocular pressure," *Journal of Clinical Investigation*, vol. 118, no. 3, pp. 1056–1064, 2008.

[39] W. Mao, J. C. Millar, W.-H. Wang et al., "Existence of the canonical Wnt signaling pathway in the human trabecular meshwork," *Investigative Opthalmology & Visual Science*, vol. 53, no. 11, pp. 7043–7051, 2012.

Hindawi
Journal of Ophthalmology
Volume 2019, Article ID 8949683, 7 pages
https://doi.org/10.1155/2019/8949683

Research Article

The Prevalence of *Demodex folliculorum* and *Demodex brevis* in Cylindrical Dandruff Patients

Jing Zhong, Yiwei Tan, Saiqun Li, Lulu Peng, Bowen Wang, Yuqing Deng, and Jin Yuan

State Key Laboratory of Ophthalmology, Zhongshan Ophthalmic Center, Sun Yat-Sen University, Guangzhou 510064, China

Correspondence should be addressed to Jin Yuan; yuanjincornea@126.com

Received 8 November 2018; Revised 3 February 2019; Accepted 12 March 2019; Published 3 April 2019

Academic Editor: Alejandro Cerviño

Purpose. To compare the prevalence of and factors associated with *Demodex brevis* and *Demodex folliculorum* in patients with cylindrical dandruff (CD group) and healthy controls. *Methods*. Eyelashes were taken from 1680 patients with CD and 1700 healthy controls in China from March 2015 to May 2017. All patients underwent a complete eye examination, and *Demodex* spp. were counted. The prevalence was analyzed according to age, gender, and clinical features. *Results*. Mean patient age was 42.93 ± 16.52 (3–88) and 39.4 ± 13.6 (7–81) years old in the CD and healthy control groups, respectively. In the CD and healthy groups, the positive rate for *Demodex folliculorum* was 27.92% and 8.47%, respectively, while that for *Demodex brevis* was 31.67% and 6.65%, respectively. In the CD group, the prevalence of *Demodex brevis* was higher than that of *Demodex folliculorum*, no matter in the females (33.65% versus 29.01%) or the males (28.54% versus 23.88%) in the CD group. Moreover, the numbers of *Demodex folliculorum* and *Demodex brevis* were significantly and positively correlated with age, in both children and old patients (both $P < 0.001$), as well as with the severity of eyelid congestion (all $P < 0.05$). *Conclusions*. In a large sample population, the prevalence of *Demodex brevis* and *Demodex folliculorum* was higher in the CD group than in healthy volunteers. In addition, the severity of eyelid congestion might be exacerbated by the number of *Demodex* spp., which may therefore provide a good clinical reference and objective guide.

1. Introduction

Demodex, one of the most common parasites in humans, resides in sites with numerous hair follicles and pilosebaceous glands, such as the eyelids [1], face [2], scalp [3], and upper chest [4]. Among more than 140 species of mites, only *Demodex folliculorum* and *Demodex brevis* are found on the human body. *Demodex folliculorum* is approximately 0.3–0.4 mm long, while *Demodex brevis* is approximately 0.2–0.3 mm long [5]. Their life cycle is approximately 14–16 days long, they move mostly at night, and they live in regions such as the sebaceous glands in facial skin, including the nose, nasolabial folds, eyelids, cheek, forehead, chin, and neck [6].

In ophthalmology, ocular demodicosis is typically accompanied by eyelash loss or abnormal alignment and chronic inflammation of the meibomian gland [7], leading to lipid tear deficiency in the conjunctiva [8]; in turn, this deficiency leads to conjunctivitis and sight-threatening keratitis in the cornea [9]. Several studies have also linked the presence of *Demodex* with chronic blepharitis because the mite can perpetuate the follicular inflammatory process [1, 10, 11]. Some researchers consider the mites to be merely passengers on skin because they are found on almost all normal adult skin and thus are coincidentally found on diseased skin [12, 13]. However, clinical observations have revealed that after ineffective conventional therapy, acaricidal therapy can eliminate the clinical symptoms of blepharitis [14]. Nevertheless, direct, absolute proof of a causal relationship has not yet been established because *Demodex* is a host-specific obligate parasite that currently cannot be cultured *in vitro* to parasitize and infect other animal hosts [15]. Therefore, clinical observations based on large samples are important for exploring the relationship between *Demodex* and clinical signs.

Cylindrical dandruff (CD) in the eyelashes, also known as cylindrical casts, are scales that form clear cuffs that collar the lash root and may be composed of keratins and lipids [16, 17]. CD is one of the clinical manifestations of ocular

demodicosis, and Tseng's study showed that eyelashes with CD did indeed have a significantly higher rate of *Demodex* infestation than was found in eyelashes without CD [6]. CD in the eyelashes is a common finding in some patients with ocular demodicosis, but whether it is pathognomonic of *Demodex* infestation remains controversial. This debate is partially attributed to the accuracy of methods used to sample and count *Demodex* [18]. Therefore, a modified sampling and counting method was established to enhance the accuracy of *Demodex* diagnosis [6].

However, the exact prevalence of *Demodex* and the pathogenic potential of these mites in eyes with CD remain uncertain. Thus, we performed a study of 1680 patients with CD and 1700 healthy volunteers in China that was designed to determine the prevalence of *Demodex* and the effect of the hosts' factors such as gender, age, and eyelid inflammation score, on the presence or absence of *Demodex*.

2. Materials and Methods

2.1. Patient Data. A total of 1680 patients with eyelashes showing CD (representative pictures are shown in Figure 1(a)) and who complained of ocular surface irritation and 1700 healthy volunteers who visited our hospital between March 2015 and June 2017 were included in our study. In the healthy group, there were 1166 (68.6%) females and 534 (31.4%) males with a mean age of 39.4 ± 13.6 (7–81) years; in the CD group, there were 1165 (69.4%) females and 515 (30.6%) males with a mean age of 42.9 ± 16.5 (3–88) years. The collected data included basic information such as gender and age, the status of eyelid inflammation, and the results of *Demodex* counting. This study followed the tenets of the Declaration of Helsinki and was approved by the Ethics Committee of the Zhongshan Ophthalmic Center (Guangzhou, China). A total of 3380 individuals in both groups all signed a consent document to participate in the study.

2.2. Demodex Sampling and Counting. The methods used here were previously described by Kheirkhah et al. [19]. Briefly, two lashes with CD were removed from each lid of each subject by fine forceps and were placed separately on each end of a glass slide for examination under a slit-lamp biomicroscope (SL220; Carl Zeiss, Oberkochen, Germany) at a magnification of ×25. Thus, for each subject, a total of 8 lashes were prepared on 4 slides. A coverslip was mounted on each lash before 20 μL of saline was slowly pipetted at the edge of the coverslip until it surrounded the lash. Then, 20 μL of 100% alcohol (Sigma-Aldrich, St. Louis, MO) was pipetted at the edge of the coverslip; this prolonged the counting time for up to 20 minutes and allowed the embedded *Demodex* to migrate from the CD. Under the microscope, the number of *Demodex* was counted three times, and all samples were photographed in a conventional manner by the same specialist (Doc Tan). The presence of *Demodex* in at least one of the 8 eyelashes was defined as *Demodex*-positive.

2.3. Eyelid Inflammation Evaluation. The status of eyelid inflammation was based on the presence of vascular congestion in the eyelid margin, as observed by external photography. These findings were subjectively rated on a four-point scale, as follows: 0, no vascular congestion; 1, mild vascular congestion; 2, moderate vascular congestion; and 3, severe vascular congestion [20].

2.4. Statistical Analysis. Data were evaluated using SPSS for Windows 11.5. An unpaired, two-tailed Student's *t*-test was used to compare the numbers of *Demodex brevis* and *Demodex folliculorum* and the numbers of *Demodex* among the different grades of eyelid congestion. The chi-square test and Fisher's exact test were used to evaluate differences in *Demodex* prevalence among different ages and genders. Correlation analysis was used to evaluate the relationship between *Demodex* numbers and age and between *Demodex* rates and eyelid congestion severity. The data were considered significant at $P < 0.05$.

3. Results

3.1. The Prevalence of Demodex Brevis and Demodex Folliculorum Was Higher in the CD Group than in the Healthy Group. Figures 1(b) and 1(c) show representative microscopic images of *Demodex folliculorum* and *Demodex brevis*. The positive rate of *Demodex folliculorum* was 27.92% and 8.47%, respectively, in the CD group and healthy group, and *Demodex brevis*'s prevalence was 31.67% and 6.65%, respectively, in these two groups (Figure 1(d)). Furthermore, the average number of *Demodex folliculorum* and *Demodex brevis* was 0.52 (0–18) and 0.86 (0–18) in the CD group, which was 0.06 (0–2) and 0.14 (0–2) in the healthy group; the average *Demodex*.spp. number of all the positive subjects was more in the CD group than in the healthy group, no matter in *Demodex folliculorum* (2.23 ± 0.07 versus 1.37 ± 0.08, $P < 0.01$) or in *Demodex brevis* (2.72 ± 0.07 versus 1.29 ± 0.13, $P < 0.05$). Moreover, the average number of *Demodex brevis* was obviously greater than *Demodex folliculorum* in the CD group ($P < 0.001$) while not in the healthy group (Figure 1(e)). Thus, the prevalence of *Demodex folliculorum* and *Demodex brevis* was higher in CD group compared with that in the healthy group, and the positive rate of *Demodex brevis* was greater than that of *Demodex folliculorum* in the CD group.

3.2. The Number of Demodex Brevis Was Higher in Females than in Males. In the CD group, the positive rate of *Demodex folliculorum* was 23.88% and 29.10%, respectively, in males and females, while in the healthy group, it was 7.49% and 8.83%, respectively, in males and females. The prevalence of *Demodex brevis* showed a trend similar to that of *Demodex folliculorum,* with the positive rate of 28.54% and 33.65% in males and females in the CD group and 5.05% and 7.55% in males and females in the healthy group. The prevalence of *Demodex folliculorum* and *Demodex brevis* were higher in the CD group than in the healthy group in both males and females and higher in females than in males in both groups (Figure 2).

3.3. The Number of Demodex Increased with Age in Eyelashes with CD. In the CD and healthy groups, the prevalence of

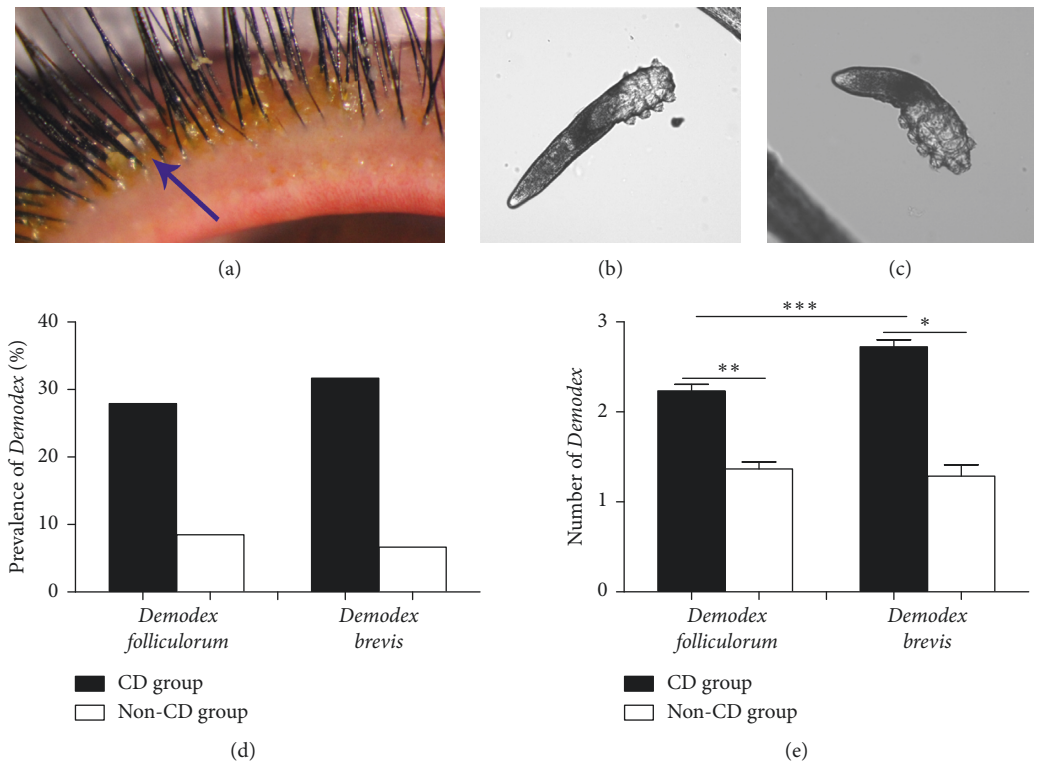

Figure 1: Representative images of cylindrical dandruff (a) (blue arrow; magnification 40x), *Demodex folliculorum* (b), and *Demodex brevis* (c); the prevalence of *Demodex brevis* was higher than that of *Demodex folliculorum*, and the average number of *Demodex folliculorum* was significantly lower than that of *Demodex brevis* (d, e). $^{*}P < 0.05$; $^{**}P < 0.01$; $^{***}P < 0.001$.

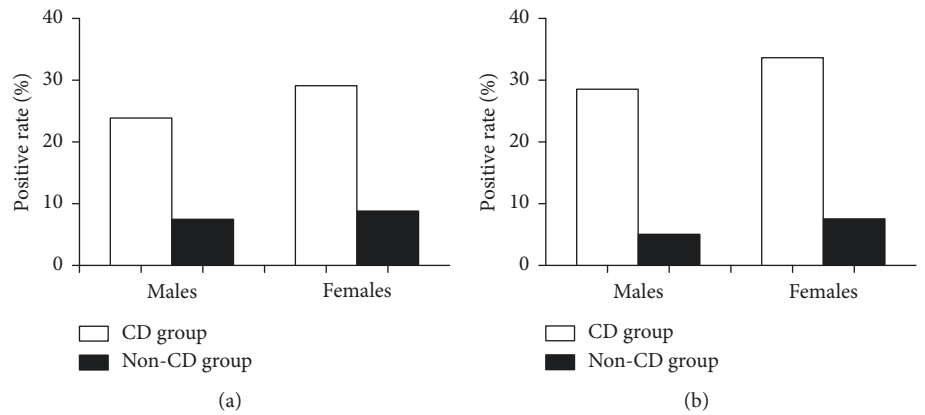

Figure 2: The positive rate of *Demodex folliculorum* (a) and *Demodex brevis* (b) in males and females in the CD and healthy groups. $^{*}P < 0.05$; $^{**}P < 0.01$; $^{***}P < 0.001$.

Demodex folliculorum was 13.33% and 0% in children (<6 years old), 22.22% and 1.78% in juveniles (7–17 years old), 21.74% and 8.71% in youth (18–40 years old), 24.31% and 9.18% in middle-aged patients (41–65 years old), and 30.97% and 12.87% in old patients (66–88 years old) (Table 1). In the CD and healthy groups, the prevalence of *Demodex brevis* were 26.67% and 2.63% in children, 30.00% and 3.55% in juveniles, 29.55% and 6.46% in youth, 32.67% and 7.75% in middle-aged patients, and 37.42% and 8.77% in old patients. The prevalence of *Demodex brevis* and *Demodex folliculorum* appeared lower in younger age groups than in older age groups, respectively (Table 1). The prevalence differed among different groups, and old patients had the higher prevalence in *Demodex folliculorum* and *Demodex brevis*. Furthermore, in the CD group, the number of *Demodex folliculorum* and *Demodex brevis* per patient was positively correlated with age across all age groups (both $P < 0.001$). The following equations were used: number of *Demodex folliculorum* = 1.180 + 0.035 (age) ($r = 0.237$, $P < 0.001$) (Figure 3(a)) and number of *Demodex brevis* = 0.650 + 0.037 (age) ($r = 0.286$, $P < 0.001$) (Figure 3(b)).

Table 1: Distribution of *Demodex folliculorum* and *Demodex brevis* by age in the CD and healthy groups.

Age (years)	*Demodex folliculorum*, positive/*n* (%)		*Demodex brevis*, positive/*n* (%)	
	CD group	Healthy group	CD group	Healthy group
0–6	2/15 (13.33%)	0/38 (0%)	4/15 (26.67%)	1/38 (2.63%)
7–17	20/90 (22.22%)	3/169 (1.78%)	27/90 (30.00%)	6/169 (3.55%)
18–40	142/653 (21.74%)	62/712 (8.71%)	193/653 (29.55%)	46/712 (6.46%)
41–65	186/765 (24.31%)	56/610 (9.18%)	250/765 (32.67%)	46/610 (7.75%)
66–88	48/155 (30.97%)	22/171 (12.87%)	58/155 (37.42%)	15/171 (8.77%)

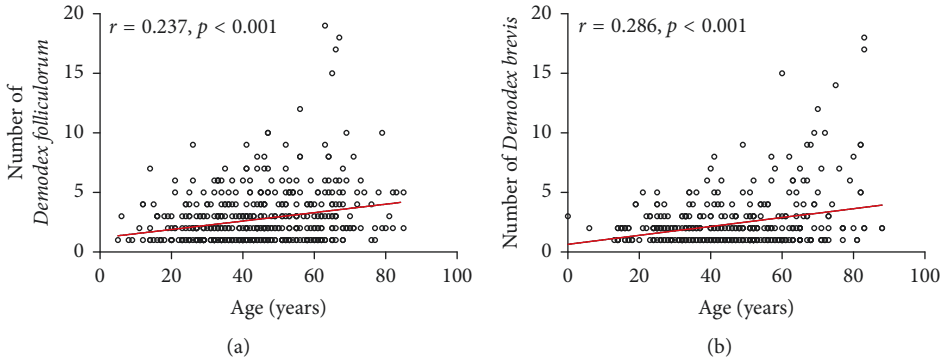

Figure 3: The average number of *Demodex folliculorum* (a) and *Demodex brevis* (b) are significantly correlated with increasing age, from children to older patients. $^{*}P < 0.05$; $^{**}P < 0.01$; $^{***}P < 0.001$.

3.4. The Prevalence and Number of Demodex Brevis Were Positively Correlated with the Severity of Eyelid Congestion. In the CD group, we concluded that the severity of eyelid congestion was positively correlated with the prevalence of both *Demodex folliculorum* and *Demodex brevis* (both $P < 0.05$) (Figure 4(a)) according to the following equations: prevalence of *Demodex folliculorum* (%) = 18.25 + 10.19 (grade) ($r = 0.999$, $P = 0.029$) and prevalence of *Demodex brevis* (%) = 13.40 + 8.75 (grade) ($r = 1.000$, $P = 0.015$). The prevalence of *Demodex folliculorum* increased from 22.26% in Grade I to 30.66% in Grade II to 39.75% in Grade III, while the prevalence of *Demodex brevis* increased from 28.70% to 38.09% and 49.01% in Grade I, II, to Grade III, respectively. Furthermore, the highest numbers of *Demodex folliculorum* and *Demodex brevis* individuals were observed in Grade III cases, whereas the fewest were observed in the Grade I cases (all $P < 0.05$) (Figure 4(b)). Specifically, the prevalence and number of *Demodex folliculorum* and *Demodex brevis* increased with the severity of eyelid congestion.

4. Discussion

Demodex is a parasite commonly observed on human skin [21], and some investigators have suggested that there is a symbiotic relationship between mites and humans that may even beneficial for the hosts because these mites ingest bacteria that can grow in the follicular canal [22, 23]. However, a growing body of evidence indicates that these mites may also act as pathogens in a number of skin diseases, such as rosacea [24], alopecia [25], and chronic blepharitis [11].

The prevalence of *Demodex folliculorum* and *Demodex brevis* was clearly higher in the CD group than in healthy volunteers in our study; although the positive rate of 27.92% and 31.67% was lower than the prevalence of 100% in Tseng's study [6], it also provided strong evidence to support the high prevalence in CD lashes. The eye is surrounded by protruding body parts such as the nose, brow, and cheek; the eyelid is not as accessible as the face is to daily cleansing hygiene. Therefore, once a *Demodex* infestation is established in the face, it is likely to spread and flourish in the eyelids. Microabrasions caused by the mite's claws can induce epithelial hyperplasia and reactive hyperkeratinization around the base of the lashes, forming CD [26], which is closely associated with *Demodex* infestation. In addition, differences in sample size and regions among studies have led to a lack of consistent results until now. For example, Wesolowska et al. [27] reported that the overall prevalence of *Demodex* spp. is 41% in Poland, a rate of positivity of 37.3% was reported for *Demodex* spp. in Turkish volunteers [28], and a prevalence rate of 21.2% was found in Shangqiu City of Henan Province [29], 36.3% in Tangshan [30], and 51.5% in inner Mongolia [31]. Thus, the difference in prevalence between our and Tseng's results might be normal.

Moreover, we found that the prevalence of *Demodex folliculorum* and *Demodex brevis* was higher in females than in males. The prevalence of *Demodex brevis* was 33.65%, which is similar to the rate of 39.3% found in women in the Malatya province in Turkey [32] but lower than the prevalence of 100% reported in Tseng's study [6]. However, the gender distribution of *Demodex* spp. in the present study was not in agreement with the results of Elston's study [33],

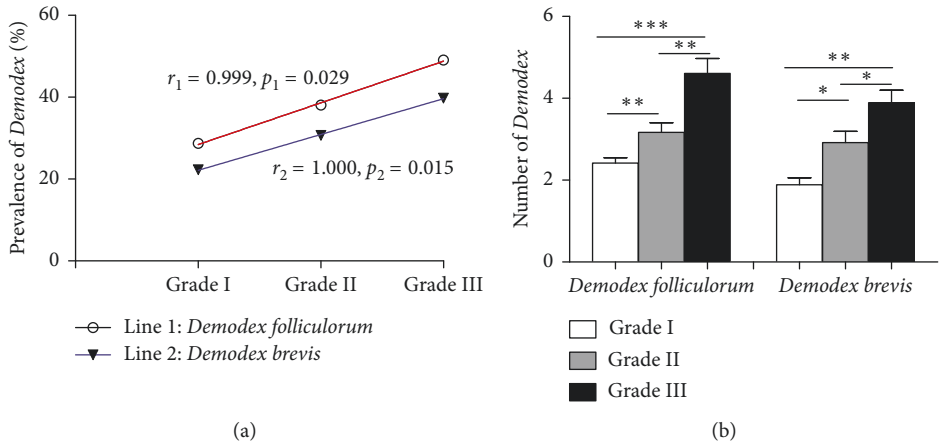

FIGURE 4: (a) The relationship between congestion severity and the number of *Demodex* in the CD group. (b) In the CD group, the number of *Demodex folliculorum* and *Demodex brevis* was highest in Grade III cases and the lowest in Grade I cases. $^{*}P < 0.05$; $^{**}P < 0.01$; $^{***}P < 0.001$.

in which men were typically more heavily infested than women with *Demodex*. The application of exogenous lipids in cosmetics may also affect the growth of *Demodex* mites in females because females have lower androgen levels, and the meibomian gland is an androgen target organ. Therefore, females may be more susceptible to meibomian gland dysfunction, the resultant lipid insufficiency, and therefore *Demodex* spp. attack [34].

Demodex spp. are acquired shortly after birth during nursing and become more abundant during puberty [33]. In our study, the total number of *Demodex folliculorum* and *Demodex brevis* per patient was significantly correlated with increasing age from children to older patients, and their prevalence was significantly higher in older patients than in youths or children. Why do mites proliferate much more in older patients? Some of the physical barrier characteristics of an elderly person's facial skin, such as increased skin pH [35], reduced skin surface hydration levels [36], and abnormal fatty acid composition [37], are conducive to mite proliferation. Additionally, in healthy skin, *Demodex* mites can cause host damage, so they may seize the opportunity to proliferate as immunity decreases or the host becomes immunocompromised [22]. Thus, the elderly, who have comparatively poor sanitary conditions and practices, abnormal skin barriers, and relatively compromised immunity, would be easily invaded by *Demodex* spp. Moreover, the prevalence of *Demodex brevis* was more common than *Demodex folliculorum* in the CD group and healthy subjects, which might be due to the fact that *Demodex folliculorum* resides in the lash follicle, whereas *Demodex brevis* burrows deep into the lash's sebaceous gland and the meibomian gland [38]. Although some studies reported that *Demodex folliculorum* can be more easily isolated than *Demodex brevis* and thus the prevalence of *Demodex folliculorum* was higher compared with the *Demodex brevis* [39], we deduced that the tendency might be different in *Demodex brevis*-related or *Demodex folliculorum*-related ocular diseases, and *Demodex brevis* might be more common in the sebaceous gland- or meibomian gland-related diseases, such as Chalaza [6], while *Demodex folliculorum* was more commonly seen in lash follicle-related diseases, such as posterior blepharitis, or keratoconjunctivitis [38].

In addition to CD, eyelid margin inflammation is one of the main clinical manifestations of ocular demodicosis; thus, the severity of eyelid inflammation may indicate the prognosis [40]. The increased number and extrafollicular localization of mites enhance the probability of a hypersensitivity reaction, inflammation, and the secretion of inflammatory cytokines. Regardless of the prevalence or number of *Demodex folliculorum* and *Demodex brevis*, both were positively correlated with eyelid congestion severity; these results demonstrate that the *Demodex* spp. infestation may act as a pathogen in ocular pathologic features. This result is in agreement with Tseng's results [41].

In conclusion, we explored a large sample population and found that the prevalence of *Demodex brevis* and *Demodex folliculorum* were higher in the CD group than in healthy volunteers. Our results demonstrate that in eyelashes with CD, the prevalence of *Demodex brevis* is higher than that of *Demodex folliculorum*. We also found that the number of *Demodex* spp. increases with age and that females are attacked more easily than males by *Demodex* spp. In patients with CD eyelashes, the severity of eyelid congestion was exacerbated by the prevalence and number of *Demodex* spp. Further studies should focus on the specific mechanism of *Demodex* spp. infection, build diagnostic criteria for eyelid demodicosis, and explore the relationship between *Demodex* spp. and ocular immunology to develop therapies against *Demodex*.

Data Availability

The datasets will be provided via a link if required after publication.

Conflicts of Interest

None of the authors has any proprietary interests or conflicts of interest related to this submission. None of the authors has any conflicts of interest to disclose.

Authors' Contributions

Jing Zhong and Yiwei Tan contributed equally to this work.

Acknowledgments

This study was supported by grants from the National Natural Science Foundation of China to JY (81670826)

References

[1] M. Galea, R. Sharma, S. Srinivasan, and F. Roberts, "*Demodex* blepharitis mimicking eyelid sebaceous gland carcinoma," *Clinical & Experimental Ophthalmology*, vol. 42, no. 2, pp. 208–210, 2014.

[2] M. M. Hom, K. M. Mastrota, and S. E. Schachter, "*Demodex*," *Optometry and Vision Science*, vol. 90, no. 7, pp. e198–e205, 2013.

[3] W. Helou, E. Avitan-Hersh, and R. Bergman, "*Demodex folliculitis* of the scalp," *American Journal of Dermatopathology*, vol. 38, no. 9, pp. 658–663, 2016.

[4] Y. E. Zhao, L. P. Wu, Y. Peng, and H. Cheng, "Retrospective analysis of the association between *Demodex* infestation and rosacea," *Archives of Dermatology*, vol. 146, pp. 896–902, 2010.

[5] A. Horváth, D. Neubrandt, Á. Ghidán, and K. Nagy, "Risk factors and prevalence of *Demodex* mites in young adults," *Acta Microbiologica et Immunologica Hungarica*, vol. 58, no. 2, pp. 145–155, 2011.

[6] Y.-Y. Gao, M. A. Di Pascuale, W. Li et al., "High prevalence of *Demodex* in eyelashes with cylindrical dandruff," *Investigative Opthalmology & Visual Science*, vol. 46, no. 9, pp. 3089–3094, 2005.

[7] K. G. Patel and V. K. Raju, "Ocular demodicosis," *West Virginia Medical Journal*, vol. 109, pp. 16–18, 2013.

[8] W. Chen and G. Plewig, "Human demodicosis: revisit and a proposed classification," *British Journal of Dermatology*, vol. 170, no. 6, pp. 1219–1225, 2014.

[9] S. H. Lee, Y. S. Chun, J. H. Kim, E. S. Kim, and J. C. Kim, "The relationship between *Demo*dex and ocular discomfort," *Investigative Opthalmology & Visual Science*, vol. 51, no. 6, pp. 2906–2911, 2010.

[10] V. Bhandari and J. Reddy, "Blepharitis: always remember *Demodex*," *Middle East African journal of ophthalmology*, vol. 21, no. 4, pp. 317–320, 2014.

[11] F. Laspina, M. Samudio, M. Arrúa et al., "*Demodex* spp. en pacientes con blefaritis crónica," *Revista Chilena de Infectología*, vol. 32, no. 1, pp. 37–42, 2015.

[12] M. Kemal, Z. Sümer, M. I. Toker, H. Erdoğan, A. Topalkara, and M. Akbulut, "The prevalence of *Demo*dex *folliculorumin* blepharitis patients and the normal population," *Ophthalmic Epidemiology*, vol. 12, no. 4, pp. 287–290, 2005.

[13] S. Talghini, D. F. Fouladi, S. Babaeinejad, R. Shenasi, and S. M. Samani, "*Demodex* mite, rosacea and skin melanoma; coincidence or association?," *Turkish Journal of Parasitology*, vol. 39, no. 1, pp. 41–46, 2015.

[14] M. Türk, I. Oztürk, A. G. Sener, S. Küçükbay, I. Afşar, and A. Maden, "Comparison of incidence of *Demodex folliculorum* on the eyelash follicule in normal people and blepharitis patients," *Turkiye Parazitol Dergisi*, vol. 31, pp. 296-297, 2007.

[15] F. Forton, M.-A. Germaux, T. Brasseur et al., "Demodicosis and rosacea: epidemiology and significance in daily dermatologic practice," *Journal of the American Academy of Dermatology*, vol. 52, no. 1, pp. 74–87, 2005.

[16] F. P. English, "*Demodex folliculorum* and oedema of the eyelash," *British Journal of Ophthalmology*, vol. 55, no. 11, pp. 742–746, 1971.

[17] D. I. Kosik-Bogacka, N. Łanocha, A. Łanocha et al., "*Demodex folliculorum* and *Demodex* brevisin healthy and immunocompromised patients," *Ophthalmic Epidemiology*, vol. 20, no. 3, pp. 159–163, 2013.

[18] A. M. S. Cheng, H. Sheha, and S. C. G. Tseng, "Recent advances on ocular *Demodex* infestation," *Current Opinion in Ophthalmology*, vol. 26, no. 4, pp. 295–300, 2015.

[19] A. Kheirkhah, G. Blanco, V. Casas, and S. C. G. Tseng, "Fluorescein dye improves microscopic evaluation and counting of *Demodex* in blepharitis with cylindrical dandruff," *Cornea*, vol. 26, no. 6, pp. 697–700, 2007.

[20] N. K. Kuscu, A. B. Toprak, S. Vatansever, F. M. Koyuncu, and C. Guler, "Tear function changes of postmenopausal women in response to hormone replacement therapy," *Maturitas*, vol. 44, no. 1, pp. 63–68, 2003.

[21] A. Ozer, U. Karaman, S. Degerli, C. Colak, M. Karadan, and E. Karci, "Investigation of *Demodex* Spp. prevalence among managers and workers of health hazard bearing and sanitary establishment," *Journal of the Formosan Medical Association*, vol. 111, no. 1, pp. 30–33, 2012.

[22] N. Lacey, S. Ní Raghallaigh, and F. C. Powell, "*Demodex* mites—commensals, parasites or mutualistic organisms?," *Dermatology*, vol. 222, no. 2, pp. 128–130, 2011.

[23] K. Fischer and S. Walton, "Parasitic mites of medical and veterinary importance—is there a common research agenda?," *International Journal for Parasitology*, vol. 44, no. 12, pp. 955–967, 2014.

[24] W. Chen and G. Plewig, "Are *Demodex* mites principal, conspirator, accomplice, witness or bystander in the cause of rosacea?," *American Journal of Clinical Dermatology*, vol. 16, no. 16, pp. 67–72, 2015.

[25] S. F. Li, X. T. Zhang, S. L Qi et al., "Allergy to dust mites may contribute to early onset and severity of alopecia areata," *Clinical and Experimental Dermatology*, vol. 40, no. 2, pp. 171–176, 2015.

[26] C. L. Bevins and F. T. Liu, "Rosacea: skin innate immunity gone awry?," *Nature Medicine*, vol. 13, no. 8, pp. 904–906, 2007.

[27] M. Wesolowska, B. Knysz, A Reich et al., "Prevalence of *Demodex* spp. in eyelash follicles in different populations," *Archives of Medical Science*, vol. 2, pp. 319–324, 2014.

[28] U. Karaman, Z. Koloren, O. Enginyurt, and A. Ozer, "The epidemiology of *Demodex* mites at the college students living in dormitories in the city of Ordu," *Turkish Journal of Parasitology*, vol. 38, no. 3, pp. 166–171, 2014.

[29] J. H. Cui and C. Wang, "Facial *Demodex* infestation among urban and rural residents in Shangqiu city of Henan province," *Zhongguo Ji Sheng Chong Xue Yu Ji Sheng Chong Bing Za Zhi*, vol. 30, no. 4, pp. 283–285, 2012.

[30] Y. S. Cao, Q. X. You, L Wang et al., "Facial *Demodex* infection among college students in Tangshan," *Zhongguo Ji Sheng Chong Xue Yu Ji Sheng Chong Bing Za Zhi*, vol. 27, no. 3, pp. 271–273, 2009.

[31] Q. Hu and Y. Wang, "Investigation on the prevalence of human *Demodex* among 2,248 medical students in inner Mongolia," *Zhongguo Ji Sheng Chong Xue Yu Ji Sheng Chong Bing Za Zhi*, vol. 19, no. 4, pp. 239-240, 2001.

[32] O. Enginyurt, U. Karaman, F. Cetin, and A. Ozer, "The prevalence of *Demodex* species and its relationship with the metabolic syndrome in women of Malatya province, Turkey," *Jundishapur Journal of Microbiology*, vol. 8, no. 10, article e24322, 2015.

[33] C. A. Elston and D. M. Elston, "*Demodex* mites," *Clinics in Dermatology*, vol. 32, no. 6, pp. 739–743, 2014.

[34] D. A. Sullivan, B. D. Sullivan, J. E Evans et al., "Androgen deficiency, meibomian gland dysfunction, and evaporative dry eye," *Annals of the New York Academy of Sciences*, vol. 966, no. 1, pp. 211–222, 2002.

[35] C. Gokce, O. Aycan-Kaya, E Yula et al., "The effect of blood glucose regulation on the presence of opportunistic *Demodex folliculorum* mites in patients with type 2 diabetes mellitus," *Journal of International Medical Research*, vol. 41, no. 5, pp. 1752–1758, 2013.

[36] T. Yoshikawa and H. Kanazawa, "Association of plasma adiponectin levels with cellular hydration state measured using bioelectrical impedance analysis in patients with COPD," *International Journal of Chronic Obstructive Pulmonary Disease*, vol. 7, pp. 515–521, 2012.

[37] S. Ni Raghallaigh, K. Bender, N. Lacey, L. Brennan, and F. C. Powell, "The fatty acid profile of the skin surface lipid layer in papulopustular rosacea," *British Journal of Dermatology*, vol. 166, no. 2, pp. 279–287, 2012.

[38] J. Liu, H. Sheha, and S. C. Tseng, "Pathogenic role of *Demodex* mites in blepharitis," *Current Opinion in Allergy and Clinical Immunology*, vol. 10, no. 5, pp. 505–510, 2010.

[39] E. Zeytun and Y. Karakurt, "Prevalence and load of *Demodex folliculorum* and *Demodex brevis* (Acari: Demodicidae) in patients with chronic blepharitis in the province of Erzincan, Turkey," *Journal of medical entomology*, vol. 56, no. 1, pp. 2–9, 2019.

[40] S. L. Maskin, "Intraductal meibomian gland probing relieves symptoms of obstructive meibomian gland dysfunction," *Cornea*, vol. 29, no. 10, pp. 1145–1152, 2010.

[41] A. Kheirkhah, V. Casas, W. Li, V. K. Raju, and S. C. Tseng, "Corneal manifestations of ocular *Demodex* infestation," *American Journal of Ophthalmology*, vol. 143, no. 5, pp. 743–749, 2007.